



UNIVERSITY of the
WESTERN CAPE

The development of functionalized metallic nanoparticles for the treatment of brain cancer

by

Vincent Lukhanyiso Fipaza

Student Number: 3343880

A mini-thesis submitted in fulfillment of the requirements for the degree:

Magister Scientiae in Nanoscience

Department of Medical Biosciences

Faculty of Natural Sciences

University of the Western Cape

Supervisor

Prof Okobi Ekpo

November, 2019

©University of the Western Cape

All Rights Reserved

DECLARATION

I declare that “*The development of functionalized metallic nanoparticles for the treatment of brain cancer*” is my own work, that it has not been submitted for any degree or examination in this and any other university, and that all the sources I have used or quoted have been indicated and acknowledged by complete references.

Full name..... Vincent Fipaza Date..... 13/11/2019

Signed..... 



UNIVERSITY of the
WESTERN CAPE

:

:

ACKNOWLEDGEMENTS

- ❧ Firstly, I would like to express my sincere gratitude to my BSc (Hons) and MSc supervisor and mentor Prof. Okobi Ekpo for his continuous support towards my postgraduate studies and research. Without his patience, motivation, knowledge and guidance, this thesis would not have been possible and I shall be eternally grateful for his assistance.
- ❧ My sincere thanks also go to Miss Taahirah Boltman for helping and guiding me with the laboratory experiments. Her support, encouragement and insightful comments helped me grow as a researcher.
- ❧ I thank Miss Valencia Jamalie for offering me a position into the Nanoscience programme even though my application was late. I would also like to thank her for always availing herself whenever I needed help.
- ❧ Many thanks to the Laboratories of Profs. Mervin Meyer, Abraham Madiehe in Biotechnology Departments at UWC; staff of the Electron Microscopy Unit at UWC as well as Lab staff and postgraduate students in Chemistry department.
- ❧ I would like to thank my colleagues: Simone Barry, Raudine Hoffman, Tusekile Kangwa and Maryam Hassan, for assisting with some of my lab work, for the weekends and sleepless nights we spent in the lab working and for all the support you guys gave me. In addition, I thank Sibongile Lusizi for allowing me to use her computer for analyzing my data.
- ❧ Last but not the least; I would like to thank my family: Ntombekhaya Fipaza, Thenjiwe Fipaza, Nosiphiwo Fipaza-Matyila, Simphiwe Matyila, Yonela Desemele, Olwethu Fipaza, Lonwabo Fipaza, Endinako Fipaza and Mvano Fipaza for all the sacrifices and support that you gave me throughout my life. Thank you to my late big brother for looking out for me up in heaven.

ABSTRACT

Background: Cancers of the nervous system often result from abnormal and uncontrolled growth of cells in nervous tissue. Glioblastoma Multiforme (GBM) and neuroblastoma (NB) are among the most common nervous system-associated cancers known to be relatively difficult to treat. GBM is an aggressive cancer in adults while NB mostly develops in infants and children younger than five years old. Current chemotherapeutic treatment options for GBM and NB have a number of drawbacks, including non-specific toxicity, drug resistance and the inability to cross the blood-brain barrier (BBB). Therefore, there is a need to develop new treatment options that can cross the BBB with minimal or no side effects to normal neural tissues. Gold (Au) and platinum (Pt) nanoparticles (NPs) have been shown to play a role in drug delivery by crossing the BBB to selectively target cancer tissue. However, these metallic nanoparticles have a short life span in the circulatory system and often elicit immune reactions. The functionalization of nanoparticles with polyethylene glycol (PEG) helps to improve their stability and biocompatibility.

The aim of this study was therefore to develop PEGylated metallic nanoparticles and investigate their potential *in vitro* cytotoxic effects on SH SY5Y (NB) and U87 (GBM) cell lines.

Methods: The citrate capped and PEGylated nanoparticles were characterized using ultraviolet-visible spectroscopy (UV-Vis), Fourier Transform infrared spectroscopy (FTIR), High resolution Transmission electron microscopy (HRTEM), Energy dispersive X-ray spectroscopy (EDS) and Dynamic Light scattering spectroscopy (DLS). The WST-1 assay was used to study cytotoxicity and subsequently the

determination of the IC₅₀. Oxidative stress induction and mitochondrial membrane potential were analyzed by flow cytometry. The cellular morphological changes were evaluated using an inverted microscope. Inductively Coupled plasma Mass Spectrometry (ICP-MS) was used to quantify the cellular uptake of the PEGylated nanoparticles.

Results: The UV-Vis spectra confirmed the synthesis and functionalization of the metallic nanoparticles, which were citrate-capped and PEGylated gold as well as gold-platinum. The analysis of HRTEM images revealed that all the nanoparticles were spherical, well dispersed with an average core size of approximately 5nm. The EDS results confirmed the elemental compositions of gold and gold-platinum nanoparticles. FTIR and DLS confirmed that the nanoparticles were citrate-capped as well as PEGylated, and that they were stable.

In vitro studies showed that the PEGylated nanoparticles were stable in biological solvents. In addition, the PEGylated metallic nanoparticles were taken up by the U87 and SH SY5Y cell lines and induced a significant decrease in cell viability. These findings tend to suggest that PEGylated metallic nanoparticles were cytotoxic possibly mediated through oxidative stress.

Conclusion: Gold and gold-platinum nanoparticles were successfully synthesized, citrate-capped, PEGylated and characterized. All the biological assays tend to suggest that these NPs have cytotoxic effects on U87 and SH SY5Y cells but further studies are required to justify the potential use of these NPs as anticancer agents.

Key words: nanoparticles, PEGylation, characterization, cancer, treatment, stability, cytotoxicity, ROS, gold, platinum

LIST OF ABBREVIATIONS

ATP	Adenosine triphosphate
Au	Gold
AuNPs	Gold nanoparticles
AuPtNPs	Gold platinum nanoparticles
BAX	Bcl-2 associated X protein
BBB	Blood-brain barrier
Bcl-2	B-cell lymphoma 2
BID	BH3 interacting domain death agonist
BSA	Bovine Serum Albumin
C- AuNPs	Citrate capped gold nanoparticles
C- AuPtNPs	Citrate capped gold-platinum nanoparticles
CNS	Central Nervous System
CA ²⁺	Calcium
CO ₂	Carbon dioxide
COO ⁻	Carboxylate group
CT	Computerized tomography
DCFH-DA	2',7'-Dichlorodihydrofluorescein diacetate
DMEM	Dulbecco's Modified Eagle's medium

EDX	Energy dispersive X-rays
ETC	Electron transport chain
Fcc	Face-centered cubic
FBS	Fetal Bovine Serum
FTIR	Fourier-transform infrared spectroscopy
GBM	Glioblastoma multiforme
h	Hour
H ₂ O ₂	Hydrogen peroxide
HCl	Hydrochloric acid
HNO ₃	Nitric acid
HRTEM	High resolution transmission electron microscopy
HVA	Homovanillic acid
IC ₅₀	half maximal inhibitory concentration
ICP-MS	Inductively coupled plasma mass spectrometry
IR	Infrared
KBr	Potassium Bromide
KeV	Killo electronvolt
MAC	Mitochondrial apoptosis-induced channel
Mg ²⁺	Magnesium

mIBG	metaiodobenzylguanidine
MMP	Mitochondrial membrane potential
MRI	Magnetic resonance Imaging
NaBH ₄	Sodium borohydride
NB	Neuroblastoma
NPs	Nanoparticles
OH	Hydroxyl group
P/S	penicillin–streptomycin
PBS	Phosphate-buffered Saline
PEG	Polyethylene glycol
pH	Potential of Hydrogen
PNS	Peripheral nervous system
Pt	Platinum
PtNPs	Platinum nanoparticles
PTFE	Polytetrafluoroethylene
RBCs	Red blood cells
RI	Refractive Index
ROS	Reactive oxygen species
rpm	Rate per minute

SAED	Selected area electron diffraction
SD	Standard deviation
SPR	Surface Plasmon Resonance
TEM	Transmission electron microscopy
UV	Ultraviolet light
UV-Vis	Ultraviolet-Visible
UWC	University of the Western Cape
v as	Anti-symmetric vibration
v s	Symmetric vibration
VMA	Vanillylmandelic acid
WST-1	Water Soluble Tetrazolium salt 1



Table of Contents

Magister Scientiae in Nanoscience	i
DECLARATION	ii
ACKNOWLEDGEMENTS	iii
ABSTRACT	iv
LIST OF ABBREVIATIONS	vi
LIST OF FIGURES	xii
LIST OF TABLES	xiv
CHAPTER ONE	1
INTRODUCTION	1
1.1 The nervous system.....	1
1.2 Neurons.....	1
1.3 Neuroglia	2
1.4 Tumours of the nervous system	3
1.5 Current treatment modalities for cancer	9
1.6 Functionalized metallic nanoparticles for pharmaceutical applications	9
1.7 Aim	10
1.8 Objectives	10
1.9 Significance of the study	11
CHAPTER TWO	12
LITERATURE REVIEW	12
2.1 Nanotechnology	12
2.2 Nanomaterials	13
2.3 Metallic nanoparticles.....	14
2.4 Characterization methods for metallic nanoparticles	17
2.5 Applications of metallic nanoparticles in cancer research.....	24
2.6 Research problem statement.....	27
CHAPTER THREE	28
MATERIALS AND METHODS	28
3.1 Materials	28
3.2. Synthesis and functionalization of metallic nanoparticles.....	29
3.3 Physicochemical Characterization	32
3.4 <i>In vitro</i> Colloidal Stability Studies	35
3.5 Cell culture.....	35
3.6 Cell viability assay	37
3.7 Observation of morphological changes	38
3.8 Measurement of intracellular reactive oxygen species	38
3.9 Flow cytometric measurement of mitochondrial membrane potential	39
3.10 Quantitative evaluation of cellular uptake of PEGylated nanoparticles	40
3.11 Statistical analysis	40
CHAPTER FOUR	41

RESULTS OF THE PHYSIOCHEMICAL CHARACTERIZATION OF NANOPARTICLES	41
4.1 Ultraviolet-visible spectroscopy study	41
4.2 Dynamic Light Scattering	43
4.3 High Resolution Transmission Electron Microscopy and Energy Dispersive X-ray Spectroscopy analysis.....	45
4.4 Fourier Transform Infrared Spectroscopy study	52
CHAPTER FIVE	56
RESULTS OF THE IN VITRO BIOLOGICAL STUDIES	56
5.1 <i>In vitro</i> stability study	56
5.2 <i>In vitro</i> Cytotoxicity assessment	59
5.3 Morphological changes	67
5.4 Oxidative stress assessment	69
5.5 Mitochondrial membrane potential	71
5.6 Quantification of the cellular uptake	73
CHAPTER SIX	76
DISCUSSION	76
6.1 Physiochemical properties of nanoparticles	77
6.2 <i>In vitro</i> colloidal stability	86
6.3 Cytotoxicity and quantification of cellular uptake studies	88
6.4 Assessment of Cyto-Morphological changes	91
6.5 Assessment of Oxidative stress	92
6.6 Assessment of mitochondrial membrane potential (MMP)	93
6.7 Conclusion	94
6.8 Limitations	95
6.9 Future recommendations	95
REFERENCES	97

LIST OF FIGURES

Figure 1. 1 Types of glial cells with their functions	2
Figure 1. 2 Morphology of U87 cells	6
Figure 1. 3 Morphology of SH SY5Y cells.....	9
Figure 2. 1 Types of nanoparticles.....	14
Figure 2. 2 Illustration of the top-down and bottom-up approach.....	15
Figure 2. 3 Structure of citrate.....	17
Figure 2. 4 The Stokes-Einstein Equation.....	20
Figure 2. 5 Typical infrared correlation spectra.....	22
Figure 2. 6 Bimetallic structures: (a) cluster in cluster, (b) core-shelled and (c) alloyed.....	26
Figure 4. 1 UV-Vis Absorption spectra of (A) Citrate-capped AuNPs (red) and PEG AuNPs (dark blue). (B) Citrate-capped AuPtNPs (light blue) and PEG AuPtNPs (orange).....	42
Figure 4. 2 TEM images of citrate-capped gold nanoparticles at high (left) and low (right) magnification. The bars for the high magnification are indicated 5 nm and for the low magnification 50 nm.....	46
Figure 4. 3 TEM images of citrate-capped gold-platinum nanoparticles at high (left) and low (right) magnification. The bars for the high magnification are indicated 5 nm and for the low magnification 50 nm.....	46
Figure 4. 4 TEM images of PEGylated gold nanoparticles at high (left) and low (right) magnification. The bars for the high magnification are indicated 5 nm and for the low magnification 50 nm.....	47
Figure 4. 5 TEM images of PEGylated gold-platinum nanoparticles at high (left) and low (right) magnification. The bars for the high magnification are indicated 5 nm and for the low magnification 50 nm.....	48
Figure 4. 6 EDS elemental composition of citrate-capped gold nanoparticles.....	49
Figure 4. 7 EDS elemental composition of citrate-capped gold-platinum nanoparticles.....	50
Figure 4. 8 EDS elemental composition of PEGylated gold nanoparticles.....	51
Figure 4. 9 EDS elemental composition of PEGylated gold-platinum nanoparticles.....	52
Figure 4. 10 FTIR spectra of citrate-capped gold-platinum nanoparticles (purple), citrate-capped gold nanoparticles (green), PEGylated gold-platinum nanoparticles (blue) and PEGylated gold nanoparticles (maroon).....	53
Figure 5. 1 UV-Vis absorption spectra of citrate-capped gold nanoparticles showing <i>in vitro</i> stability of the nanoparticles in different solutions.....	56
Figure 5. 2 UV-Vis absorption spectra of PEGylated gold nanoparticles showing <i>in vitro</i> stability of the nanoparticles in different solutions.....	57
Figure 5. 3 UV-Vis absorption spectra of citrate-capped gold-platinum nanoparticles showing <i>in vitro</i> stability of the nanoparticles in different solutions.....	58
Figure 5. 4 UV-Vis absorption spectra of PEGylated gold-platinum nanoparticles showing <i>in vitro</i> stability of the nanoparticles in different solutions.....	58

Figure 5. 5 Effects of citrate-capped gold nanoparticles on the viability of SH SY5Y (A and C) and U87 (B and D) cell lines.....	60
Figure 5. 6 Citrate-capped gold-platinum nanoparticles effect on the viability of SH SY5Y (A and C) and U87 (B and D) cell lines evaluated using WST-1 assay after exposure for 24 hours (A and B) and 48 hours (C and D).....	62
Figure 5. 7 PEGylated gold nanoparticles effect on the viability of SH SY5Y (A and C) and U87 (B and D) cell lines evaluated using WST-1 assay after exposure for 24 hours (A and B) and 48 hours (C and D).....	64
Figure 5. 8 PEGylated gold-platinum nanoparticles effect on the viability of SH SY5Y (A and C) and U87 (B and D) cell lines evaluated using WST-1 assay after exposure for 24 hours (A and B) and 48 hours (C and D).	65
Figure 5. 9 Morphology of control, PEGylated gold nanoparticles and PEGylated gold-platinum nanoparticles treated SH SY5Y cells.....	68
Figure 5. 10 Morphology of control, PEGylated gold nanoparticles and PEGylated gold-platinum nanoparticles treated U87 cells	69
Figure 5. 11 Flow cytometric analyses of intracellular ROS using DCF staining on U87 cells.....	70
Figure 5. 12 Flow cytometric analyses of intracellular ROS using DCF staining on SH SY5Y cells.....	71
Figure 5. 13 The mitochondrial membrane potential was quantitated by a flow cytometric analysis with rhodamine123.....	72
Figure 5. 14 The mitochondrial membrane potential was quantitated by a flow cytometric analysis with rhodamine123.....	73
Figure 5. 15 Cellular uptake of the IC ₅₀ PEGylated gold nanoparticles concentration by U87 and SH SY5Y cells.....	74
Figure 5. 16 Cellular uptake of the IC ₅₀ PEGylated gold-platinum nanoparticles concentration by U87 and SH SY5Y cells;.....	75

LIST OF TABLES

Table 4.1 Hydrodynamic size, polydispersity index (PDI) and zeta potential of various NPs. Data are provided as mean \pm S.D. (n = 6).	43
Table 4.2 Core size of various NPs. Data are provided as mean \pm S.D. (n = 10).....	45
Table 4.3 Summary of the effects of PEGylated gold and gold-platinum NPs.....	55
Table 5.1 IC ₅₀ values of SH SY5Y and U87 cells treated with PEGylated gold nanoparticles and PEGylated gold-platinum nanoparticles for 24 and 48 hours respectively. The IC ₅₀ values were obtained from Graph pad Prism 8 statistical software.....	66



CHAPTER ONE

INTRODUCTION

1.1 THE NERVOUS SYSTEM

The nervous system (NS) is a major system in the body that plays a role in maintaining homeostasis (McEwen, 2016). Its main function is to detect and collect sensory input from the internal and external environment, to process and interpret this sensory input and respond to it (Butler, 2000). There are two classes of cells in the nervous system, namely neurons and neuroglia cells (Tai, 2012) and both these cell classes work in harmony to execute the functions of the NS.

1.2 NEURONS

A neuron is the basic unit of the nervous system. It has three major parts, namely the cell body (soma), dendrites (short branching projections) and an axon (elongated projection) with the dendrites and axons usually referred to as nerve fibers (Kristan, 2016). Most axons may branch out, forming collateral axons called telodendria and each telodendron has axon terminals (synaptic bouton, or terminal bouton) which are involved in synapses (Maple, 2005). Dendrites receive stimuli from receptors or other neurons and bring electrical impulses to the cell body, whereas axons conduct electrical impulses away from the cell body towards the axon terminals (Lodish *et al.*, 2000).

Neurons could be functionally classified according to the direction in which they transmit electrical impulses. Sensory (afferent) neurons carry information to the central nervous system (CNS) while motor (efferent) neurons conduct signals away from the

CNS. Interneurons on the other hand conduct impulses from sensory to motor neurons (Lovinger, 2008).

1.3 NEUROGLIA

Neuroglia, also known as glial cells, are specialized non-neuronal connective tissue cells found in the nervous system (Vasile *et al.*, 2017). These cells maintain homeostasis, form myelin, and provide support and protection for neurons (**Figure 1.1**).

In the CNS, glial cells include oligodendrocytes, astrocytes, ependymal cells, and microglia whereas in the peripheral nervous system (PNS), they include Schwann cells and satellite cells (Butt and Verkhratsky, 2018).

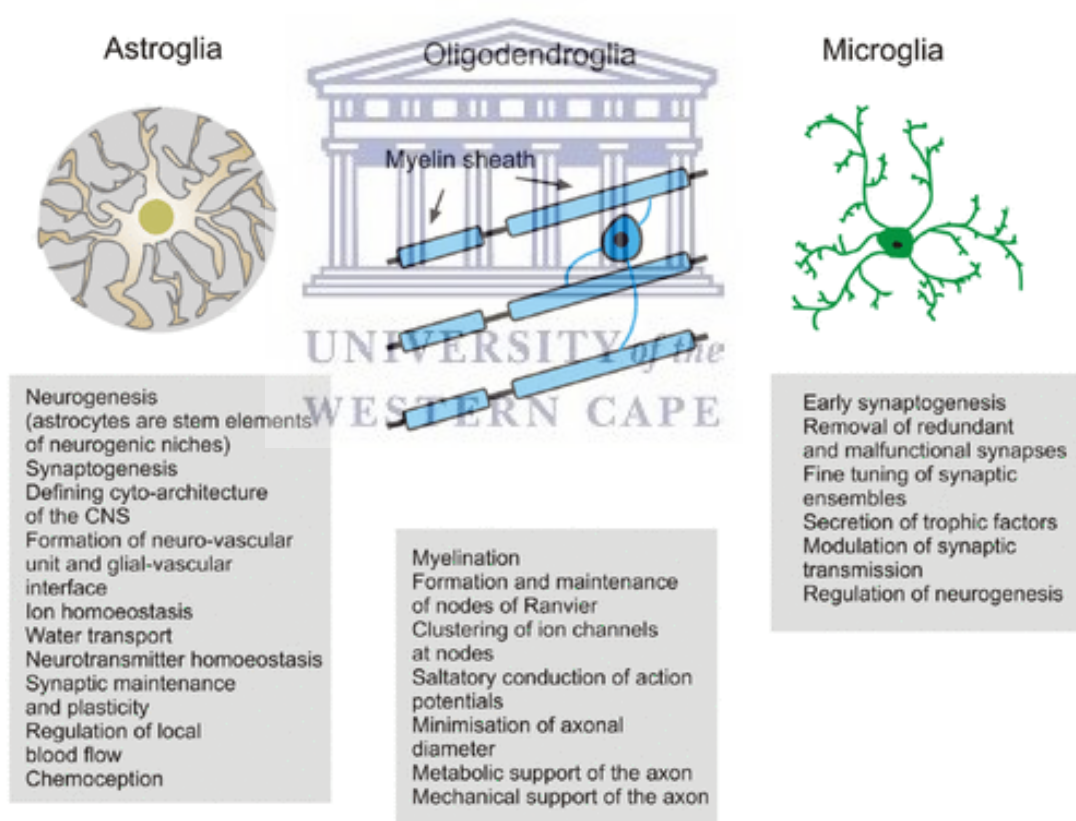


Figure 1. 1 Types of glial cells with their functions (Butt and Verkhratsky, 2018).

1.3.1 Astrocytes

Astrocytes are the most abundant glial cells in the CNS. They are star-shaped; their many processes anchor neurons to their blood supply while forming the blood-brain barrier. They thus assist in the transportation of nutrients and waste to and from the neurons (Genzen *et al.*, 2009).

1.3.2 Oligodendrocytes

Oligodendrocytes are large cells with slender extensions. These cells coat axons in the CNS with their cell membrane, forming a specialized membrane differentiation called myelin, producing the myelin sheath (Baba and Cătoi, 2007). The myelin sheath provides protection and insulation to the axon that allows electrical signals to propagate more efficiently. Schwann cells perform a similar function but in the PNS.

1.3.3 Ependymal cells

Ependymal cells line the fluid-filled cavities of CNS. They are ciliated simple cuboidal epithelial cells. Their function is to produce, transport and circulate the cerebrospinal fluid (CSF) with the help of the cilia and villi on their surface (Gladson *et al.*, 2010).

1.4 TUMOURS OF THE NERVOUS SYSTEM

Cancer can simply be defined as a collection of genetic diseases that result from an uncontrollable cell division. In general, all cells that have the ability to undergo cell division can be cancerous (Cooper, 2000). When this abnormal cell division occurs in solid tissues, a mass called a tumour appears. There are two types of tumours, namely the benign and malignant tumours. Malignant tumours have the potential to invade and destroy other parts of the body, through the circulatory and lymphatic system (Wittekind and Neid, 2005).

The nervous system is a very important system in the human body and when it is compromised, the consequences can be severe, even life threatening. Tumours of the nervous system can cause specific regions of the body to function abnormally, depending on the type and location of the tumour (Colon and Chung, 2011). Glioblastoma Multiforme (GBM) and neuroblastoma (NB) are some of the most common malignant tumours of the nervous system.

1.4.1 Glioblastoma multiforme (GBM)

GBM (high-grade or undifferentiated astrocytoma) are aggressive malignant tumours that have rapid, infiltrative, destructive growth. They are located in the cerebrum of the brain and comprise of cancerous glial cells (astrocytes) (Hanif *et al.*, 2017).

1.4.1.1 Epidemiology

GBM are the most common primary malignant brain tumours and the second most common CNS tumours after meningioma (Philips *et al.*, 2018). The incidence of GBM is generally higher in developed European countries with a peak incidence at 45-70 years (mean age is 53 years old), with Caucasian male adults more frequently affected. It has an incidence of 23 per 100 000 persons (Xu *et al.*, 2017). It has lower incidence in Africans and Asians (Tamimi and Juweid, 2017). However, the life expectancy of people diagnosed with GBM is short, with a mean survival of 15 months (Kriel *et al.*, 2018).

1.4.1.2 Signs and symptoms

GBM does not metastasize to outside of the brain and are commonly found on the cerebral hemispheres of an adult brain (Mughal *et al.*, 2018). They are very aggressive with symptoms depending on the location of the tumour as well as tumour vasculature.

The integrity of the blood-brain barrier (BBB) can be compromised due to the highly disorganized and permeable tumour blood vessels (Dubois *et al.*, 2014). The impairment of the BBB results in brain inflammation and edema, which often causes symptoms, such as increased intracranial pressure and hemorrhage, pain, headache, focal neurological deficits, confusion, cognitive disturbances, seizures, and incontinence, as well as the level of consciousness. In most cases, this disease can be life-threatening (Sizoo *et al.*, 2010).

1.4.1.3 Diagnosis

In general, the first diagnostic technique used is neurological examination, which includes investigation by a physician of such signs and symptoms as a patient's vision, hearing, balance, coordination, muscle strength and reflexes (Lee *et al.*, 2018). Problems in one or more of these signs/symptoms may provide information about the part of the brain that could be affected by the tumour. Once the tumour is suspected, microscopic and imaging tests may be used to explore possible abnormalities in the brain.

Imaging tests can help determine the location and size of the brain tumour (Smith and Ironside, 2007); Magnetic Resonance imaging (MRI) and Computerized tomography (CT) are often used. MRI and CT scan images of the brain are often detailed and allow the detection of tumours (Davis, 2016) and in MRI; a contrast dye is used to distinguish a tumour from normal brain tissue. Thus, MRI provides the best images of GBM (Shukla *et al.*, 2017).

A surgical biopsy can be done with a needle by removing a sample of suspicious tissue for analysis in a laboratory to determine the types of cells and their level of aggressiveness (Almenawer *et al.*, 2015). Microscopic techniques usually show a

variety of characteristics are detected such as high cellularity: small, round or oval cells; undifferentiated cells, nuclei with variable shapes, scanty and poorly outlined cytoplasm; mitotic bodies, marked pleomorphism, multi-nucleation in cells (Gladson *et al.*, 2010). One of the commonly used GBM cell lines in brain cancer research is the U87 cell line (**Figure 1.2.**)

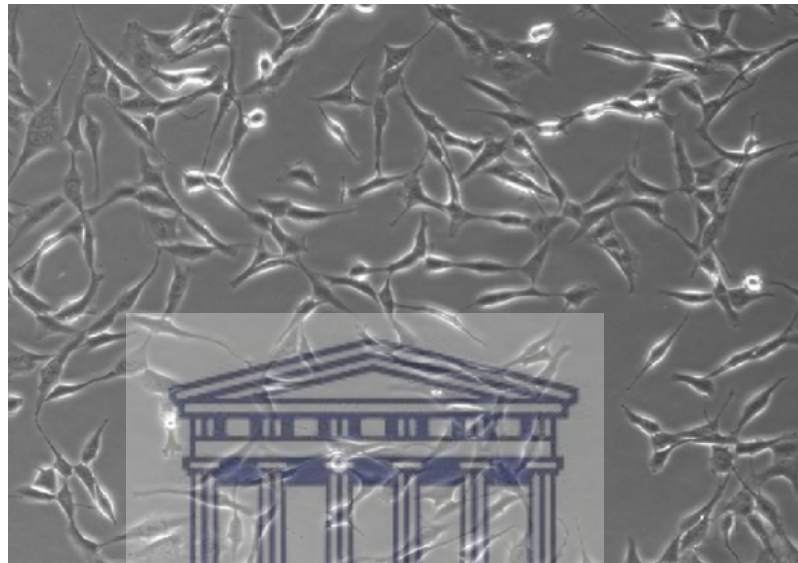


Figure 1. 2 Morphology of U87 cells (Zablocka *et al.*, 2015).

1.4.2 Neuroblastoma (NB)

NBs are malignant tumours of ganglion cell origin that derive from neural crest cells. They are located in the sympathetic component of the PNS (Tosun *et al.*, 2017). NBs arise from the adrenal glands and can spread and develop in the spinal cord, the neck (thymus gland), the abdominal (adrenal medulla, retroperitoneal space, kidneys and stomach) and thoracic region (lungs and mediastinum) (Park and Bagatell, 2016). Microscopically, the NB tumour has small, round lymphocyte-like cells, with hyperchromatic nuclei and scant cytoplasm. There is also a presence of rosette and pseudorosette structures (Colon and Chung, 2011).

1.4.2.1 Epidemiology

NB is another life-threatening nervous system cancer known globally, to be most common in childhood. In children, it is the most common solid tumour, the second most common abdominal neoplasm and the third most common cancer overall, after leukemia and CNS cancers (Berthold *et al.*, 2017).

The prevalence rate of NB is 10.5/million children under the age of 15 years, slightly more common in young boys, with no racial profiling and the median age at presentation is 22 months. About 15% of all cancer deaths in children are due to NB (Mullassery and Losty, 2016).

1.4.2.2 Signs and symptoms

Symptoms are caused by pressure from the tumour in their respective locations (Ishola and Chung, 2007). Early signs can develop slowly and be similar to symptoms of other common childhood illnesses. The first symptoms are often vague and may include irritability, being very tired, loss of appetite, and fever. In the abdomen, a tumour may cause a swollen belly and constipation and in the chest, a tumour may cause breathing problems. A tumour pressing on the spinal cord may cause weakness, thus an inability to stand, crawl, or walk. While a tumour in the area around the eyes or orbits may cause distinct bruising and swelling (Alvi *et al.*, 2017).

1.4.2.3 Diagnosis

The medical history and a physical exam are initially assessed and the physician will observe any abnormal mass or swelling in the body as well as examine signs and symptoms. If the history and examination suggest that the patient might have NB, more tests will be performed (Rich and La Quaglia, 2012). CT scan is the most common

imaging test, and the most common regions imaged as the gold standard include the neck, chest, and/or abdomen, as the solid mass is easier to define than in MRI (Dumba *et al.*, 2015). Ultrasound can also be used to characterize the tumour mass (Kembhavi *et al.*, 2015). In addition, meta-iodobenzylguanidine (mIBG) scan is often used once the patient is diagnosed with NB and this helps in determining the size and spread of the NB (Brisse *et al.*, 2011).

In most cases, NB diagnostic findings will include elevated levels of urine or blood catecholamines or their metabolites (Smith *et al.*, 2010), mainly because sympathetic nerve cells release such catecholamine as epinephrine, norepinephrine and dopamine which enter the bloodstream and eventually break down into metabolites, notably homovanillic acid (HVA), and vanillylmandelic acid (VMA). There are also increased levels of nonspecific biomarkers such as lactate dehydrogenase, ferritin, and neuron-specific enolase (Verly *et al.*, 2017).

Neuroblastoma cell lines are heterogeneous and there are three distinct cellular phenotypes that are frequently present in human neuroblastoma cell lines. These are neuroblastic N-type cells, substrate-adherent S-type cells and intermediate I-type cells (Bell *et al.*, 2013). The neuroblastic N-type cells are the most common and grow as poorly attached aggregates of small, rounded cells with short neuritic processes. S-type cells resemble non-neuronal precursor cells and attach strongly to the substrate and show contact inhibition of cell growth (Walton *et al.*, 2004). One of the most common neuroblastoma cell lines is the SH SY5Y cell line (**Figure 1.3**).

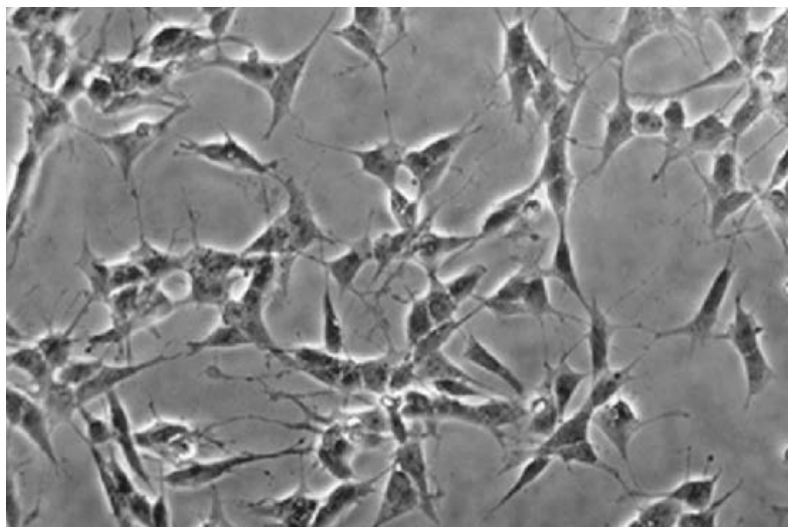


Figure 1. 3 Morphology of SH SY5Y cells (Kovalevich *et al.*, 2013).

1.5 CURRENT TREATMENT MODALITIES FOR CANCER

Most cancers can be treated by surgery, chemotherapy, radiation therapy and hormonal therapy. The choice of therapy depends upon the location and grade of the tumour and the stage of the disease, as well as the general state of the patient (Pal and Hurria, 2012). These conventional therapies may improve the quality of life and overall survival of patients but have several limitations: tumour cells may become resistant to conventional therapies, nearby tissues are susceptible to damage, especially in nervous tissue which has very limited capacity to repair itself. In addition, many drugs cannot cross the BBB to act on the tumour (Zimmermann *et al.*, 2014).

1.6 FUNCTIONALIZED METALLIC NANOPARTICLES FOR PHARMACEUTICAL APPLICATIONS

Metallic nanoparticles have been suggested to possess the properties required to overcome the limitations related to conventional therapy for NB and GBM. These nanoparticles play a powerful role in cancer therapy and can provide better targeting, cancer detection and drug delivery options (Sharma *et al.*, 2018). Metallic nanoparticles can be functionalized with targeting polymers to improve the efficiency of drug and

gene delivery to the target cells and tissues. Surface functionalization of the metallic nanoparticles with polyethylene glycol (PEG) is a commonly used approach and it shields the surface of nanoparticles from aggregation and opsonization (Laudon *et al.*, 2011).

1.7 AIM

The aim of the study was to synthesize functionalized metallic nanoparticles and evaluate their potential cytotoxic properties on U87 and SH SY5Y cell lines.

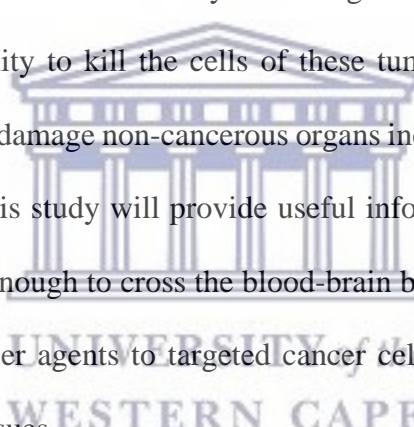
1.8 OBJECTIVES

- To chemically synthesize citrate-capped metallic nanoparticles
- To functionalize the synthesized citrate-capped nanoparticles with PEG and:
 - evaluate the optical properties of the nanoparticles
 - determine the core size of the nanoparticles
 - determine the size distribution of the nanoparticles
 - determine the hydrodynamic size of the nanoparticles
 - evaluate the chemical composition of the nanoparticles
 - evaluate the functional groups and bonds on the surface of the nanoparticles
- To characterize the physiochemical properties of the citrate-capped and PEGylated nanoparticles.
- To evaluate the *in vitro* stability of the citrate-capped and PEGylated nanoparticles on biological solvents.
- To determine the cytotoxicity of the citrate-capped and PEGylated nanoparticles on U87 and SH SY5Y cell lines

- To investigate the effects of the PEGylated nanoparticles on cell morphology.
- To quantify the cellular uptake of PEGylated nanoparticles using ICP-MS
- To monitor and quantify the intracellular Reactive Oxygen Species (ROS) generated by the cells.
- To measure the effects of the PEGylated nanoparticles on mitochondrial membrane potential of the cells.

1.9 SIGNIFICANCE OF THE STUDY

Both GBM and NB are malignant tumours, with the former mostly occurring in Caucasian males, and the latter mostly occurring in young children. Conventional therapies have the ability to kill the cells of these tumours but in the process, such treatment agents could damage non-cancerous organs including the brain. It is expected that the results from this study will provide useful information on the use of metallic NPs, which are small enough to cross the blood-brain barrier, can be functionalized to deliver potent anticancer agents to targeted cancer cells and cause minimal harm to surrounding normal tissues.



CHAPTER TWO

LITERATURE REVIEW

2.1 NANOTECHNOLOGY

Nanotechnology can be defined as a field of scientific research and innovation that deals with the manipulation of matter at the atomic level in order to develop, characterize, produce and apply structures, devices and systems (Whatmore, 2006). It is the application of nanoscience in different scientific disciplines (Biology, Chemistry, Physics and Material sciences) for the manipulation of materials at the nanoscale (1-100 nm) (Dowling, 2004).

Nanotechnology has been used since the 10th century, where gold nanoparticles were used as colour pigments in stained glasses (Dowling, 2004). However, the development of modern nanotechnology which has produced many scientific innovations started in the last century, with Richard Feynman considered the father of modern nanotechnology, mostly because he gave the first lecture on nanotechnology in 1959. In his lecture titled '*There's Plenty of Room at the Bottom*', he explained the possibility of synthesizing materials via direct manipulation of atoms. Modern science started to explore nanotechnology shortly thereafter (Pitkethly, 2008).

Quantum dots were discovered in the early 1980's (Ornes, 2016) and have been described as nanoscaled semi-conductor particles with unique optical and electrical properties that function as both size and shape. They are used in transistors and solar cells (Pawar *et al.*, 2018).

In the late 1980's and early 1990's, nanotechnology mostly involved the use of carbon-derived structures, mainly buckminsterfullerene (C_{60}) and carbon nanotubes (CNT) (Goodarzi *et al.*, 2017). C_{60} particles are soccer ball-like structures used in lubricants, while CNT are tube-like structures used in radio antennas (Schnorr and Swager, 2011). In the 21st century, research in nanotechnology advanced dramatically and has become the foundation for most applications that impact daily human life (Hulla *et al.*, 2015). The National Nanotechnology Initiative (NNI) was launched in the United States (US), mainly to pursue the novel and economic applications anticipated for nanotechnology (Roco, 2011).

The South African Department of Science and Technology (DST), which ensures that the country remains competitive in the fast-developing field of nanotechnology, coordinates its development. There are two National Nanotechnology Innovation Centres committed to the advancement of nanotechnology namely, the Council for Scientific and Industrial Research (CSIR) and MINTEK (Saidi and Douglas, 2017). Research into the diverse applications of nanotechnology is ongoing in universities and research centers all over South Africa.

2.2 NANOMATERIALS

Particles that have at least one external dimension in the nanoscale, which is between 1 and 100 nanometers in diameter, are considered nanomaterials. These can be classified based on the number of dimensions that are not confined to the nanoscale range (Spear *et al.*, 2015). Two-dimensional (2D) nanomaterials have two of their dimensions not confined to the nanoscale and have one in the nanoscale, and exhibit plate-like shapes; examples include nanofilms, nanolayers, and nano coatings (Huang and Gao, 2018). One-dimensional (1D) nanomaterials are outside the nanoscale and have two external

dimensions in the nanoscale, which leads to needle-like-shaped nanomaterials such as nanotubes, nanorods, and nanowires (Khan, 2013). Zero-dimensional (0D) materials have all the dimensions measured within the nanoscale and their electrons are fully confined and delocalized (no freedom of movement). The most common representation of zero-dimensional nanomaterials are nanoparticles (Foss and Rahman, 2016). There are different types of nanoparticles with different shapes and surface chemistry (**Figure 2.1**).

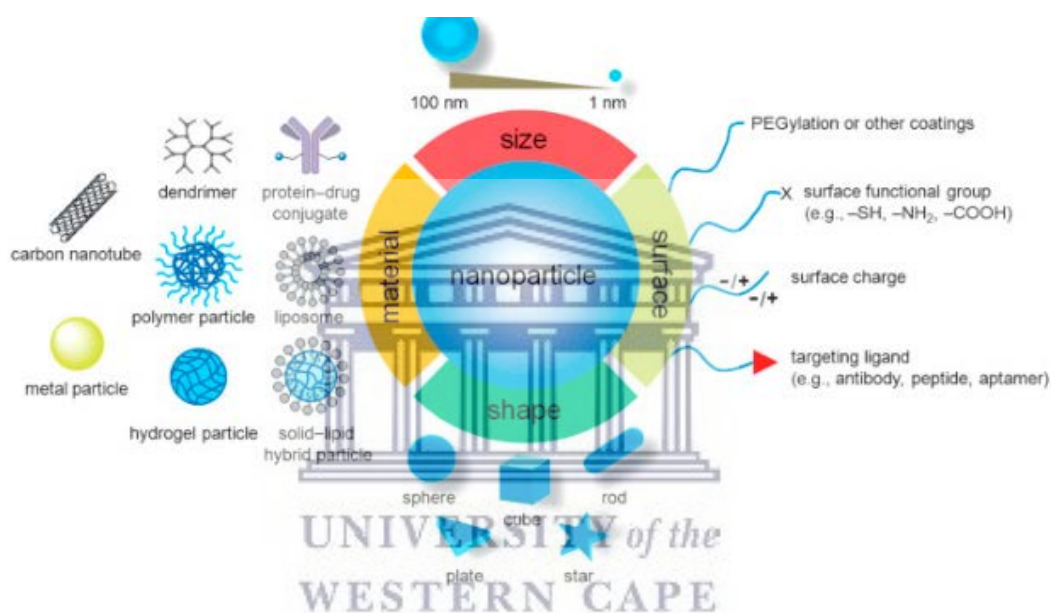


Figure 2. 1 Types of nanoparticles (Heinz *et al.*, 2017).

2.3 METALLIC NANOPARTICLES

Metallic nanoparticles are zero-dimensional nanomaterials that are made up of metals. They have different properties compared to having the same metals in the bulk state (Dahman and Dahman, 2017). These unique properties are due to their quantum confinement, large surface-to-volume ratio (SVR), surface plasmon excitation and large surface energies. The large SVR is one of the main factors that enhances the reactivity, strength and electrical properties of nanomaterials (Elhissi, 2013).

2.3.1 Synthesis of metallic nanoparticles

There are two approaches used to synthesize and control the size and shape of metallic nanoparticles; these are the bottom-up approach and the top-down approach (**Figure 2.2**). The top-down approach reduces larger molecules until they reach the level of nanoscale units. This approach is mostly used in the microelectronics industry and has four processes, namely lithography, etching, deposition and doping (Ahmed *et al.*, 2015). The most common example of a top-down approach is the lithographic patterning technique that uses short wavelength optical source. This approach is a cheaper, well-developed technique, which is dominant when doing fabrication in the micro scale (Gritsch *et al.*, 2017). However, it is limited in nanofabrication and chances of contamination are quite high (Sharma *et al.*, 2019).

In the bottom-up approach, the nanoparticles are synthesized by building them up from atomic and molecular scale components (Fichtner, 2009) and this approach is often preferred because nanomaterials with less defects and a narrow size distribution can be synthesized (Roopan and Elango, 2016).

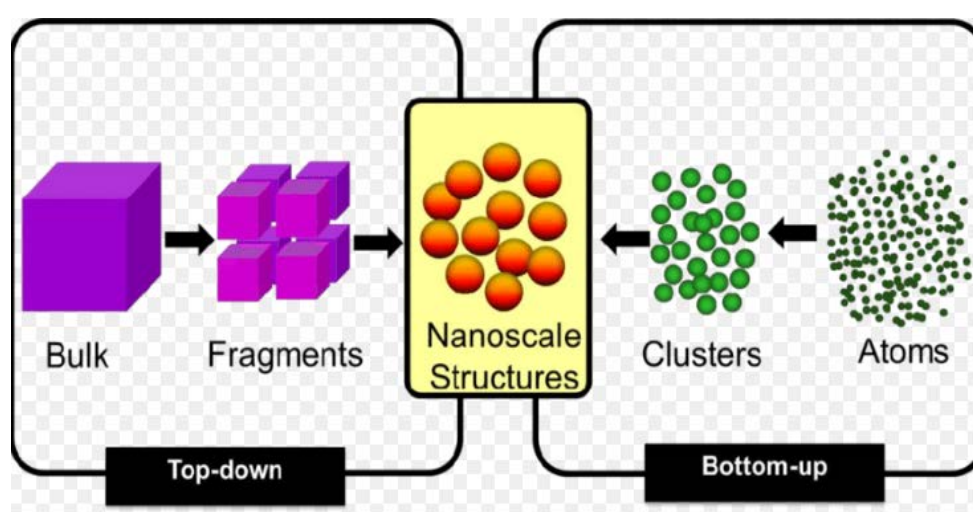


Figure 2. 2 Illustration of the top-down and bottom-up approach (Rawat, 2015).

One of the most common methods of synthesizing nanoparticles in the bottom-up approach is the chemical method (wet chemical).

2.3.1.1 Chemical synthesis method

The chemical synthesis method is a simple and inexpensive technique that has the ability to produce nanoparticles with a variety of shapes and sizes (Paszkievicz *et al.*, 2015). Chemical synthesis of metallic nanoparticles often begins with the nucleation process, followed by the crystallization process. In the nucleation process, metallic ions are reduced into zero valent metallic atoms (nuclei) by reducing agents, through the donation of electrons to the metal ions. The most commonly used reducing reagents are sodium borohydride, sodium citrate and hydrazine, with sodium borohydride being the strong reducing agent (Liu *et al.*, 2012). Once the metallic ions are reduced to metallic nuclei, they start to cluster in the solvent.

The second step is the crystallization process in which crystal growth of the clusters occurs through the arrangement of atoms in a defined and periodic manner that defines the crystal structure. The growth of smaller crystals to larger crystals is thermodynamically favoured due to the decrease in the specific surface energy during crystal growth (Rezaei *et al.*, 2012). The growth of crystals must be prevented by a suitable capping agent, which plays the role of covering the surface of the nanoparticles to prevent them from overgrowing and aggregating. This is achieved by reducing reactivity at the outside of the particle (Li *et al.*, 2013). Thus, nanoparticles are normally synthesized at room temperature because capping agents are fragile to heat. The most common capping agents are sodium citrate and tannic acid (Beyer, 2012).

Sodium citrate acts as both capping and reducing agent, and is the most commonly used capping agent due to its high degree of electrostatic stabilization (Oliveira *et al.*, 2017). Citrate is a tri-carboxylic acid tri-anion and is thus negatively charged, as shown in **Figure 2.3**. Adsorption of citrate ions (electrolytes) to the surface creates an electrical double layer, which results in a Coulombic repulsion force between individual particles with a highly negative zeta potential at pH 7. These repulsive forces can exceed the van der Waals attraction forces between the nanoparticles, thus preventing aggregation (Chowdhury *et al.*, 2016).



Figure 2. 3 Structure of citrate (Perera *et al.*, 2015).

2.4 CHARACTERIZATION METHODS FOR METALLIC NANOPARTICLES

Metallic nanoparticles have unique physical and chemical (physiochemical) properties. Physical properties include size, size distribution, shape, aggregation state, structure (crystallinity) and solubility. Chemical properties include molecular structure, chemical composition, surface chemistry (composition and charge) and hydrophilicity. These properties on the synthesized metallic nanoparticles can be analysed by using different characterization methods, which could be either microscopic or spectroscopic methods (Oliveira *et al.*, 2017).

2.4.1 Microscopic characterization using electron microscopy

Electron microscopes use electron beams to produce detailed images. They work in a similar technique to optical microscopes, except they use electron beams to probe materials instead of light. Electrons have a much shorter wavelength compared to light and thus can interact with nanoparticles (Brinsko *et al.*, 2011), yielding much greater resolution than the light microscopes. Electron microscopic techniques include the transmission electron microscopy (TEM) and scanning electron microscopy (SEM).

The morphology, particle size and particle size distribution are the most basic set of information that can be collected and analysed using the TEM technique, which is based on electron transmission. Electrons are transmitted through a thin section sample, and are used to create an image of the sample on a fluorescent screen. Some electrons scatter when they pass through this thin section sample. In the regions that are less dense in the sample, less electrons are scatter and more are transmitted, thus an image formed in brighter. Denser regions scatter more electrons and appear darker (Diallo *et al.*, 2015).

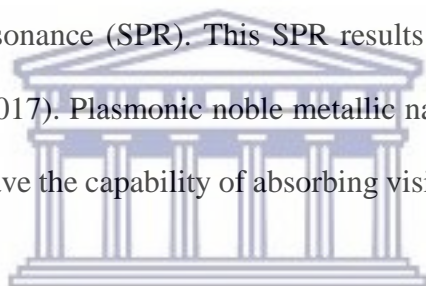
A TEM study by Diallo *et al.*, (2015) showed that Co_3O_4 nanoparticles were non-agglomerated quasi-spherical shape with an average diameter range of 2-7 nm.

2.4.2 Spectroscopic characterization

Spectroscopy is the study of the interaction between electromagnetic radiation energy and matter. Electromagnetic radiation is energy that is generated as both electrical and magnetic waves travel in packets of energy called photons (Bell *et al.*, 2013). Electromagnetic radiation includes light (ultraviolet, visible and infrared), microwaves, radio waves, gamma rays and X-rays. When these are absorbed in the medium through which they pass, they give up their energy to produce electrons (Cox *et al.*, 2010).

2.4.2.1 Ultraviolet-visible absorption spectroscopy

Nanoparticles have unique optical properties that are sensitive to the size, shape and agglomeration state, which makes the ultraviolet-visible (UV-Vis) spectroscopy a valuable tool for identifying and characterizing Metallic nanoparticles. UV-Vis spectroscopy, refers to the absorption spectroscopy in the ultraviolet and visible region (Nilapwar *et al.*, 2011). When white light (from deuterium and tungsten lamp) is irradiated, it enters the monochromator, which narrows down the wavelength band of the radiation. When the incident light interacts with the metallic nanoparticles, the free electrons in the conduction band on the metal surface are driven by the alternating electric field to collectively oscillate in phase with the incident light, which is known as surface plasmon resonance (SPR). This SPR results in a strong absorption signal (Mäntele and Deniz, 2017). Plasmon noble metallic nanoparticles (gold, copper and silver nanoparticles) have the capability of absorbing visible light via SPR (Nadagouda and Varma, 2008).



UNIVERSITY of the
WESTERN CAPE

The transmitted light (light not absorbed) enters the detector where its intensity is measured. The SPR property of metallic nanoparticles is determined by several factors, such as the size, shape, and geometry of the plasmonic nanoparticles, the dielectric properties of the surrounding medium, and the inter-particle coupling interactions (Behzadi *et al.*, 2015).

2.4.2.2 Dynamic Light scattering

Dynamic light scattering (DLS) or Photon correlation spectroscopy is an important tool in assessing hydrodynamic size and particle size distribution. Nanoparticles dispersed in solvents have a random (Brownian) motion. This Brownian motion is due to the nanoparticles colliding with the particles of the solvent, causing a certain amount of

energy to be transferred, which in turn causes movement (Hackley and Clogston, 2011). When a laser light is illuminated to a sample, it interacts with the nanoparticles and gets scattered in all directions on the surface of the nanoparticles. The scattered light from all the nanoparticles in the sample is added together to create a changing destructive or constructive interference. This leads to fluctuation in the intensity of the scattered light which is detected at a certain angle over time and this signal is used to determine the diffusion coefficient (velocity) and the particle size (hydrodynamic radius) using the Stokes-Einstein equation (**Figure 2.4**). The Boltzmann constant (K) is $1.38064852 \times 10^{-23} \text{ m}^2 \text{ kg s}^{-2} \text{ K}^{-1}$.

Stokes-Einstein Equation

$$d_H = \frac{kT}{3\pi\eta D}$$

d_H = hydrodynamic diameter (m)
 k = Boltzmann constant (J/K=kg·m²/s²·K)
 T = temperature (K)
 η = solvent viscosity (kg/m·s)
 D = diffusion coefficient (m²/s)

Figure 2.4 The Stokes-Einstein Equation (Rangamani and Iyengar, 2007).

In some literature, the zeta potential measurements fall under DLS and this will apply in the present study. The electrical potential on the surface of the nanoparticles is generally analysed with a Malvern ZetaSizer Nano ZS, which is also utilized for size measurements. The magnitude of the zeta potential indicates the degree of electrostatic repulsion between adjacent, similarly charged particles in a dispersion (Clogston and Patri, 2011). The zeta potential could therefore indicate the stability of colloidal dispersions.

Zeta potential measurements are performed by applying an electric field across the sample, allowing the particles to move toward the electrode of opposite charge with a velocity proportional to the magnitude of the zeta potential. The sample is irradiated with Helium-neon (He-Ne) laser light, which interacts with the nanoparticles, causing some scattering. The scattered light at an angle is measured and the particle velocity is determined from the frequency shift. Electrophoretic Mobility is then readily obtained as the ratio of velocity to electric field strength (Bhattacharjee, 2016). Zeta potential is directly proportional to the electrophoretic mobility and it can be determined by substituting the electrophoretic mobility in a Smoluchowski model (Kaszuba *et al.*, 2010).

2.4.2.3 Fourier-transform infrared spectroscopy

The surface chemistry of nanomaterials can be analysed with Fourier-transform infrared spectroscopy (FTIR). The infrared spectroscopy captures the vibrational motions of molecules and provides information on the nature of the bonding and the functional groups in a molecule. Atoms in molecules are continuously vibrating and the vibrational energy is quantified (Baker *et al.*, 2014). When the molecules are exposed to infrared light, they absorb the energy from the radiation at particular wavelengths causing chemical bonds present to stretch. Wavenumbers are used as units of measurement (**Figure 2.5**), since they are directly proportional to frequencies and energy, making it more convenient.

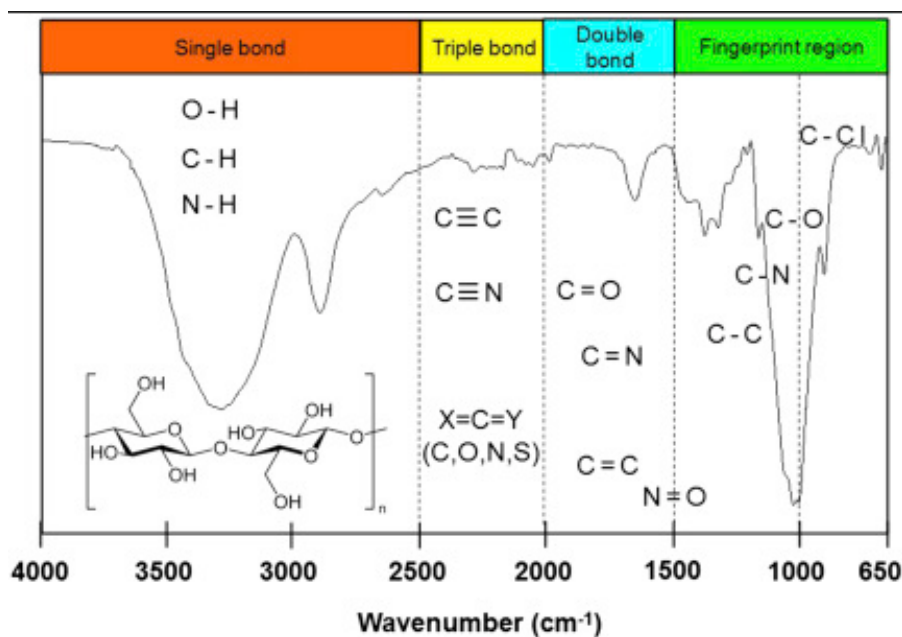


Figure 2. 5 Typical infrared correlation spectra (Mohamed *et al.*, 2017).

In one study, the presence of polyphenolic biomolecules in dried tea extract and their interaction with the surface of the gold nanoparticles was confirmed by FTIR spectra. The infrared (IR) bands observed at 3395, 1654 and 1323 cm^{-1} in the dried tea powder were characteristics of O-H, C=O and C-O stretching modes of the carboxylic acid group, respectively (Boruah *et al.*, 2012).

2.4.2.4 Energy Dispersive X-ray Spectroscopy

The Energy Dispersive X-ray Spectroscopy (EDS) is an analytical technique where an electron beam (typically in the range of 10-20 keV) is irradiated into the sample (Kumar *et al.*, 2016). This excites an electron in the inner shell and ejects it from the shell, thus creating an electron vacancy that is filled by an electron from an outer shell (Neikov *et al.*, 2019). The shells can be either K, L or M. The shell closest to the atomic nucleus is the K shell, followed outward by the L and M shells, respectively (Jensen, 2003).

The difference in energy between the outer shell and the inner shell may be released in the form of X-rays. Hence, EDS emits specific wavelengths of X-rays that are

characteristics of the atomic structure of elements and the X-ray emission at different wavelengths may then be measured by a photon-energy sensitive detector (Scimeca *et al.*, 2018). Elemental composition of the metallic nanoparticles can thus be analysed with EDS (Chandra and Kumar, 2012). Elements with low atomic number are difficult to detect with insufficient X-ray emission.

This EDS technique was used to determine the elemental composition of platinum nanoparticles. The EDS results showed platinum (Pt), carbon (C) and copper (Cu) peaks, which suggested the presence of platinum nanoparticles. The Cu and C peaks corresponded to the carbon coated copper grids that were used (Alshatwi *et al.*, 2015).

2.4.2.5 Mass Spectroscopy

Mass spectrometry is a powerful analytical technique used to quantify ions from known chemical materials. It has slightly different principles to the other spectroscopic techniques. The first step in the mass spectrometric analysis of compounds is the vaporization of the sample into gas phase (Bustos *et al.*, 2013) followed by ionization at low pressure. Ionization is when neutral atoms gain or lose electrons in order to become ions (Rockwood *et al.*, 2018). Ions are accelerated to high speeds by an electric field and pass through a perpendicular magnetic field, which bends the path of the ions depending on their mass-to-charge ratio (Stauffer *et al.*, 2008). Heavier ions are deflected less than lighter ions and ions are separated in the mass spectrometer according to their mass-to-charge ratio, and are detected in proportion to their abundance by a detector. A mass spectrum of the molecule is thus produced (Johnston *et al.*, 2006).

2.5 APPLICATIONS OF METALLIC NANOPARTICLES IN CANCER RESEARCH

The physiochemical properties of metallic nanoparticles are important for different applications. Some known biological applications include antimicrobial techniques, drug delivery, cancer therapy and general diagnostics (Wang and Wang, 2014). The most commonly used metallic nanoparticles in drug delivery and cancer therapy research include gold and platinum nanoparticles (Yamada *et al.*, 2015).

2.5.1 Gold nanoparticles (AuNPs)

Gold nanoparticles (AuNPs) are the most commonly used nanoparticles in cancer research, possibly due to their unique size- and shape-related optoelectronic properties, excellent biocompatibility, low toxicity, large surface area and high level of conductivity (Dykman and Khlebtsov, 2011). AuNPs have a size-relative SPR, due to their unique interaction with light (Mody *et al.*, 2010). As the particle size increases, the SPR shifts to longer wavelengths with a darker red/ purplish color, meaning that blue light is reflected. The color is an important indicator that gold nanoparticles have been successfully synthesized (Ismail *et al.*, 2018).

AuNPs are known to be non-toxic particles but in order to avoid agglomeration these NPs are often capped with such chemical agents as citrate, which can be toxic to cells (Guo *et al.*, 2017). Citrate-capped AuNPs can in turn be modified with other molecules such as polymers, oligonucleotides, antibodies and proteins for targeted delivery.

Polyethylene glycol (PEG) is a polar polymer with a high aqueous solubility and steric stabilization (Pinzaru *et al.*, 2018) which for colloidal particles, occurs by chemically attaching polymers to the surfaces of the particles. This means that there is a physical barrier of chains that block the Van der Waals attractive forces from fully operating

between nanoparticles. The short range of repulsive layer around the nanoparticles imparts long-term stability in high concentrations of salts and extreme pH.

PEG has antifouling properties and thus inhibits some non-specific interaction with proteins. This delays the opsonization process while reducing NP uptake in macrophages (Bunker, 2012). In addition, this increases the circulation in blood by avoiding reticuloendothelial cells (Suk *et al.*, 2016).

2.5.2 Platinum nanoparticles (PtNPs)

Platinum-based compounds (such as cisplatin, oxaliplatin and carboplatin) exert their cytotoxic effect by selectively bonding with atoms of purine bases in deoxyribonucleic acid (DNA), thus causing changes in the DNA structure (Dasari and Tchounwou, 2014). Cisplatin has been shown to be very effective against testicular and ovarian cancers but it is not target-specific for cancer cells, leading to enormous damage to normal cells. Kutwin *et al.*, (2017) have demonstrated that PtNPs have potent cytotoxic effects against U87, MCF-7 and HepG-2 cell lines. Bendale *et al.*, (2017) has also shown that PtNPs were cytotoxic against A549, PA-1 and Mia-Pa-Ca-2 cells but did not adversely affect normal cells, thus making platinum nanoparticles perfect candidates in cancer research.

2.5.3 Bimetallic nanoparticles (bNPs)

The monometallic nanoparticles AuNPs and PtNPs consist of a single metal and the metal atom involved determines the property of the nanoparticle formulation (Paszkievicz *et al.*, 2016). When two different metals are reduced simultaneously with a reducing agent in the presence of a suitable capping agent, the atoms of these two metals can combine to form bNPs (Sharma *et al.*, 2019).

There are three different forms of bNPs based on the distribution modes of the two elements (Paszkievicz *et al.*, 2015). These are cluster-in-cluster, alloys and core-shell bimetallic NPs (**Figure 2.6**). Cluster-in-cluster materials are heterogeneous intermetallic compounds while alloys have an intermixed pattern, which may be random or ordered and core-shell NPs have one metal at the core and the other one surrounding the core as the 'shell'. The type of bNPs formed is dependent on a number of factors including, the metal-metal bond, surface energies, relative atomic size and the preparation method (Zaleska-Medynska *et al.*, 2016).

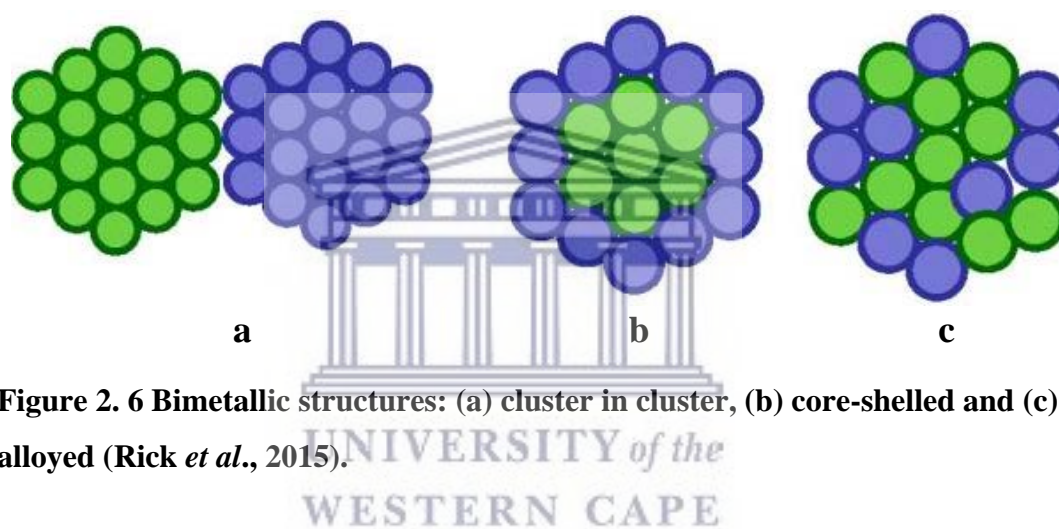


Figure 2. 6 Bimetallic structures: (a) cluster in cluster, (b) core-shelled and (c) alloyed (Rick *et al.*, 2015).

Bimetallic nanoparticles are normally used as catalysts due to their decreased particle sizes and increased surface area (An and Somorjai, 2015). They also enhance catalysis in chemical reactions and in environmental remediation. Gold-silver bNPs (AuAgNPs) are mostly used in biosensors and have been shown to have anti-cancer effects against HCT116, 4T1, HUH7 and HEK293 cell lines (Katifelis *et al.*, 2018).

2.5.4 Gold-Platinum bimetallic nanoparticles (AuPtNPs)

AuPtNPs are made up of Au and Pt metals and are also used in biosensors (Rick *et al.*, 2015). The Au metal ions are located at the core whereas the Pt metal ions are usually located at the surface or shell, to enhance the catalytic potential of Pt.

In cancer research, AuPtNPs have been shown to induce cell-specific cytotoxicity (Maney and Singh, 2017) and have been used in thermal treatment and drug delivery (Srinoi *et al.*, 2018). In all cases, the AuPtNPs were conjugated with drugs, however, not much has been reported on the application of AuPtNPs in cancer.

2.6 RESEARCH PROBLEM STATEMENT

Drug resistance, non-specific toxicity and the BBB are some of the challenges of current anticancer chemotherapeutic agents used for nervous system cancers such as NB and GBM cancers (Housman *et al.*, 2014). Thus, research on the development of more effective chemotherapeutic agents that will have minimal side effects while targeting nervous system cancers continues to receive attention and support. The targeted intracellular delivery of PEGylated metallic nanoparticles to only cancer cells will be an effective method for nervous system cancers.

Both AuNPs and PtNPs are known to play an important role in cancer research, especially in the development of potent treatment agents. However, to the best of our knowledge, there is no published report in literature on the *in vitro* effects of PEGylated gold-platinum bNPs (PEGylated AuPtNPs) on any cancer cell line. Therefore, the present study was done with the aim of synthesizing “citrate-capped” and “PEGylated” gold and gold-platinum bNPs and evaluating their cytotoxicity on the human primary glioblastoma cell line U87 MG as well as the human-derived neuroblastoma cell line SH SY5Y.

CHAPTER THREE

MATERIALS AND METHODS

The present study was done in the Experimental Neurobiology Laboratory of the Medical Bioscience Department in the Life Sciences Building of the University of the Western Cape.

3.1 MATERIALS

Ultrapure millipore water (having resistivity 18.2 M Ω .cm at 25°C) was obtained from the University of the Western Cape Pharmacy Department and used as a solvent for the synthesis of gold, platinum and gold-platinum bNPs. Gold (III) chloride trihydrate (>99.9% trace me), Chloroplatinic acid hydrate (>99.9% trace me), sodium citrate tribasic dehydrate (>98%), sodium borohydride (99%) and Brand[®] magnetic stir bar [Polytetrafluoroethylene (PTFE), 5mm length x 2mm diameter] were all purchased from Sigma-Aldrich (South Africa). Polyethylene glycol-ethanol (PEG-OH) with molecular weight of 468 g/mol was purchased from Prochimia Surfaces (United States of America). All chemicals used were of analytical grade. Glassware such as Erlenmeyer flasks and glass vials as well as the 0.22 μ m filters were purchased from Biosmart (South Africa). All glassware and magnetic stirring bars were cleaned with aqua regia [3:1 mixture of concentrated Hydrochloric acid (HCl) and Nitric acid (HNO₃)], then autoclaved together with pipette tips and a bottle of Ultrapure millipore water.

3.2. SYNTHESIS AND FUNCTIONALIZATION OF METALLIC NANOPARTICLES

Metallic nanoparticles were synthesized using established methods. The benches as well as the Magnetic stirrers (ISG Hot Plate and Magnetic Stirrer) were first sprayed with 70% ethanol and thoroughly wiped with Nampak Tissue paper before commencing experiments.

3.2.1 Chemical synthesis of citrate-capped gold nanoparticles

3.2.1.1 Preparation of stock solutions

An amount of 0.0197g of Gold (III) chloride trihydrate was weighed out into a glass vial and 5 ml Ultrapure millipore water was added into the glass vial to dissolve the Gold (III) chloride trihydrate. The glass vial was then wrapped with aluminium foil and kept in the dark at 4°C (DEFY refrigerator 385).

Similarly, an amount of 0.029g of sodium citrate tribasic dehydrate was weighed out into a glass vial and 10 ml of Ultrapure millipore water was added to dissolve the sodium citrate tribasic dehydrate. The glass vial was kept at room temperature in the dark (wrapped in aluminium foil).

An amount of 0.0057g of sodium borohydride was also weighed out into a glass vial, and dissolved in 1.5 ml iced cold Ultrapure millipore water. The glass vial was wrapped with aluminium foil and placed on ice until use. This solution was freshly prepared for every synthesis.

3.2.1.2 Procedure for the synthesis of citrate-capped gold nanoparticles

A modified method of Oliveira *et al.*, (2017) was used to synthesize citrate-capped gold nanoparticles was performed in Erlenmeyer flasks with the magnetic stirring bars.

Aqueous solution of Gold (III) chloride trihydrate (1.25 ml, 0.01M) was added to 47.5 ml of Ultrapure millipore water and stirred for 2 minutes on a low speed (speed knob at 5 on the magnetic stirrer) at room temperature. Sodium citrate tribasic dehydrate (1.25 ml, 0.01M) was added to the Erlenmeyer flask and stirred on slow speed for 3 minutes at room temperature. The speed of the magnetic stirrer was increased (speed knob at 7 on the magnetic stirrer) and subsequently, sodium borohydride (1.5 ml, 0.1M) was added to the mixture on the Erlenmeyer flask. The pale yellow mixture turned to bright red colour after the addition of the sodium borohydride and after 40 seconds, the stirring was stopped and the Erlenmeyer flask was wrapped with aluminium foil. This Erlenmeyer flask was left undisturbed in the incubator (Yinder Hybridization shaking oven OH-800D) at 23.5°C for 5-7 hours after which the mixture was filtered with a 0.22µm Millipore filter into a 50 ml tube, covered with aluminium foil and kept at 4°C to reduce photo-induced oxidation.

3.2.2 Chemical synthesis of citrate-capped Gold-Platinum nanoparticles

3.2.2.1 Preparation of stock solutions

An amount of 0.0236g of Gold (III) chloride trihydrate and 0.0246g of Chloroplatinic acid hydrate were weighed out into separate glass vials and 6 ml Ultrapure millipore water respectively were added to dissolve the Gold (III) chloride trihydrate and Chloroplatinic acid hydrate respectively. The glass vials were then wrapped with aluminium foil and kept in the dark at 4°C.

An amount of 0.1471g of sodium citrate tribasic dehydrate was weighed out into a glass vial and 5 ml of Ultrapure millipore water was added to dissolve the sodium citrate tribasic dehydrate. This glass vial was kept at room temperature in the dark (it was wrapped with aluminium foil).

Finally, 0.0023g of sodium borohydride was weighed out into a glass vial, and dissolved in 600 μ l iced cold Ultrapure millipore water. The glass vial was wrapped with aluminium foil and placed on ice until use. This solution was freshly prepared for every synthesis.

3.2.2.2 Procedure for the synthesis of citrate-capped gold-platinum nanoparticles

A modified method of Qu *et al.*, (2011) was used to synthesize citrate-capped gold-platinum nanoparticles was performed in Erlenmeyer flasks with the magnetic stirring bars. Aqueous solution of Chloroplatinic acid hydrate (1 ml, 1 mM) was added to 18 ml of Ultrapure millipore water and stirred for one minute on a low speed (speed knob at 5 on the magnetic stirrer) at room temperature. Gold (III) chloride trihydrate (1 ml, 1 mM) was added to the Erlenmeyer flask and stirred for one minute on the low speed (speed knob at 5 on the magnetic stirrer) at room temperature. Sodium citrate tribasic dehydrate (800 μ l, 100 mM) was added to the Erlenmeyer flask and stirred on slow speed for one minute at room temperature and the speed of the magnetic stirrer was later increased (speed knob at 7 on the magnetic stirrer). Subsequently, sodium borohydride (600 μ l, 100 mM) was added to the mixture on the Erlenmeyer flask and the pale yellow mixture turned to dark-brown colour. After 40 seconds, the stirring was stopped and the Erlenmeyer flask was wrapped with aluminium foil and left undisturbed in the incubator at 23.5°C for 5-7 hours. After incubation, the mixture was filtered into a 50 ml tube using 0.22 μ m Millipore filter, covered with foil and kept at 4°C.

3.2.3 Synthesis of polyethylene glycol functionalized nanoparticles (PEGylated NPs)

A modified method of Sosibo *et al.*, (2015) was used. Briefly, a volume of 5 ml of each of the synthesized citrate-capped gold and gold-platinum nanoparticles respectively was added into separate glass vials and stirred at room temperature. To each 5 ml of the respective citrate-capped nanoparticles, a volume of 5.265 μl of PEG-OH (18.8 mg/ml) was added, stirred for 8 hours and covered with aluminium foil until use.

3.2.4 Purification

All the citrate-capped metallic as well as the PEGylated nanoparticles were purified by centrifugation (Eppendorf Centrifuge 5417R). A volume of 10 ml of all the citrate-capped metallic nanoparticles were centrifuged at 14000rpm for an hour at 4°C followed by a dispersion of the pellet in 9 ml ultrapure millipore water, while 10 ml of the PEGylated nanoparticles was centrifuged at 14000rpm for two hours at 4°C followed by dispersion of the pellet in 9 ml ultrapure millipore water.

3.3 PHYSICOCHEMICAL CHARACTERIZATION

The synthesized citrate-capped, PEGylated gold and gold-platinum nanoparticles were characterized within 24 hours after synthesis by different techniques, including the ultraviolet-visible (UV-Vis) spectroscopy and dynamic light scattering (DLS). Characterization with High- Resolution Transmission Electron Microscope (HRTEM) and Fourier-transform infrared spectroscopy (FTIR) was done a week post-synthesis, due to these faulty machines and booking challenges.

3.3.1 Ultraviolet-visible spectroscopic analysis

The citrate-capped and PEGylated nanoparticles were initially characterized with UV-Vis spectroscopy. The UV-Vis spectroscopy (POLARstar OMEGA at the Department of Biotechnology, University of the Western Cape) was the primary tool for the detection of the optical properties of metallic nanoparticles. The path length correlation selected was a volume of 300 μ l with wavelength intervals ranging from 250- 1000 nm, with a resolution of 1 nm on the spectrophotometer.

3.3.2 Dynamic Light scattering analysis

The stability of the synthesized citrate-capped and PEGylated nanoparticles was evaluated as the zeta potential as determined by the Malvern Zetasizer Nano ZS90 at the Department of Biotechnology, University of the Western Cape. An amount of 750 μ l of the nanoparticles was slowly filled into a sterilized, folded capillary cell (DTS1070) with gold electrodes and allowed to flow down the U-shaped tube to stop bubbles from forming but when air bubbles formed, the cell was tapped gently. The cell (with the Malvern logo facing towards the front) was inserted and pushed on the Zetasizer machine until it stopped. The temperature was set at 25°C, with equilibration time of 30 seconds. The measurements were done in triplicates at 90° angle, the number of runs was seven, and each run lasted for 30 seconds. The measurement of zeta potential is generally based on the direction and velocity of particles under the influence of a known electric field.

The hydrodynamic size as well as the size distribution of the NPs were determined by a Dynamic Light Scattering (Malvern Zetasizer Nano ZS90) following similar procedures as for zeta potential above. The standard disposable polystyrene cuvettes were tilt-filled with 1 ml of the citrate-capped and PEGylated nanoparticles and the

samples were allowed to flow down inside the cuvette to avoid air bubbles. Readings were taken at 25°C temperature, 0.8872 cP viscosity of water. There were seven experimental runs of 10 seconds duration. The hydrodynamic size was determined based on measuring the time-dependent fluctuation of scattering laser light (He-Ne laser of wavelength 633 nm) by the nanoparticles undergoing Brownian motion. Size distribution was determined at a 90° angle using the Stokes-Einstein relationship.

3.3.3 High Resolution Transmission Electron Microscopy and Energy-dispersive X-ray spectroscopy

To determine the core size and morphology of the nanoparticles, a less than 20 µl drop of all the nanoparticles was placed on carbon-coated nickel grids. There were insufficient number of carbon-coated nickel grids, therefore carbon-coated copper grids were used when the carbon-coated nickel grids were depleted and the nanoparticles were left to dry at room temperature. HRTEM was undertaken with a Tecnai F20 microscope (200 keV) at The Electron Microscope Unit, Department of Physics at the University of the Western Cape. The image analysis tool ImageJ software (version 1.4) was used for analysis of HRTEM images.

The Energy Dispersive X-ray (EDX) spectra equipped in Tecnai F20 microscope at an energy range of 0–20 keV was used to confirm the primary elements found in the nanoparticles. The same sample was used for both TEM and EDS,.

3.3.4 Fourier Transform Infrared Spectroscopy

Infrared (IR) spectra were obtained using a BIORAD FTS 3000MX Excalibur series spectrometer fitted with a DRIFTS accessory. This was used to identify the functional group compounds that were on the surface of the nanoparticles. A volume of 5 ml of

all the nanoparticles was centrifuged (14000 rpm, 4°C) for 60 minutes, the supernatant discarded and pellets dried at room temperature. The dried samples were then mixed separately with potassium bromide (KBr) and ground using agate mortar and pestle to produce a fine mixed powder which was inserted in the 7mm die-collar and put into the Qwik Handi-Press for 2 minutes to form the disc. These were subjected to the FTIR analysis and all spectra were recorded at a resolution of 4 cm⁻¹ over a wave number range of 400 – 4000 cm⁻¹.

3.4 *IN VITRO* COLLOIDAL STABILITY STUDIES

The *in vitro* stability study of the citrate-capped and PEGylated nanoparticles was performed by mixing the centrifuged nanoparticles to aqueous solutions that mimic biological environments such as Dulbecco's Modified Eagle's medium (DMEM) media supplemented with 10% (v/v) fetal bovine serum (FBS); phosphate buffered-saline (PBS) at pH 7.4; 0.5% bovine serum albumin (BSA) and millipore water. A volume of 700 µl of the nanoparticles was added to 300 µl of the mentioned solvents and incubated at 37°C. The stability was measured by monitoring the UV-Vis spectra absorbance over a period of 0h, 4h, 24h and 48h. A negligible change in UV-Vis plasmon band confirmed the retention of the composition of the nanoparticles in all mixtures.

3.5 CELL CULTURE

SH SY5Y and U87 cells already available in the Medical Biosciences laboratories were stored in the -80°C freezer. The U87 is a primary glioblastoma cell line (astrocytoma) derived from human malignant gliomas with the phenotype of adherent epithelial cells with an infinite life span and high reproducibility (Ledur et al., 2017). On the other hand, SH SY5Y cells were originally derived from a bone marrow biopsy of a

neuroblastoma patient. Both cell lines can be cultured by incubating at 37 °C in DMEM supplemented with 10% FBS and 1% penicillin–streptomycin (P/S). All the chemicals used in these experiments were obtained from Sigma-Aldrich (South Africa). The cell culture plates used were the non-pyrogenic, non-cytotoxic and DNase/RNase-free sterile plates from SPL Life Sciences.

3.5.1 Sub-culturing SH SY5Y and U87 cell lines from a monolayer

At 70-80% confluency, the cells were sub-cultured and the medium from the plates was removed with a sterile pipette. The adhering cell monolayer was washed with 1 ml of PBS to remove any residual FBS that may prevent the action of trypsin. Pre-warmed trypsin-EDTA was then added to the sides of the petri dish, enough to cover the cell monolayer (approximately 1- 1.5 ml) and the plate was then placed in the incubator for 2 minutes. The cells were viewed under the inverted microscope to check if they lifted. When the cells were not sufficiently detached, the trypsin was removed and cells were incubated for further three minutes at 37°C until more than 90% of the cells detached and with a change in morphology when viewed under the inverted microscope. The cells were put back into the laminar flow hood, 2 ml of complete medium added and dispersed by pipetting over the cell layer surface and the resulting cell suspensions transferred into a centrifuge tube. A volume of 1 ml of each of these cell suspensions was added to a 90 mm petri dish containing 9 ml of medium. The plate was labelled then subsequently incubated at 37°C with the passage number increasing. Only cells that had a passage number less than 20 were used in the experiments as cells with higher passage numbers tend to display alterations in morphology, gene expressions, response to stimuli and high chances of cross-contamination (Kwist *et al.*, 2016).

3.6 CELL VIABILITY ASSAY

Cell viability was evaluated using the Water Soluble Tetrazolium salt 1 (WST-1) product (Sigma, South Africa) following manufacturer's recommendations and the method described by Sigma.

WST-1 assay is a cell proliferation assay based on the metabolic activity (viability) of a population of cells. Metabolically active cells produce lactate dehydrogenase enzymes. WST-1 is a tetrazolium salt usually reduced to formazan dye when exposed to the lactate dehydrogenase enzymes. Thus, the amount of the formazan dye is directly proportional to the number of lactate dehydrogenase enzymes (metabolically active cells) (Riss *et al.*, 2004).

Briefly, both SH SY5Y and U87 cell lines were seeded at a density of 4×10^3 cells per well in a flat-bottomed 96 well microplates with a volume of 100 μ l per well. The cells were incubated and allowed to attach to the wells. Thereafter, the medium was carefully removed from the wells and the attached cells were treated with 100 μ l of the respective citrate-capped and PEGylated gold and gold-platinum nanoparticles with series dilutions of 75, 150 and 225 μ g/ml. All the concentrations of the nanoparticles were made in medium and each concentration was added to the plate in quadruplets. After 24 and 48 hours of incubation, a volume of 10 μ l of the WST-1 solution was added to each well and incubated for an additional 4 hours at 37°C. Different plates were used for each time period and after 4 hours, the plates were shaken thoroughly for 1 minute on the shaker. The absorbance of the formazan product of each well was subsequently recorded at a wavelength of 450 nm on a spectrophotometer (POLARStar OMEGA), with reference wavelength of 600 nm. Blank wells contained no cells but only the nanoparticles and WST-1. Untreated wells contained cells but no nanoparticles added

and hence were considered 100% viable. The background noise was eliminated by subtracting the value of the blank from the values obtained in these tests.

The half maximal inhibitory concentration (IC_{50}) was used to measure the potency of the PEGylated nanoparticles on the U87 and SH SY5Y cells. The IC_{50} values were calculated from a non-linear regression (dose-response curves) using GraphPad Prism 8 software. For each cell line, two IC_{50} values were obtained, one for the 24 hour period and the other for the 48 hour period and the IC_{50} obtained in the 24 hour period was used for the quantification of cellular uptake while IC_{50} values obtained for 48 hours were used for the rest of the experiments.

3.7 OBSERVATION OF MORPHOLOGICAL CHANGES

After 48 h of exposure of the SH SY5Y and U87 cells (both at density of 1×10^6 cells/dish) to the IC_{50} concentrations of the PEGylated nanoparticles, cell morphology was investigated using a Carl Zeiss inverted light microscope (Olympus, Tokyo, Japan). Images were captured using a ProgRes c12 camera (Jenoptik, Jena, Germany). Cells cultured without the PEGylated nanoparticles were used as controls.

3.8 MEASUREMENT OF INTRACELLULAR REACTIVE OXYGEN SPECIES

The level of Intracellular ROS was monitored using the fluorescent probe 2',7'-Dichlorodihydrofluorescein diacetate (DCFH-DA) according to the manufacturer's instructions (Thermo Fisher Scientific, South Africa). DCFH-DA is a stable non-fluorescent molecule. DCFH-DA is lipophilic and a hydrogen donor. Since it is lipophilic, it can be taken up by the cells where there are esterases inside the cells that cleave the lipophilic groups in the DCFH-DA, resulting in the DCFH-DA compound with the inability to leave the cells. Intracellular H_2O_2 or low-molecular weight

peroxides, oxidize DCFH-DA to the highly fluorescent compound dichlorofluorescein (DCF).

SH SY5Y and U87 cells were seeded in 90mm cell culture dishes at a density of 1×10^6 cells per well, then incubated with each IC_{50} concentrations of PEGylated gold and gold-platinum nanoparticles for 48 hours. One dish was not treated and used as a control. Cells were washed twice with an iced cold PBS, then incubated with $10 \mu\text{M}$ of the DCFH-DA (prepared in DMEM media without phenol red) under cell culture conditions for 40 minutes and were covered with aluminium foil to protect from the light. Phenol red contains esterases, which could have cleaved the lipophilic groups of the DCFH-DA, inhibiting it from entering the cells (Wu and Yotnda, 2011). The cells were washed twice with pre-warmed PBS and finally the fluorescence intensity of DCF was measured in a BD ACCURI flow cytometer at an excitation wavelength of 485 nm and emission wavelength of 538 nm. For each sample, 10000 events were collected.



3.9 FLOW CYTOMETRIC MEASUREMENT OF MITOCHONDRIAL MEMBRANE POTENTIAL

The level of mitochondrial transmembrane potential was determined by flow cytometry after cells were stained with the cationic fluorescent dye rhodamine 123, according to the manufacturer's instructions (Sigma-Aldrich, South Africa). This dye partitions into metabolic active mitochondria based on the highly negative mitochondrial membrane potential.

Briefly, SH SY5Y and U87 cells were seeded at a density of 1×10^6 cells per plate and after treatment with IC_{50} concentrations of the PEGylated gold and gold-platinum nanoparticles for 48 hours, the cells were trypsinized, washed twice with PBS and incubated at 37°C for 1 hour in the presence of $5 \mu\text{M}$ Rhodamine 123. After incubation

in the dark, the cells were collected by pipetting, washed with PBS and the fluorescence intensity was analysed using BD ACCURI flow cytometer. This was to estimate the mitochondrial transmembrane potential changes with excitation settings of 488 nm and emission settings of 530 nm. For each sample, 10000 events were collected.

3.10 QUANTITATIVE EVALUATION OF CELLULAR UPTAKE OF PEGYLATED NANOPARTICLES

SHS Y5Y and U87 cells were seeded in cell culture dishes at a density of 1×10^6 cells/dish. On the next day, the growth medium was discarded and replaced with IC_{50} concentrations of PEGylated gold and gold-platinum nanoparticles for 24 hours. The cells were washed twice with the PBS solution, then were removed from the bottom of the well using 1 ml of trypsin. The cell suspension was centrifuged at 3000 rpm for 5 min to remove any cellular debris which may clog the instrument. The pellets were digested with 0.4 ml aqua regia ($1NO_3: 3HCl$) then diluted with 8 ml millipore water. The nanoparticles were measured by Perkin Elmer Optima 4300 DV Inductively Coupled plasma Mass Spectrometry (ICP-MS), and were reported as the concentration of nanoparticles (ppm).

3.11 STATISTICAL ANALYSIS

The results for the WST-1 assay were plotted using GraphPad Prism software 8 for windows (<http://www.graphpad.com>) and were expressed as mean \pm SEM of experiments performed in triplicates. One-way ANOVA test was used to analyse the results to obtain statistical significance.

CHAPTER FOUR

RESULTS OF THE PHYSIOCHEMICAL CHARACTERIZATION OF NANOPARTICLES

4.1 ULTRAVIOLET-VISIBLE SPECTROSCOPY STUDY

A simple and sensitive ultraviolet-visible (UV-Vis) technique was employed to verify the synthesis of both the citrate-capped and PEGylated nanoparticles at the wavelength range 200-800 nm (UV-Vis region). The position of the surface plasmon resonance (SPR) and its bandwidth are dependent on size and shape of the nanoparticles (Zuber *et al.*, 2016). In this section, gold and gold-platinum nanoparticles will sometimes be denoted as AuNPs and AuPtNPs, respectively.

4.1.1 Citrate-capped and PEGylated gold nanoparticles

An absorption spectra of citrate-capped and PEGylated gold nanoparticles is shown below in **Figure 4.1**. **Figure 4.1A** showed a strong SPR peak that was observed at around 510- 512 nm for the citrate-capped gold nanoparticles (red line), while the PEGylated gold nanoparticles had an SPR peak range of 518- 520 nm (dark blue line), indicating a redshift in wavelength. The shape of both the SPR absorption bands was symmetrical and quite narrow; suggesting that both the citrate-capped and PEGylated gold nanoparticles were spherical and had narrow range of sizes.

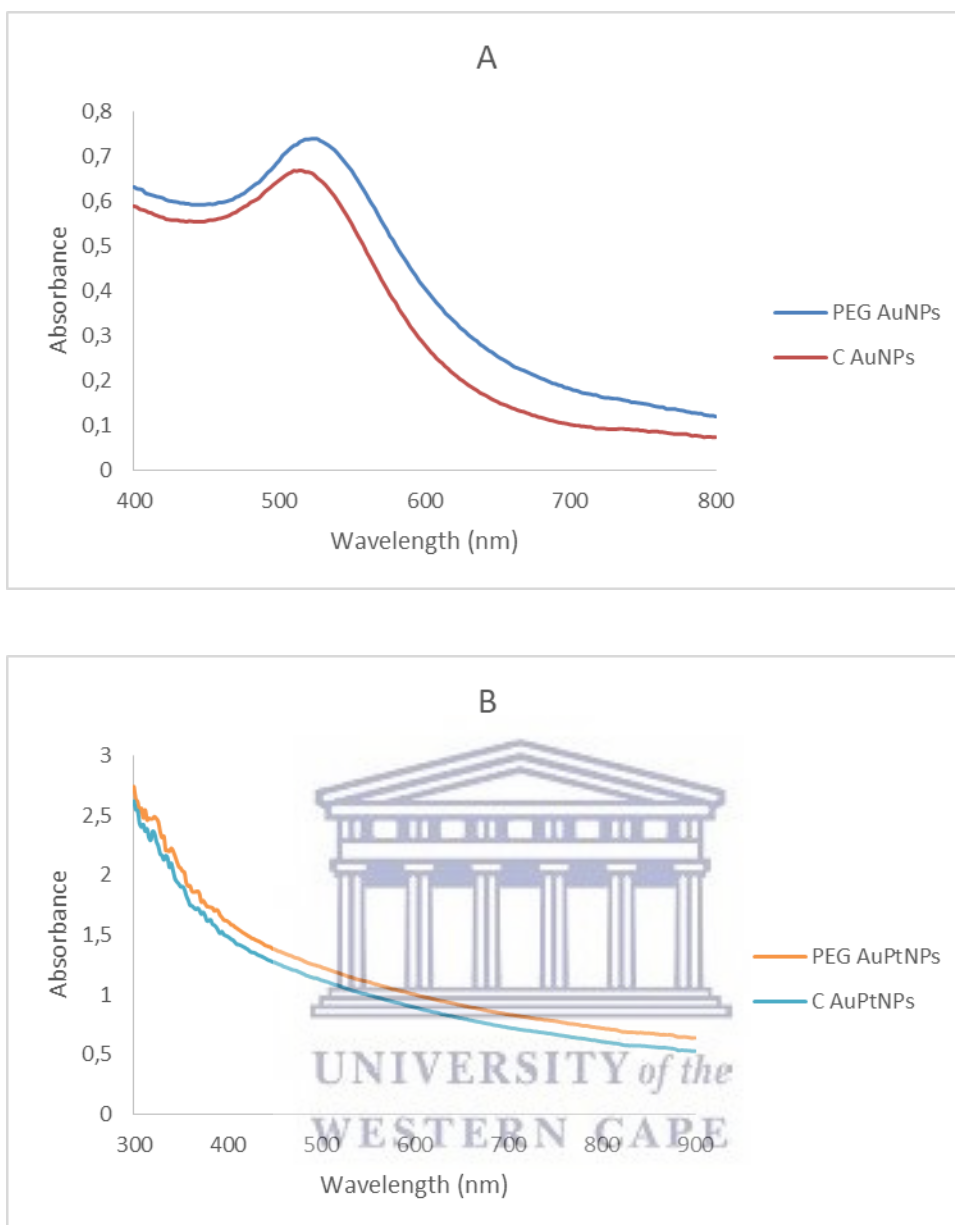


Figure 4.1 UV-Vis Absorption spectra of (A) Citrate-capped AuNPs (red) and PEG AuNPs (dark blue). (B) Citrate-capped AuPtNPs (light blue) and PEG AuPtNPs (orange).

4.1.2 Citrate-capped and PEGylated gold-platinum nanoparticles

Although it has been shown in previous studies that the choice of wavelength could start at 200 nm, we limited by the specifications of the only machine available for our use, which starts all readings at 300 nm. For the citrate-capped and PEGylated gold-platinum nanoparticles, no characteristic absorption band was observed in the UV-Vis

region (**Figure 4.1B**). Instead, a continuous scattering, which stretched across the UV-Vis region, was observed, and that is a typical scattering pattern of platinum nanoparticles. It was therefore not possible to extract information on the nanoparticle size and morphology from the recorded absorption spectra.

4.2 DYNAMIC LIGHT SCATTERING

The synthesized nanoparticles were dispersed in water and information on hydrodynamic sizes, PDI and zeta potentials are summarized in the table below.

Table 4.1 Hydrodynamic size, polydispersity index (PDI) and zeta potential of various NPs. Data are provided as mean \pm S.D. (n = 6).

Sample	Hydrodynamic size (nm)	PDI	Zeta Potential (mV)
C- AuNPs	8.5907 \pm 0.36905	0.2387 \pm 0.5930	-26.27 \pm 2.09
C- AuPtNPs	8.7045 \pm 1.01798	0.4173 \pm 0.5930	-26.22 \pm 2.57
PEG AuNPs	13.33 \pm 0.91413	0.2625 \pm 0.1355	-10.97 \pm 0.81
PEG AuPtNPs	16.1833 \pm 0.98656	0.3985 \pm 0.6024	-9.82 \pm 1.89

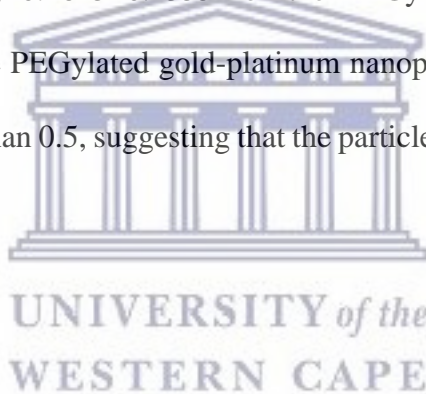
4.2.1 Hydrodynamic size

Hydrodynamic size refers to the overall size of the nanoparticles in suspension; that is, including the capping and stabilizing agent on the surfaces of the nanoparticles (Menéndez-Manjón and Barcikowski, 2011). In this study, the average hydrodynamic sizes of nanoparticles measured 8.5907 \pm 0.36905 nm and 8.7045 \pm 1.01798 nm for the citrate-capped AuNPs and citrate-capped AuPtNPs, respectively. Following functionalization with PEG, the hydrodynamic size increased to 13.33 \pm 0.91413 nm for the PEGylated AuNPs and 16.1833 \pm 0.98656 nm for the PEGylated AuPtNPs, respectively (**Table 4.1**).

4.2.2 Polydispersity index (PDI)

The measurement of the PDI was used to estimate the average dispersity (size distribution) of particles in a solution. PDI therefore indicates the broadness of the nanoparticle size distribution with values ranging between 0 and 1, with no units. PDI values greater than 0.7, indicate a broad range of sizes that are distributed in the suspension (Danaei *et al.*, 2018) while PDI values less than 0.2 (or closer to 0) indicate that the nanoparticles are monodispersed.

In this study, the average PDI of nanoparticles were measured to be approximately 0.2387 ± 0.5930 for the citrate-capped gold nanoparticles; 0.4173 ± 0.5930 for the citrate-capped gold-platinum, 0.2625 ± 0.1355 for the PEGylated gold nanoparticles and 0.3985 ± 0.6024 , for the PEGylated gold-platinum nanoparticles, respectively. All PDI values above are less than 0.5, suggesting that the particles were monodispersed (**Table 4.1**).



4.2.3 Zeta potential

The zeta potential was analysed to evaluate the chemical stability and electro-kinetic behaviour of the nanoparticles. Citrate-capped nanoparticles that have a highly negative zeta potential (usually lower than -25 mV) have moderate-to-good stability. A value of less than -5 mV indicates that there is agglomeration of the nanoparticles (Lu and Gao, 2010). PEGylated nanoparticles, however, tend to have a zeta potential that is closer to zero. The average zeta potential of the nanoparticles was measured to be -26.27 ± 2.09 mV for citrate-capped gold nanoparticles and -26.22 ± 2.57 mV for the citrate-capped gold-platinum, respectively (**Table 4.1**). PEGylated gold nanoparticles and PEGylated gold-platinum nanoparticles had a zeta potential of -10.97 ± 0.81 mV and -9.82 ± 1.89

mV, respectively (**Table 4.1**), indicating decrease in zeta potential compared to the citrate-capped nanoparticles.

4.3 HIGH RESOLUTION TRANSMISSION ELECTRON MICROSCOPY AND ENERGY DISPERSIVE X-RAY SPECTROSCOPY ANALYSIS

The morphological and elemental composition of the nanoparticles were analysed through higher resolution transmission electron microscope (HRTEM).

4.3.1 Transmission Electron Microscopy (TEM)

TEM was used to indicate the core sizes as well as the morphology of the dry nanoparticles. (**Table 4.2**).

Table 4.2 Core size of various NPs. Data are provided as mean \pm S.D. (n = 10).

Sample	Core size (nm)
C- AuNPs	5.13 \pm 0.71
PEG- AuNPs	4.96 \pm 1.44
C- AuPtNPs	5.18 \pm 0.62
PEG- AuPtNPs	5.01 \pm 1.47

4.3.1.1 Citrate-capped gold nanoparticles

The citrate-capped gold nanoparticles exhibited uniformly distributed quasi-spherical nanoparticles (**Figure 4.2**) with a mean core size of 5.13 \pm 0.71 nm (**Table 4.2**). Although, these nanoparticles appear to have agglomerated when observed at low magnification (**Figure 4.2**).

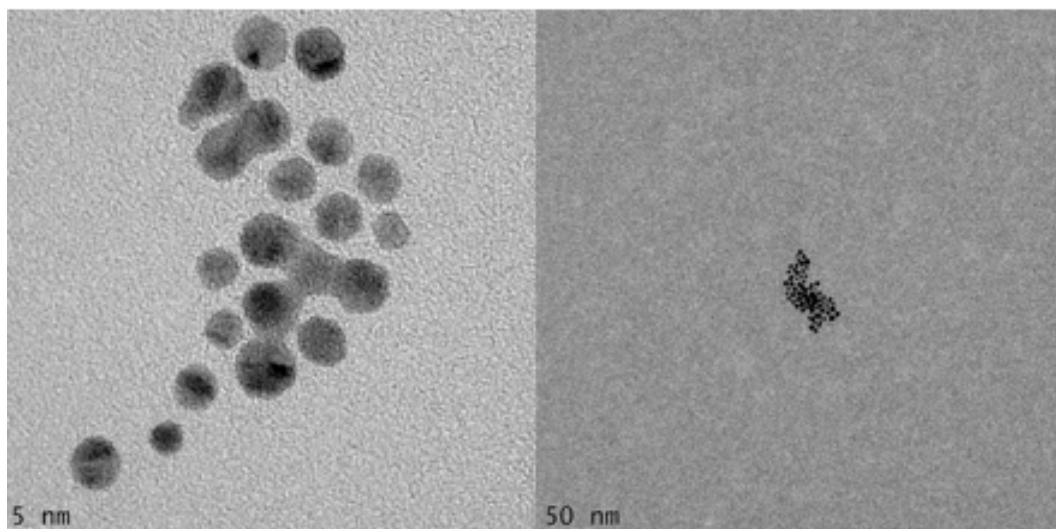


Figure 4.2 TEM images of citrate-capped gold nanoparticles at high (left) and low (right) magnification. The bars for the high magnification are indicated 5 nm and for the low magnification 50 nm.

4.3.1.2 Citrate-capped gold-platinum nanoparticles

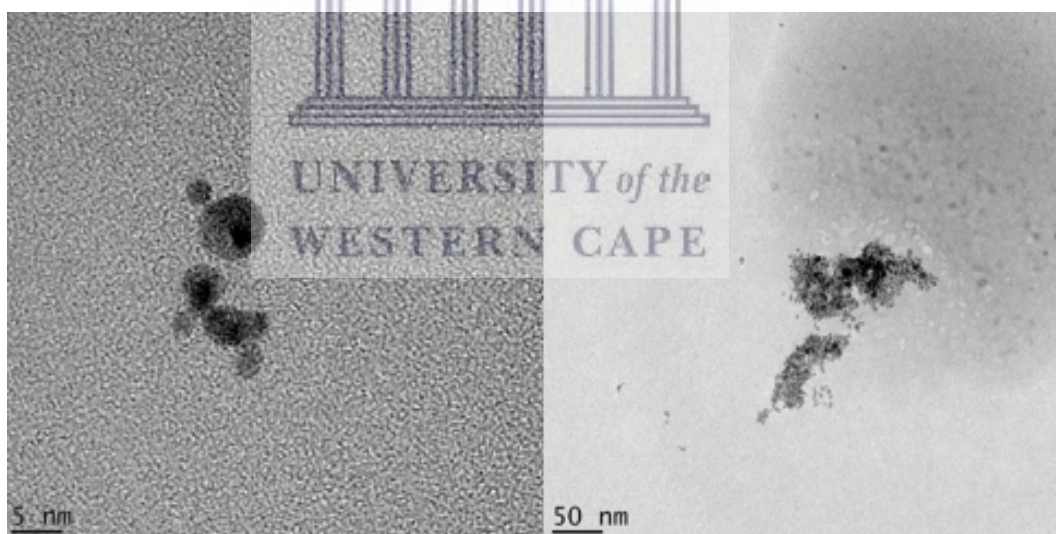


Figure 4.3 TEM images of citrate-capped gold-platinum nanoparticles at high (left) and low (right) magnification. The bars for the high magnification are indicated 5 nm and for the low magnification 50 nm.

Citrate-capped gold-platinum nanoparticles were spherical but differed in morphology. They were in close contact with one another, forming branched nano-chains with a very narrow size distribution (**Figure 4.3**). Mean core size was 5.18 ± 0.62 nm (**Table 4.2**)

although these nanoparticles appear to have agglomerated when observed at low magnification (**Figure 4.3**).

4.3.1.3 PEGylated gold nanoparticles

PEGylated gold nanoparticles were well dispersed (no agglomeration), with a narrow size distribution (**Figure 4.4**), with near spherical shapes and an average size of 4.96 ± 1.44 nm (**Table 4.2**).

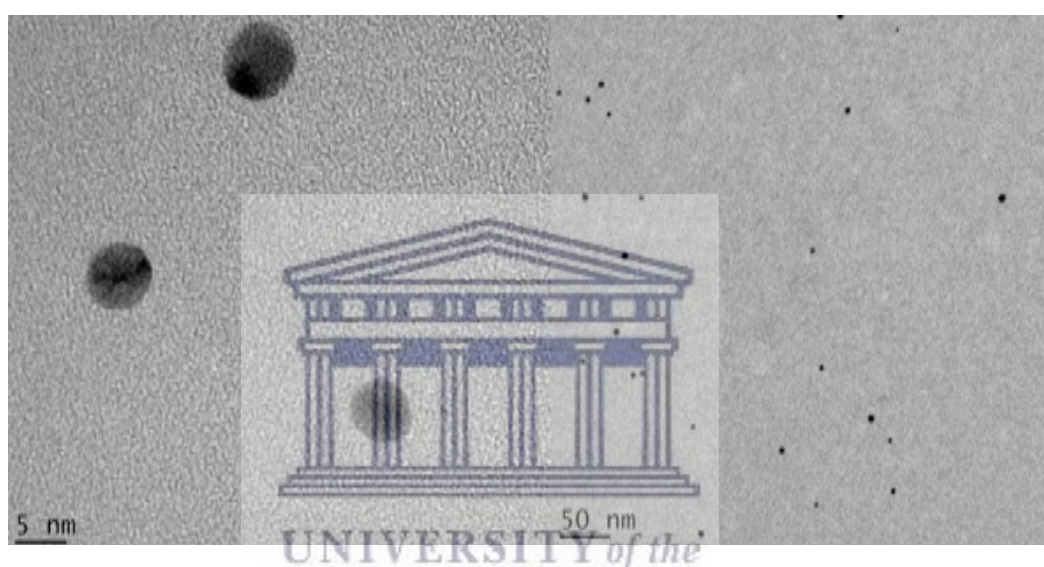


Figure 4.4 TEM images of PEGylated gold nanoparticles at high (left) and low (right) magnification. The bars for the high magnification are indicated 5 nm and for the low magnification 50 nm.

4.3.1.4 PEGylated gold-platinum nanoparticles

PEGylated gold-platinum nanoparticles were mostly spherical and in close contact with one other, forming branched nano-chains, which looked worm-like with a very narrow size distribution (**Figure 4.5**). Particles were largely spherical, with a mean core size of 5.01 ± 1.47 nm (**Table 4.2**). Even though they formed nano-chains, no agglomerations were observed.

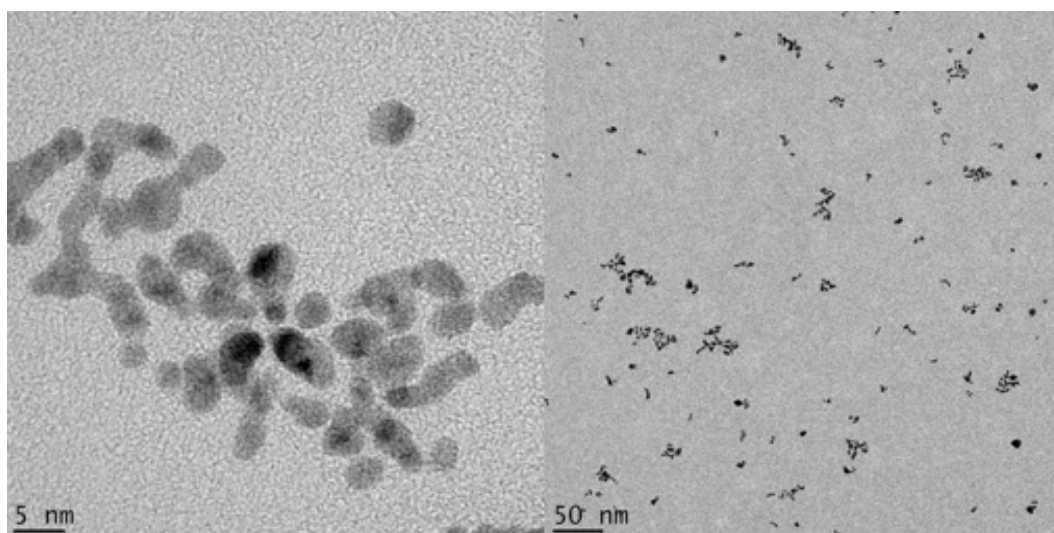


Figure 4.5 TEM images of PEGylated gold-platinum nanoparticles at high (left) and low (right) magnification. The bars for the high magnification are indicated 5 nm and for the low magnification 50 nm.

4.3.2 Energy Dispersive X-ray Spectroscopy

EDS was used to examine the elemental composition of the nanoparticles and the data is presented as a graph with energy (keV) values on the x-axis and the peak intensity on the y-axis. The Siegbahn notation was used to name the characteristic X-ray lines for each element, using K, L or M depending on which electron shell the X-ray was emitted from.

4.3.2.1 Citrate-capped gold nanoparticles

The results from the EDS analysis confirmed the presence of elemental Au in Citrate-capped gold nanoparticles and strong signals were observed from the metallic Au (M at 2.12 keV) in these nanoparticles. There were also weak Au signals (L α at 9.71 keV). The elements Ni (K α at 7.41 keV and L α at 0.85 keV), C (K α at 0.28 keV) and Cu (K α at 8.04 keV) were present due to the impurities on the carbon-coated copper grids and

carbon-coated nickel TEM grids. Also, the small peak of O ($K\alpha$ at 0.53 keV) may have originated from the citrate layer on the surface of the nanoparticles (**Figure 4.6**).

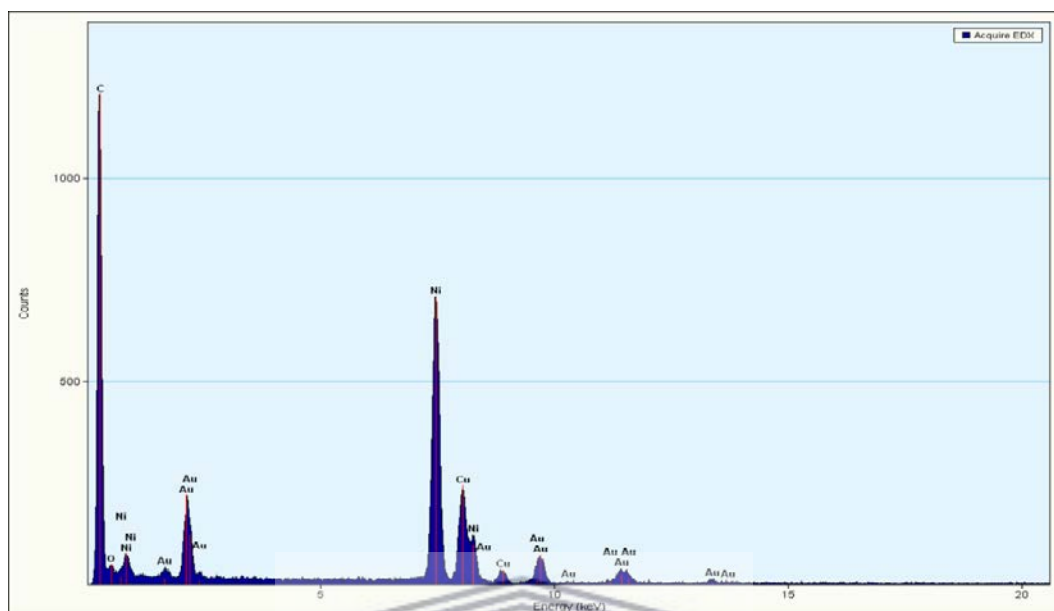


Figure 4.6 EDS elemental composition of citrate-capped gold nanoparticles.

4.3.2.2 Citrate-capped gold-platinum nanoparticles

The EDS analysis also confirmed the presence of both metallic Au and Pt elements in citrate-capped gold-platinum nanoparticles. There were multiple peaks of Au and Pt elements that were the same height, indicating that in bNPs, the metal distribution may be constant at some points. The elements C ($K\alpha$ at 0.28 keV) and Cu ($K\alpha$ at 8.04 keV) were present as impurities from the carbon-coated TEM copper grids. The Cl ($K\alpha$ at 2.62 keV) might have originated from the precursors of the platinum salts while the Na ($K\alpha$ at 1.04 keV) and O ($K\alpha$ at 0.53 keV) may have originated from the sodium citrate layer on the surface of the nanoparticles (**Figure 4.7**).

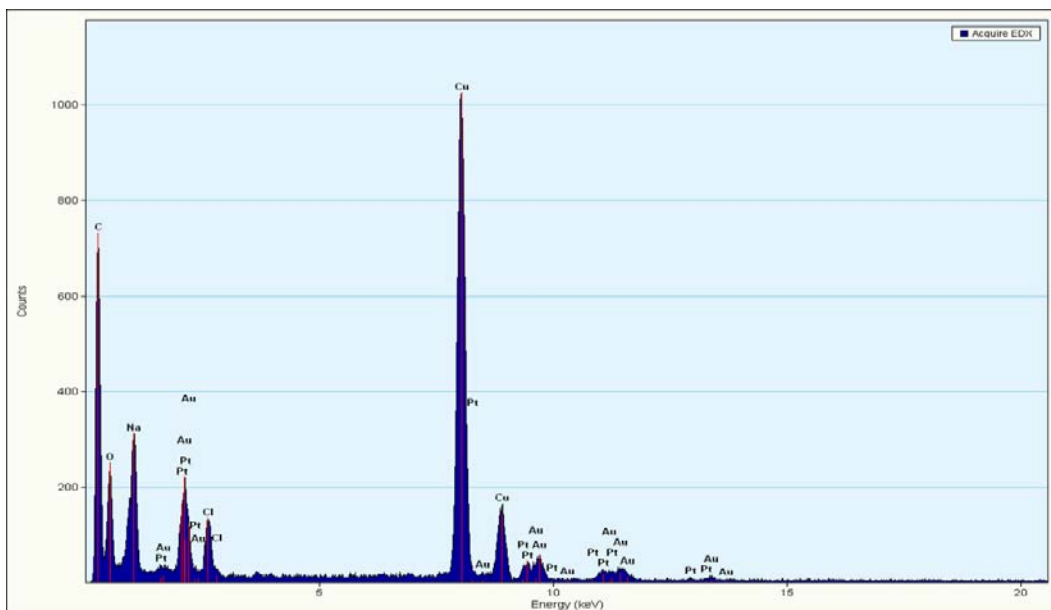


Figure 4.7 EDS elemental composition of citrate-capped gold-platinum nanoparticles.

4.3.2.3 PEGylated gold nanoparticles

The results from the EDS analysis confirmed the presence of elemental Au in PEGylated gold nanoparticles (**Figure 4.8**). Strong signals were observed from the Au in these nanoparticles M at 2.12 keV and weak Au signals (L α at 9.71 keV) were recorded. The presence of Ni (K α at 7.41 keV), C (K α at 0.28 keV) and Cu (K α at 8.04 keV) could have been due to the impurities on the carbon-coated copper grids and carbon-coated nickel TEM grids.

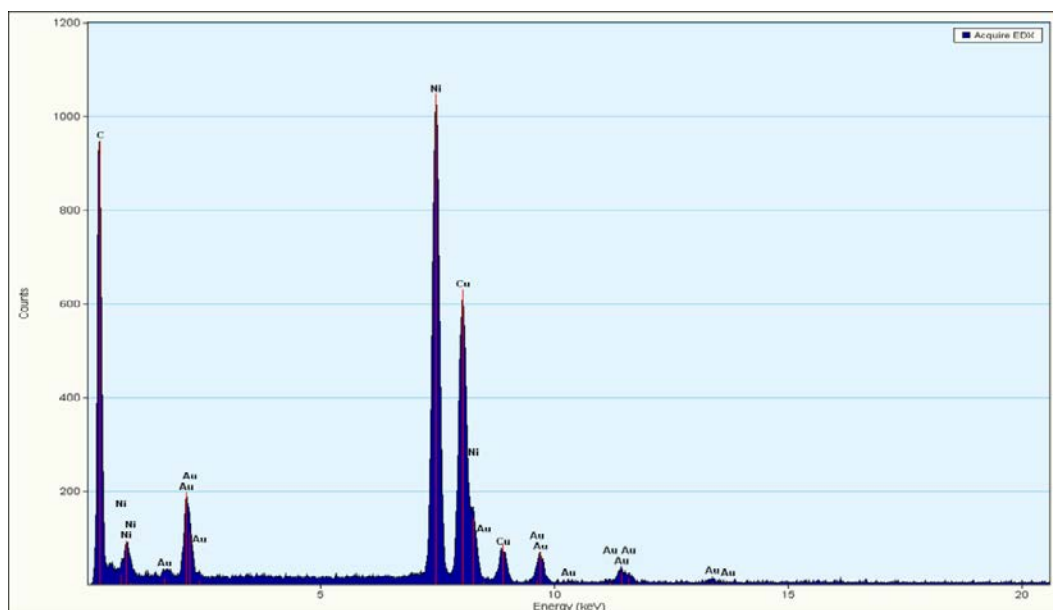


Figure 4. 8 EDS elemental composition of PEGylated gold nanoparticles.

4.3.2.4 PEGylated gold-platinum nanoparticles

The EDS analysis also confirmed the presence of both Au and Pt in PEGylated gold-platinum nanoparticles. There were multiple peaks of Au and Pt that were of the same height, indicating that in bNPs, the metal distribution may be constant at some points. The presence of Ni ($K\alpha$ at 7.41 keV), C ($K\alpha$ at 0.28 keV) and Cu ($K\alpha$ at 8.04 keV) were possibly due to the impurities on the carbon-coated copper grids and carbon-coated nickel TEM grids. Also, O ($K\alpha$ at 0.53 keV) may have originated from the PEG agent on the surface of the nanoparticles (**Figure 4.9**).

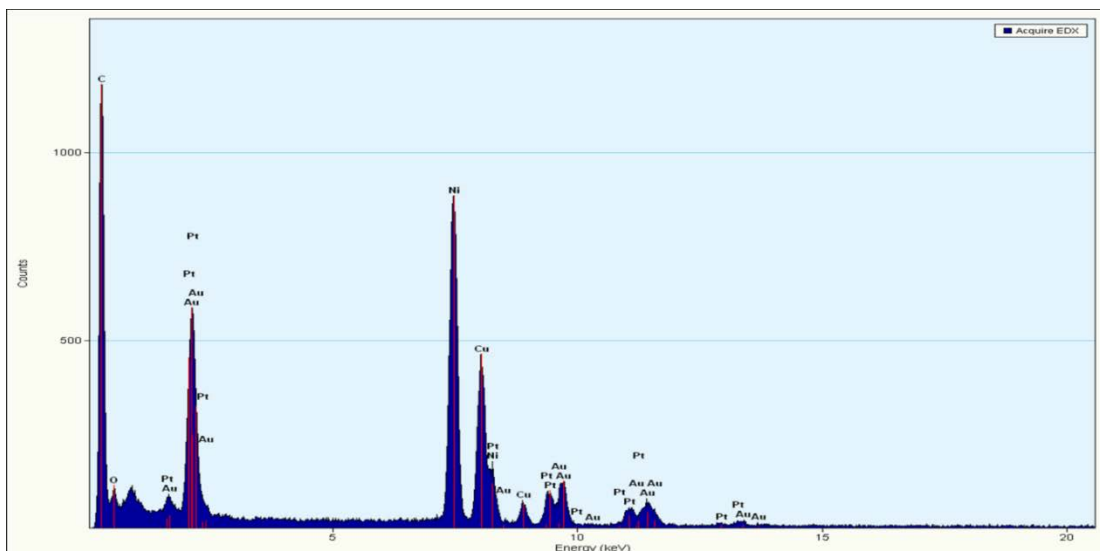
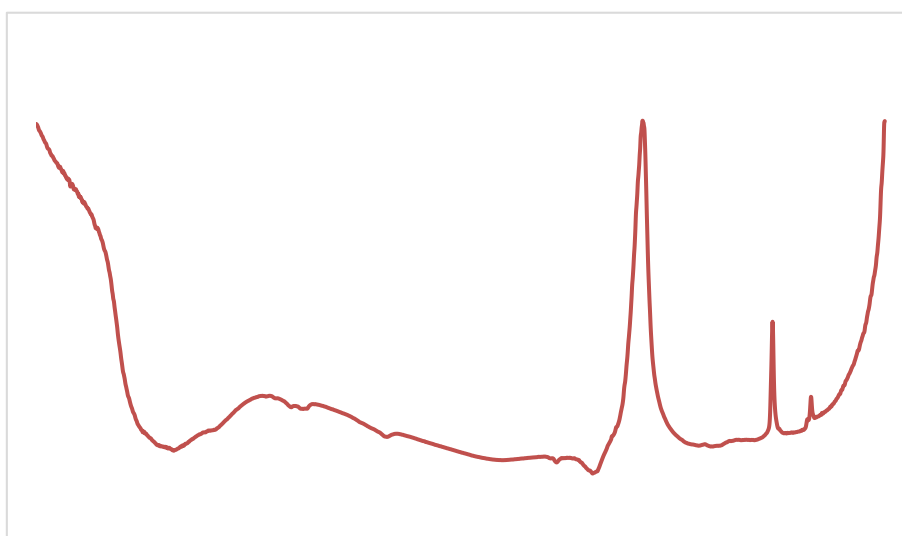


Figure 4.9 EDS elemental composition of PEGylated gold-platinum nanoparticles.

4.4 FOURIER TRANSFORM INFRARED SPECTROSCOPY STUDY

FTIR spectroscopy was carried out to determine the potential functional groups that are on the surface of the nanoparticles. Absorptions from 1000 to 600 cm^{-1} in the fingerprint region are assigned to the bending of metal to oxygen and/or hydrogen bonds. The respective metal elements were already presented in the EDS section.



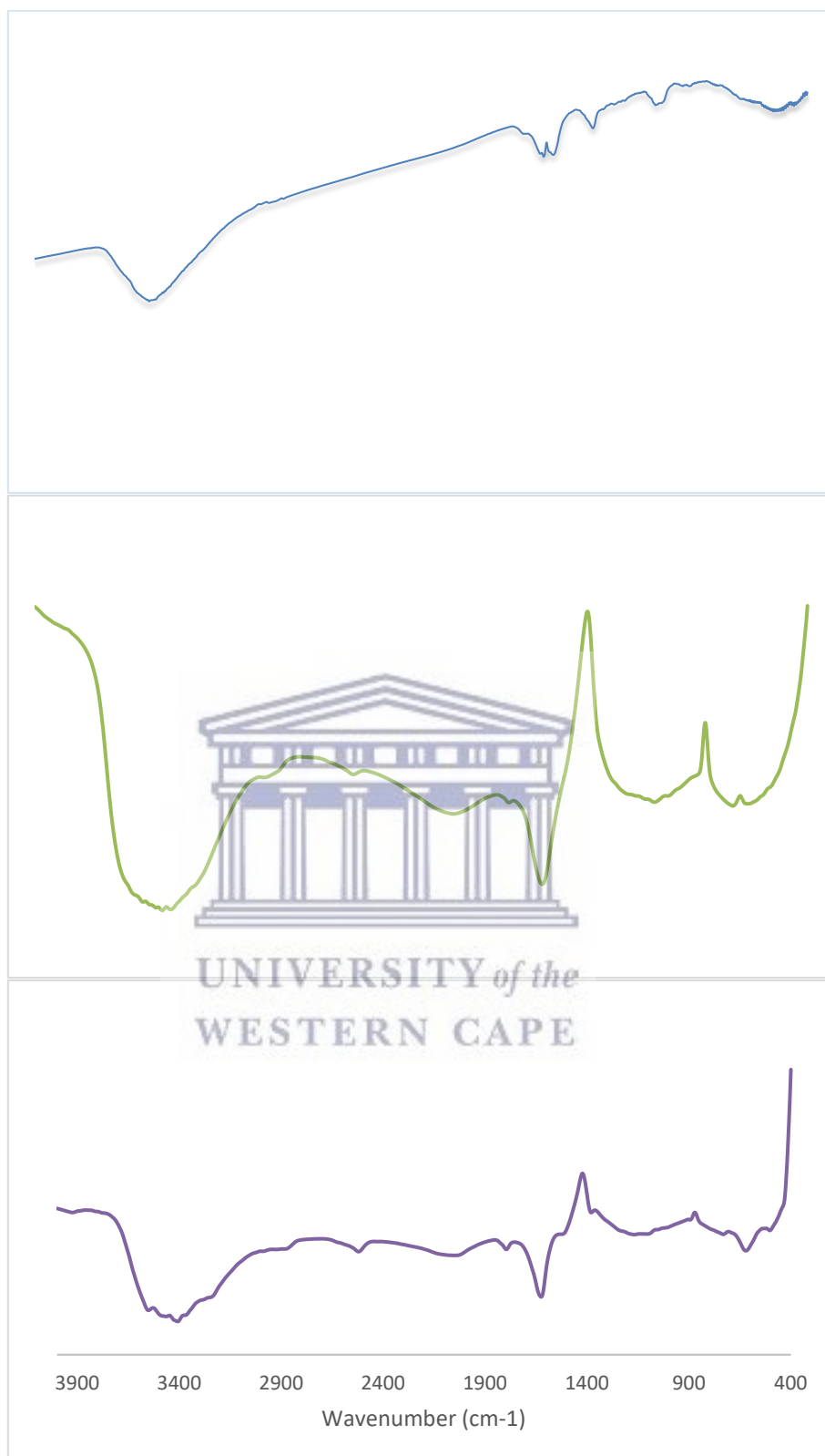


Figure 4.10. FTIR spectra of citrate-capped gold-platinum nanoparticles (purple), citrate-capped gold nanoparticles (green), PEGylated gold-platinum nanoparticles (blue) and PEGylated gold nanoparticles (maroon)

4.4.1 Citrate-capped gold-platinum nanoparticles

At higher wavenumbers, the FTIR spectra recorded on citrate-capped gold-platinum nanoparticles (purple line in **Figure 4.10**) resembles with that of the pure citrate. Two intense absorption bands were observed at 1625 cm^{-1} and 1167 cm^{-1} which are readily assigned to the asymmetric and symmetric stretching vibrations of COO^- and COO^- of citrate molecules, respectively. These results indicate that the citrate molecules have been linked on the surface of the nanoparticles being part of these nanoparticles. The broad IR absorption band at 3466 cm^{-1} is assigned to OH molecules adsorbed on the surface. The absorption band at 2520 cm^{-1} is assigned to a $\text{C}=\text{O}$ functional group of aldehydes. At 1795 cm^{-1} , an absorption band is observed, which could also belong to carbonyl group. The vibrations at 2047 cm^{-1} could possibly be assigned to a stretch in a bond between hydrogen and a metal.

4.4.2 Citrate-capped gold nanoparticles

For the citrate-capped gold nanoparticles (green line in **Figure 4.10**), there were symmetric stretching vibrations of carboxylate group (COO^-) at 1112 cm^{-1} . Furthermore, there were anti-symmetric stretching vibrations of COO^- at 1636 cm^{-1} . There is also a hydroxyl group (OH) infrared band at 3406 cm^{-1} . The exhibition of COO^- and OH groups generally indicate that the citrate molecule has been linked to the surface of the nanoparticles. A carbonyl group ($\text{C}=\text{O}$) of an aldehyde stretching was observed at 2515 cm^{-1} . Absorption band observed at wavenumbers of 2047 cm^{-1} could possibly represent a stretch in the bond between hydrogen and a metal.

4.4.3 PEGylated gold-platinum nanoparticles

The blue line on **Figure 4.10** shows some vibrational characteristics at 3445, 1620 and 1073 cm^{-1} were observed for PEG gold-platinum nanoparticles, which represented OH, C=O and C-O stretch. At 1397 cm^{-1} , a vibration was observed which represented a CH₂ scissoring.

4.4.4 PEGylated gold nanoparticles

FTIR absorption spectra analysis of PEGylated gold nanoparticles showed many characteristic peaks (maroon line in **Figure 4.10**). The prominent peak for PEG gold nanoparticles was a broad stretching band at around 3416 cm^{-1} which was attributed to the hydroxyl group (OH). Other absorption peaks were detected at 2866, 1635 and 1132 cm^{-1} which represented CH₂ of alkane, carbonyl group (C=O) and an ether (C-O) stretching, respectively. The absorption peak at 1796 cm^{-1} is assigned to a carbonyl group.

A summary of the effects of the treatment of the SH SY5Y and U87 cells with PEGylated gold and PEGylated gold-platinum NPs-treated is shown in Table 4.3.

Table 4.3. Summary of the effects of PEGylated gold and gold-platinum NPs-treated SH SY5Y and U87 cells compared to their respective controls. The cells were treated with their respective IC₅₀ values.

	SH SY5Y	U87
Dose-dependent response	decrease	decrease
ICP-MS (cellular uptake)	increase	increase
Intracellular ROS	increase	increase
MMP	decrease	decrease

CHAPTER FIVE

RESULTS OF THE *IN VITRO* BIOLOGICAL STUDIES

5.1 *IN VITRO* STABILITY STUDY

It is critical to fully understand how different nanoparticles behave in an *in vitro* environment that mimics *in vivo* conditions for any potential biomedical application. For this reason, the stability of citrate-capped and PEGylated nanoparticles was evaluated in four different biological solutions (10% supplemented DMEM medium, PBS, 0.5% BSA and water) by monitoring the SPR band.

5.1.1 Citrate-capped and PEGylated gold *in vitro* stability studies

The SPR band of the citrate-capped gold NPs ranged 510-512 nm (Figure 5.1) and for the PEGylated gold NPs was 518-522 nm (Figure 5.2).

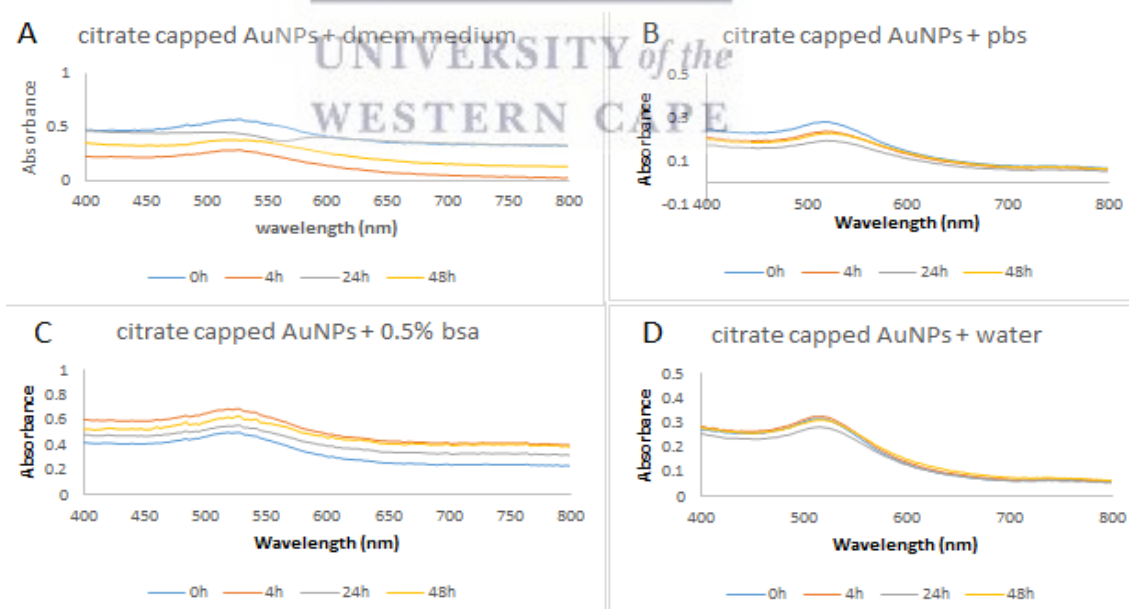


Figure 5.1 UV-Vis absorption spectra of citrate-capped gold nanoparticles showing *in vitro* stability of the nanoparticles in different solutions, A) 10% FBS supplemented DMEM medium (B) PBS (C) 0.5% BSA (D) water at 0h, 4h, 24h and 48h time intervals.

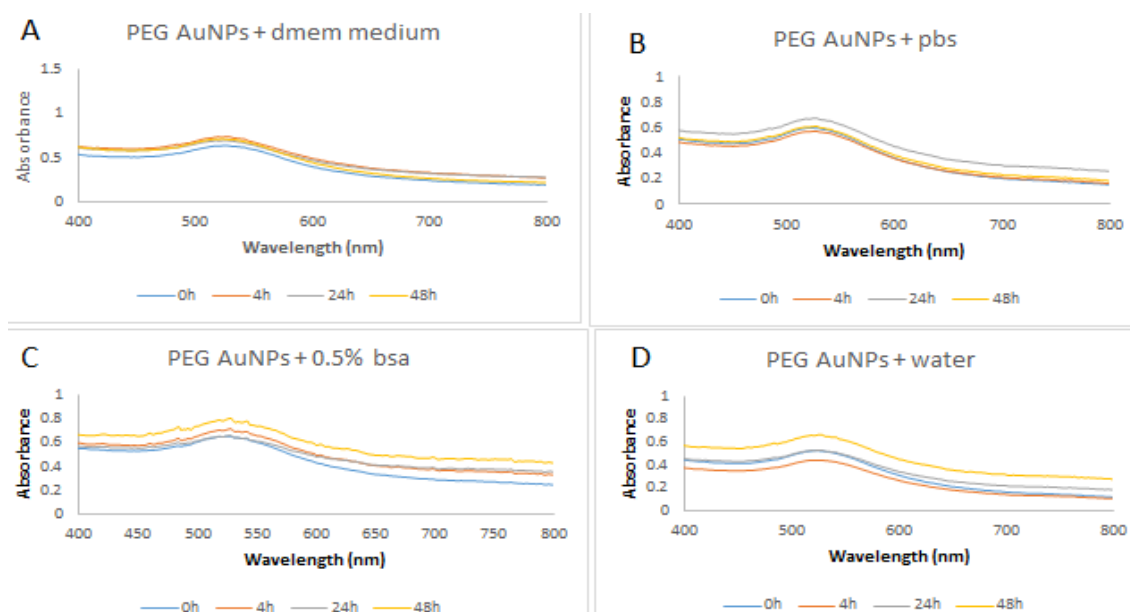


Figure 5.2 UV-Vis absorption spectra of PEGylated gold nanoparticles showing *in vitro* stability of the nanoparticles in different solutions, A) 10% FBS supplemented DMEM medium (B) PBS (C) 0.5% BSA (D) water at 0h, 4h, 24h and 48h time intervals.

Figure 5.1D shows that the citrate-capped gold nanoparticles retained their positions of SPR when dispersed in water, even up to 48 hours. For the citrate-capped gold nanoparticles, their SPR positions shifted to higher wavelengths when dispersed in DMEM medium (**Figure 5.1A**), PBS (**Figure 5.1B**) and 0.5% BSA (**Figure 5.1C**) up to 48 hours. This shift in the SPR indicated that these citrate-capped gold nanoparticles were not stable under these biological solvents. There was flocculation when the citrate-capped gold nanoparticles were dispersed in DMEM medium for 24 hours, and no clear SPR was observed.

Figure 5.2 shows that there was retention of the SPR in all the biological solvents (**Figure 5.2A, B, C and D**). This showed that the PEGylated gold nanoparticles (**Figure 5.2**) were intact, and thereby demonstrated good *in vitro* stability in biological solvents at all exposure durations.

5.1.2 Citrate-capped and PEGylated gold-platinum *in vitro* stability studies

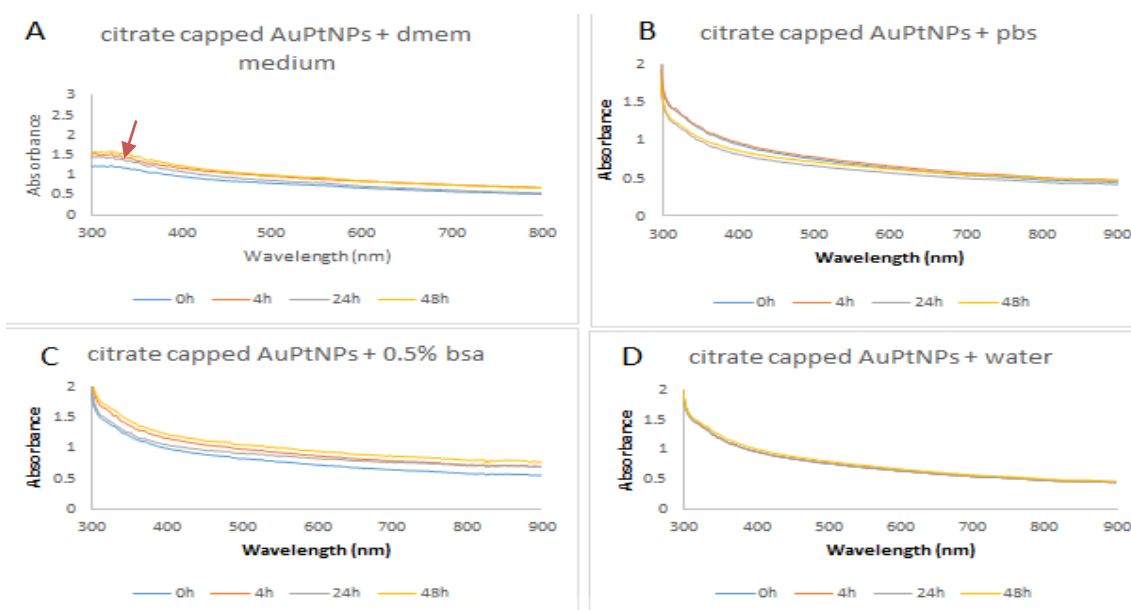


Figure 5.3 UV-Vis absorption spectra of citrate-capped gold-platinum nanoparticles showing *in vitro* stability of the nanoparticles in different solutions, A) 10% FBS supplemented DMEM medium (B) PBS (C) 0.5% BSA (D) water at 0h, 4h, 24h and 48h time intervals.

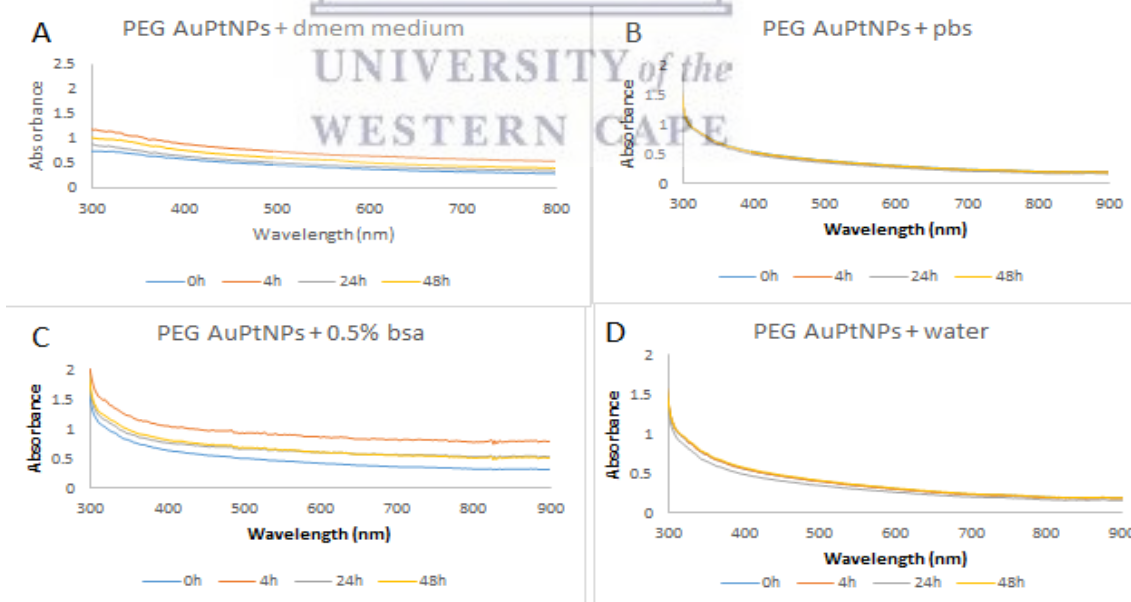


Figure 5.4 UV-Vis absorption spectra of PEGylated gold-platinum nanoparticles showing *in vitro* stability of the nanoparticles in different solutions, A) 10% FBS supplemented DMEM medium (B) PBS (C) 0.5% BSA (D) water at 0h, 4h, 24h and 48h time intervals.

The gold-platinum nanoparticles do not have a SPR peak in the visible region and therefore it was not possible to assess their state of stability by observing a shift in their peak. Instead, the absence of the SPR peak indicates that gold-platinum nanoparticles were stable, because platinum nanoparticles that have aggregated (thus unstable) are known to possess an SPR peak in the visible region.

On the citrate-capped gold-platinum nanoparticles dispersed in PBS, BSA and water, there was no SPR peak observed (**Figure 5.3B-D**). However, when they were dispersed in DMEM medium, there appear to be small SPR peaks between the wavelengths 300-350 nm (arrowed) , possibly indicating instability (**Figure 5.3A**).

All the PEGylated gold-platinum nanoparticles were shown to be stable in all the biological solvents (**Figure 5.4A-D**), as there was no SPR peak visible.

5.2 IN VITRO CYTOTOXICITY ASSESSMENT

The *in vitro* cytotoxic potential of the citrate-capped and PEGylated nanoparticles was evaluated at different concentrations (0, 75, 150 and 225 $\mu\text{g/ml}$) in a glioblastoma (U87) and neuroblastoma (SH SY5Y) cell line for 24 and 48-hour period using the WST-1 assay.

5.2.1 Cytotoxicity of Citrate-capped gold nanoparticles

Results obtained, showed that the citrate-capped gold nanoparticles showed a dose- and time-dependent decrease in both the U87 and SH SY5Y cell viability. The results shown in **Figure 5.5A** indicated that citrate-capped gold nanoparticles caused a significant decrease in cell viability of SH SY5Y cells after a 24-hour exposure with 75 $\mu\text{g/ml}$ (**P < 0.01), 150 $\mu\text{g/ml}$ (**P < 0.001) and 225 $\mu\text{g/ml}$ (**P < 0.01) treatments

respectively as compared to control. The results shown in **Figure 5.5C** indicated that citrate-capped gold nanoparticles caused a significant decrease in cell viability of SH SY5Y cells after a 48-hour exposure with 150 $\mu\text{g/ml}$ (** $P < 0.01$) and 225 $\mu\text{g/ml}$ (***) ($P < 0.001$) treatments, respectively as compared to control. However, there was no significant decrease at 75 $\mu\text{g/ml}$ compared to the control.

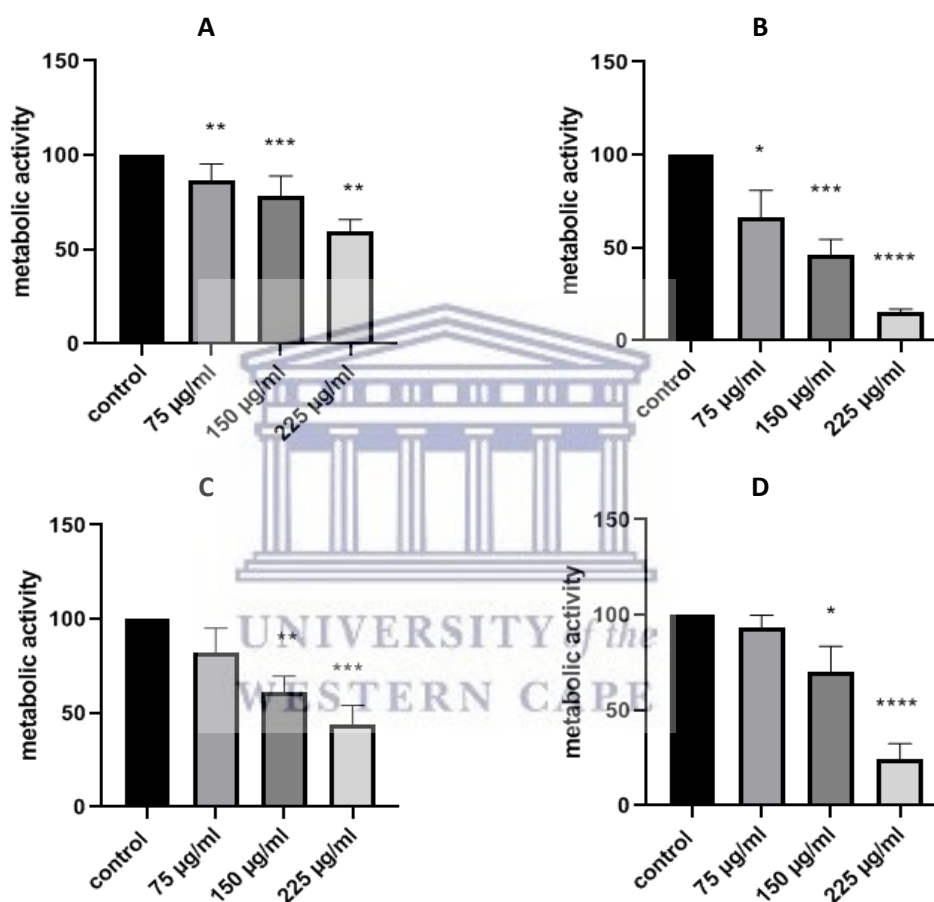


Figure 5.5 Effects of citrate-capped gold nanoparticles on the viability of SH SY5Y (A and C) and U87 (B and D) cell lines evaluated using WST-1 assay after exposure for 24 hours (A and B) and 48 hours (C and D) respectively. The graphs represent means \pm SEM of three independent experiments ($n=3$) using GraphPad Prism 8 statistical software. Statistically significant differences in concentrations relative to the control are marked by asterisks *, **, ***, **** representing $P < 0.5$, 0.01, 0.001 and 0.0001, respectively.

Results obtained, showed that the citrate-capped gold NPs showed a dose- and time-dependent decrease in both the U87 and SH SY5Y cell viability. The results shown in **Figure 5.5A** indicated that citrate-capped gold NPs caused a significant decrease in cell viability of SH SY5Y cells after a 24-hour exposure with 75 $\mu\text{g/ml}$ (** $P < 0.01$), 150 $\mu\text{g/ml}$ (*** $P < 0.001$) and 225 $\mu\text{g/ml}$ (** $P < 0.01$) treatments respectively as compared to control. The results shown in **Figure 5.5C** indicated that citrate-capped gold NPs caused a significant decrease in the viability of SH SY5Y cells after 48-hour exposure with 150 $\mu\text{g/ml}$ (** $P < 0.01$) and 225 $\mu\text{g/ml}$ (*** $P < 0.001$) treatments, respectively compared to control. However, there was no significant decrease at 75 $\mu\text{g/ml}$ compared to the control.

The results shown in **Figure 5.5B** indicated that citrate-capped gold NPs caused a significant decrease in cell viability of U87 cells after a 24-hour exposure to 75 $\mu\text{g/ml}$ (* $P < 0.5$), 150 $\mu\text{g/ml}$ (*** $P < 0.001$) and 225 $\mu\text{g/ml}$ (**** $P < 0.0001$) treatments respectively as compared to control. The results shown in **Figure 5.5D** indicated that citrate-capped gold NPs caused a significant decrease in the viability of the U87 cells after a 48-hour exposure to 150 $\mu\text{g/ml}$ (* $P < 0.1$) and 225 $\mu\text{g/ml}$ (**** $P < 0.00*1$) treatments, respectively compared to the control. However, there was no significant decrease at 75 $\mu\text{g/ml}$ compared to the control.

5.2.2 Cytotoxicity of Citrate-capped gold-platinum nanoparticles

Citrate-capped gold-platinum NPs showed a time and dose-dependent decrease in cell viability as seen in the significant difference between the control and treated cells. The results shown in **Figure 5.6A** indicated that citrate-capped gold-platinum NPs caused a significant decrease in the viability of SH SY5Y cells after a 24-hour exposure to 75 $\mu\text{g/ml}$ (* $P < 0.5$), 150 $\mu\text{g/ml}$ (* $P < 0.5$) and 225 $\mu\text{g/ml}$ (* $P < 0.5$) treatments respectively

as compared to the control. **Figure 5.6C** shows a significant decrease in the viability of SH SY5Y cells compared to the control following a 48-hour exposure to citrate-capped gold NPs at 150 $\mu\text{g/ml}$ ($***P < 0.001$) and 225 $\mu\text{g/ml}$ ($***P < 0.001$) treatments, respectively. However, no significant decrease was seen at 75 $\mu\text{g/ml}$.

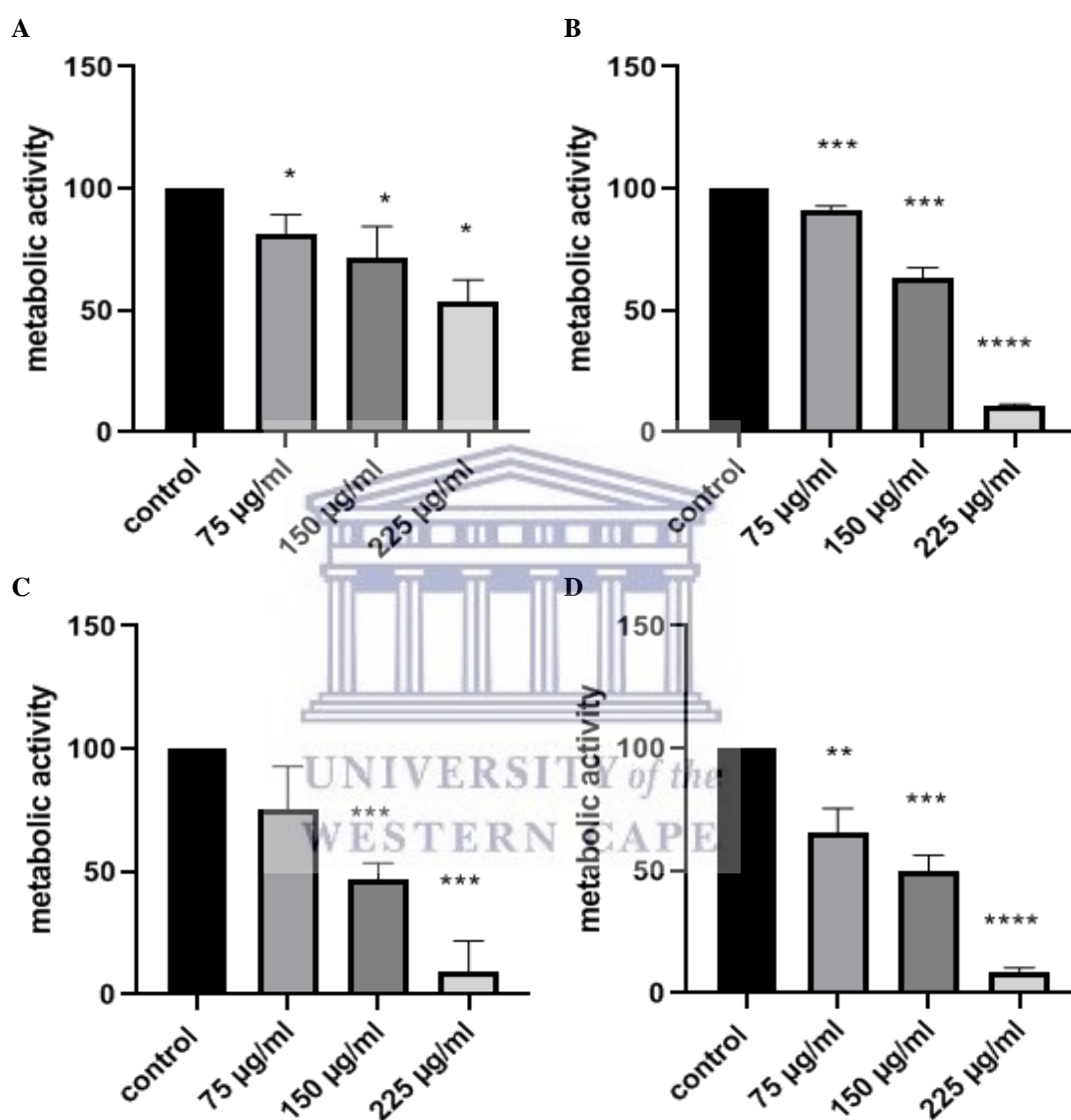


Figure 5.6 Citrate-capped gold-platinum nanoparticles effect on the viability of SH SY5Y (A and C) and U87 (B and D) cell lines evaluated using WST-1 assay after exposure for 24 hours (A and B) and 48 hours (C and D). The graphs represent mean \pm SEM of three independent experiments ($n=3$) using GraphPad Prism 8 statistical software. Statistically significant differences in concentrations relative to the control are marked by asterisks *, **, ***, **** representing $P < 0.5$, 0.01, 0.001 and 0.0001, respectively.

The results shown in **Figure 5.6B** indicated that citrate-capped gold-platinum nanoparticles caused a significant decrease in cell viability of U87 cells after a 24 hour exposure with 75 $\mu\text{g/ml}$ ($***P < 0.001$), 150 $\mu\text{g/ml}$ ($***P < 0.001$) and 225 $\mu\text{g/ml}$ ($****P < 0.0001$) treatments respectively as compared to control. The results shown in **Figure 5.6D** indicated that citrate-capped gold nanoparticles caused a significant decrease in cell viability of U87 cells after a 48-hour exposure with 75 $\mu\text{g/ml}$ ($**P < 0.01$), 150 $\mu\text{g/ml}$ ($***P < 0.001$) and 225 $\mu\text{g/ml}$ ($****P < 0.0001$) treatments, respectively as compared to control.

5.2.3 Cytotoxicity of PEGylated gold nanoparticles

It was observed that the PEGylated gold nanoparticles showed a dose-and time-dependent decrease in both the U87 and SH SY5Y cell viability. The results shown in **Figure 5.7A** indicated that PEGylated gold nanoparticles caused a significant decrease in cell viability of SH SY5Y cells after a 24 hour exposure to 75 $\mu\text{g/ml}$ ($***P < 0.001$), 150 $\mu\text{g/ml}$ ($**P < 0.01$) and 225 $\mu\text{g/ml}$ ($****P < 0.0001$) treatments respectively as compared to control. The results shown in **Figure 5.7C** indicated that PEGylated gold nanoparticles caused a significant decrease in cell viability of SH SY5Y cells after a 48-hour exposure to 75 $\mu\text{g/ml}$ ($*P < 0.5$), 150 $\mu\text{g/ml}$ ($**P < 0.01$) and 225 $\mu\text{g/ml}$ ($***P < 0.001$) treatments, respectively as compared to control.

The results shown in **Figure 5.7B** indicated that citrate-capped gold nanoparticles caused a significant decrease in cell viability of U87 cells after a 24-hour exposure to 75 $\mu\text{g/ml}$ ($**P < 0.01$), 150 $\mu\text{g/ml}$ ($****P < 0.0001$) and 225 $\mu\text{g/ml}$ ($****P < 0.0001$) treatments respectively as compared to control. **Figure 5.7D** indicated that PEGylated gold nanoparticles caused a significant decrease in cell viability of U87 cells after a 48-

hour exposure to 75 $\mu\text{g/ml}$ (** $P < 0.01$), 150 $\mu\text{g/ml}$ (** $P < 0.01$) and 225 $\mu\text{g/ml}$ (**** $P < 0.0001$) treatments, respectively as compared to control.

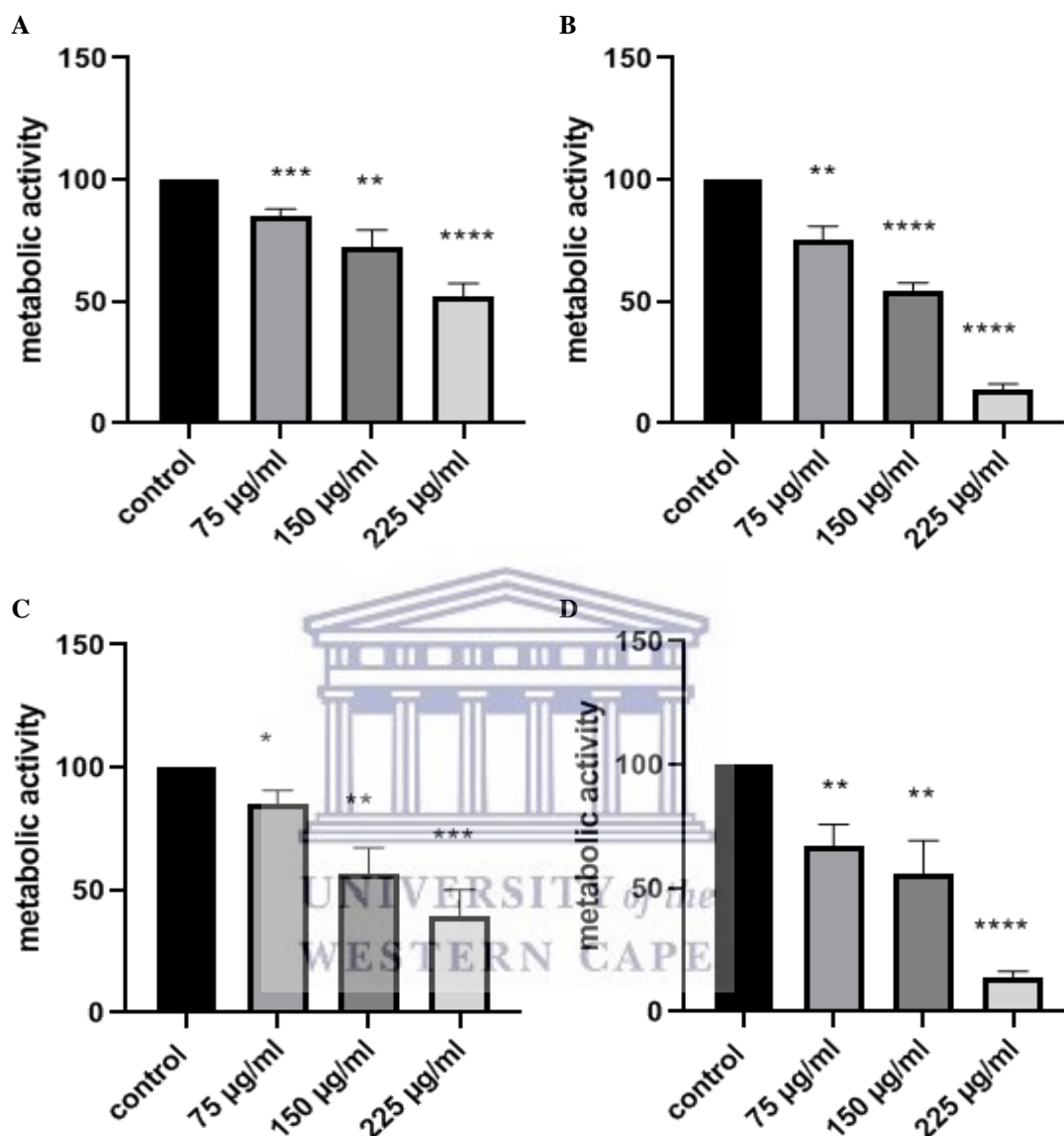


Figure 5.7 PEGylated gold nanoparticles effect on the viability of SH SY5Y (A and C) and U87 (B and D) cell lines evaluated using WST-1 assay after exposure for 24 hours (A and B) and 48 hours (C and D). The graphs represent mean \pm SEM of three independent experiments ($n=3$) using GraphPad Prism 8 statistical software. Statistically significant differences in concentrations relative to the control are marked by asterisks *, **, ***, **** representing $P < 0.05$, 0.01, 0.001 and 0.0001, respectively.

5.2.4 Cytotoxicity of PEGylated gold-platinum nanoparticles

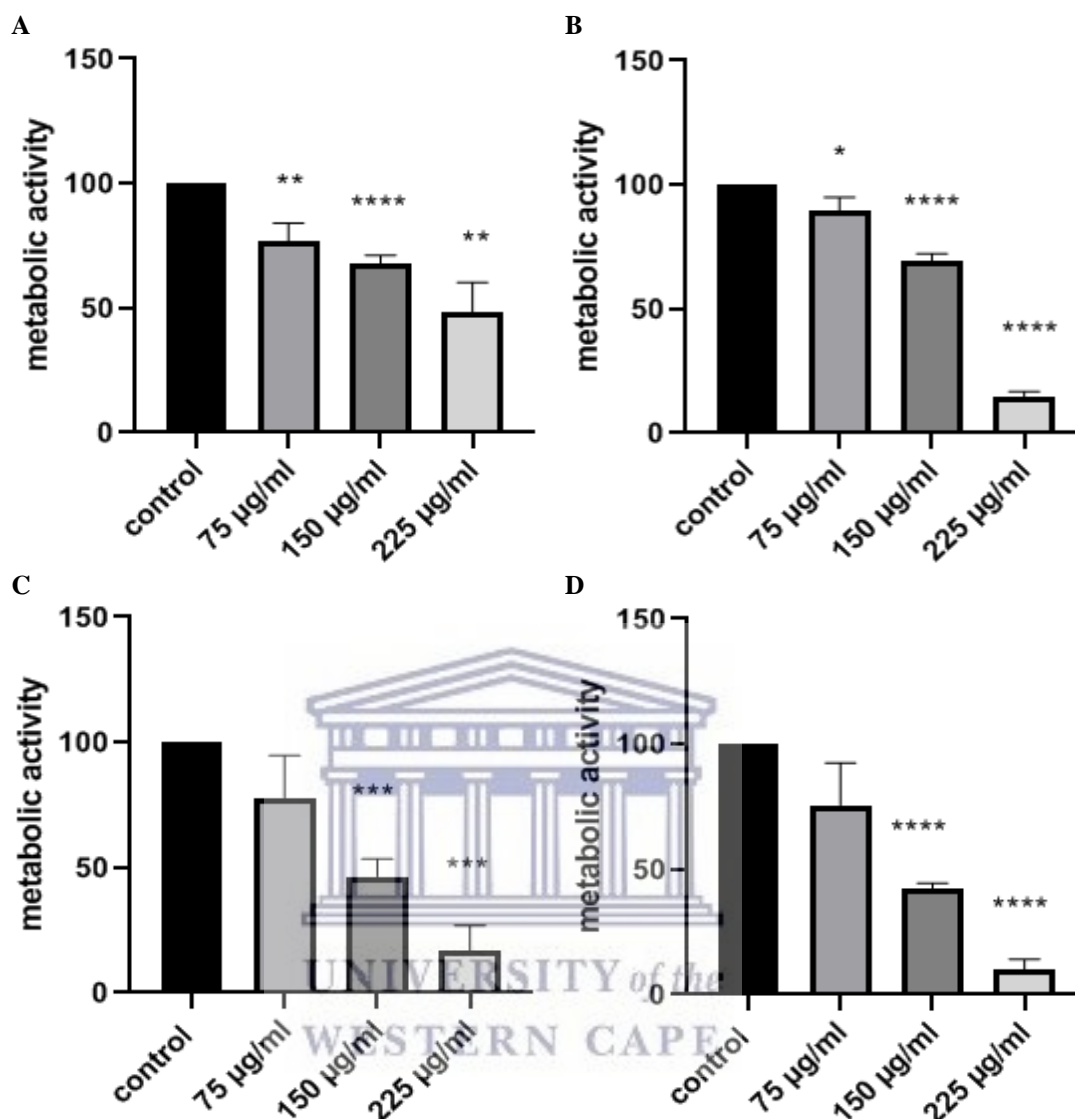


Figure 5.8 PEGylated gold-platinum nanoparticles effect on the viability of SH SY5Y (A and C) and U87 (B and D) cell lines evaluated using WST-1 assay after exposure for 24 hours (A and B) and 48 hours (C and D). The graphs represent mean \pm SEM of three independent experiments (n=3) using GraphPad Prism 8 statistical software. Statistically significant differences in concentrations relative to the control are marked by asterisks *, **, ***, **** represent P < 0.5, 0.01, 0.001 and 0.0001, respectively.

Results obtained showed that the PEGylated gold-platinum nanoparticles showed a dose- and time-dependent decrease in both the U87 and SH SY5Y cell viability. **Figure 5.8A** shows that PEGylated gold-platinum nanoparticles caused a significant decrease in cell viability of SH SY5Y cells after a 24-hour exposure to 75 $\mu\text{g/ml}$ (**P < 0.01), 150 $\mu\text{g/ml}$ (****P < 0.0001) and 225 $\mu\text{g/ml}$ (**P < 0.01) treatments respectively as compared to control. **Figure 5.8C** shows that PEGylated gold-platinum nanoparticles caused a significant decrease in cell viability of SH SY5Y cells after a 48-hour exposure to 150 $\mu\text{g/ml}$ (***P < 0.001) and 225 $\mu\text{g/ml}$ (***P < 0.001) treatments, respectively as compared to control. However, there was no significant decrease at 75 $\mu\text{g/ml}$ compared to the control.

The results shown in **Figure 5.8B** indicated that PEGylated gold-platinum nanoparticles caused a significant decrease in cell viability of U87 cells after a 24-hour exposure to 75 $\mu\text{g/ml}$ (*P < 0.5), 150 $\mu\text{g/ml}$ (****P < 0.0001) and 225 $\mu\text{g/ml}$ (****P < 0.0001) treatments respectively as compared to control. The results shown in **Figure 5.8D** indicated that PEGylated gold-platinum nanoparticles caused a significant decrease in cell viability of U87 cells after a 48-hour exposure with 150 $\mu\text{g/ml}$ (****P < 0.0001) and 225 $\mu\text{g/ml}$ (****P < 0.0001) treatments, respectively as compared to control. However, there was no significant decrease at 75 $\mu\text{g/ml}$ compared to the control.

5.2.5 Determination of the IC₅₀ concentrations

A dose-response decrease in the viability of U87 and SH SY5Y cells was observed for all the treatments after 24 and 48 hours. The IC₅₀ is the concentration of the nanoparticles that causes metabolic response to be reduced by half. The IC₅₀ values of the PEGylated nanoparticles were determined and are presented in the table below.

Time (h)	PEGylated AuNPs ($\mu\text{g/ml}$)		PEGylated AuPtNPs ($\mu\text{g/ml}$)	
	<i>SH SY5Y</i>	<i>U87</i>	<i>SH SY5Y</i>	<i>U87</i>
24	319.3	125.5	253.2	182.1
48	206.0	116.7	122.3	103.6

Table 5. 1 IC_{50} values of SH SY5Y and U87 cells treated with PEGylated gold nanoparticles and PEGylated gold-platinum nanoparticles for 24 and 48 hours respectively. The IC_{50} values were obtained from Graphpad Prism 8 statistical software.

As shown in Table 5.1, the IC_{50} values following treatment with PEGylated gold nanoparticles and incubation at 24 and 48 h respectively were 319.3 and 206.0 $\mu\text{g/ml}$ for the SH SY5Y cells, and 125.5 and 116.7 $\mu\text{g/ml}$ for the U87 cells respectively. In addition, the IC_{50} values following treatment with the PEGylated gold-platinum nanoparticles and incubation at 24 and 48 h respectively were 253.2 and 122.3 $\mu\text{g/ml}$ for the SH SY5Y cells, and 182.1 and 103.6 $\mu\text{g/ml}$ for the U87 cells respectively. PEGylated gold-platinum nanoparticles were more sensitive than the PEGylated gold nanoparticles.

The lowest IC_{50} value of the PEGylated gold and gold-platinum nanoparticles for each cell line were used for the subsequent experiments, that is, 206.0 and 122.3 $\mu\text{g/ml}$ of PEGylated gold and gold-platinum nanoparticles for SH SY5Y cells, respectively. Similarly, the lowest IC_{50} values for U87 treated cells were 116.7 and 103.6 $\mu\text{g/ml}$ for PEGylated gold and gold-platinum nanoparticles, respectively. Therefore, all the subsequent experiments were treated with these IC_{50} values for 48 hours, except for the ICP-MS experiment, which was performed using the 24-hour IC_{50} value.

5.3 MORPHOLOGICAL CHANGES

A Carl Zeiss light inverted microscope was used for monitoring microscopic observations. With this method, the untreated cells (control) were compared with cells

treated with the different IC_{50} concentrations of the PEGylated gold and gold-platinum nanoparticles of the different cell lines.

SH SY5Y cells

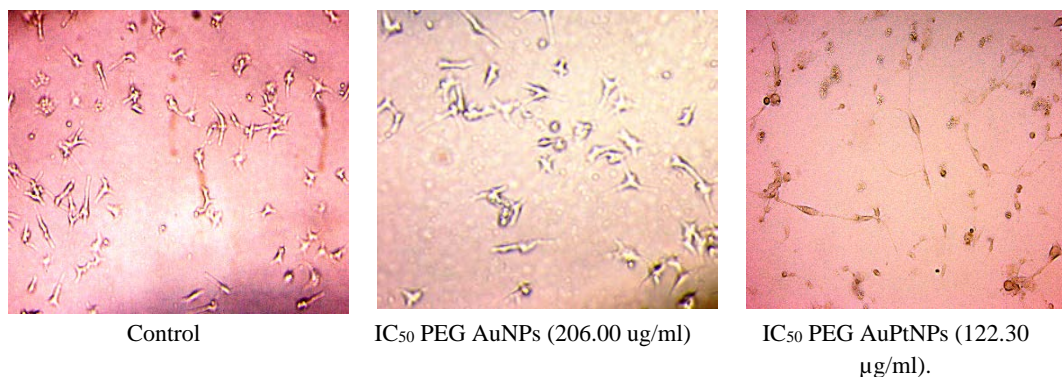


Figure 5.9 Morphology of control, PEGylated gold nanoparticles and PEGylated gold-platinum nanoparticles treated SH SY5Y cells. (a) Control; (b) IC_{50} PEG AuNPs (206.00 μ g/ml); (c) IC_{50} PEG AuPtNPs (122.30 μ g/ml).

The images on **Figure 5.9** show that the control cells were adherent to the plate and had neuronal extensions with what appeared to be pyramid-like body shapes possibly due to intact cell membranes. In addition, the cells on the control were not clustered. The cells treated with the PEGylated nanoparticles were round and formed irregular confluent aggregates compared to those of the control. With the IC_{50} PEGylated gold-platinum nanoparticles treated cells, some cells were round and floating.

U87 cells

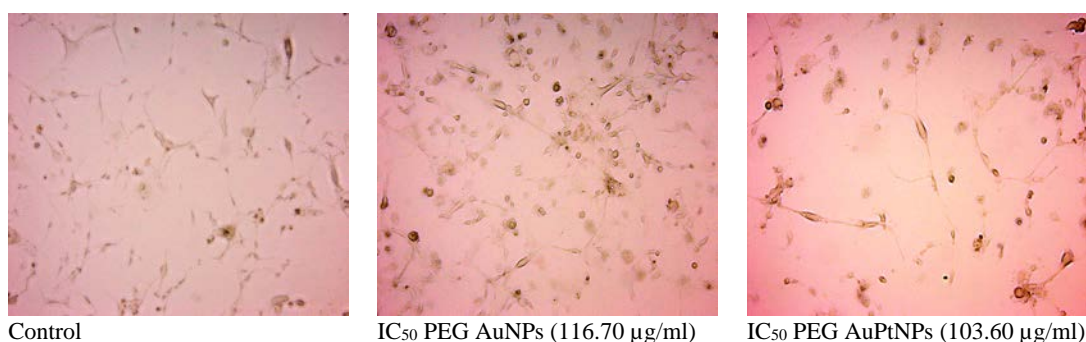


Figure 5.10 Morphology of control, PEGylated gold nanoparticles and PEGylated gold-platinum nanoparticles treated U87 cells. (a) Control; (b) IC₅₀ PEG AuNPs (116.70 µg/ml); (c) IC₅₀ PEG AuPtNPs (103.60 µg/ml).

The images on Figure 5.10 show that the control cells had an astrocyte-like morphology and had long protrusions. They were also adherent to the plate. However, when looking at the treated cells, none of them were significantly altered (except for a few round cells) compared to the control. It is to be noted that there were some floating cells on the IC₅₀ PEGylated gold-platinum nanoparticles treated cells.

5.4 OXIDATIVE STRESS ASSESSMENT

The antioxidant effects of PEGylated gold and gold-platinum nanoparticles on intracellular reactive oxygen species (ROS) was examined by monitoring DCFH-DA and flow cytometry.

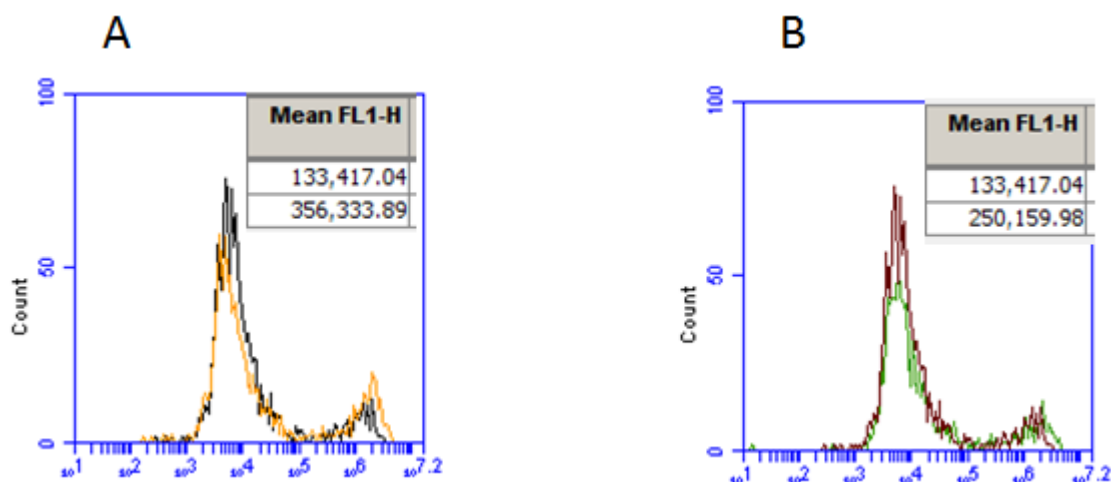


Figure 5.11 Flow cytometric analyses of intracellular ROS using DCF staining on U87 cells is shown with treatment of A) 116.70 µg/ml of PEGylated gold nanoparticles (orange line); and B) 103.60 µg/ml of PEGylated gold-platinum nanoparticles (green line). The black line on graph A indicates the control. The control on graph B is indicated by the maroon line. The horizontal axis shows the fluorescence intensity. On the Mean FL1-H insets, the top values represent the control and the bottom values represent the treated fluorescence intensity of the U87 cells.

As shown in Figure 5.11, the DCFH-DA flow cytometry revealed an increase in intracellular ROS levels from an average fluorescent intensity of 133,417.04 of the control (untreated) to an average fluorescent intensity of 356,333.89 following exposure to PEGylated gold nanoparticles in U87 cells (Figure 5.11A). Treatment with PEGylated gold-platinum nanoparticles attenuated intracellular ROS accumulation on the U87 cells to an average fluorescent intensity of 250,159.98 from 133,417.04 of the control (Figure 5.11B).

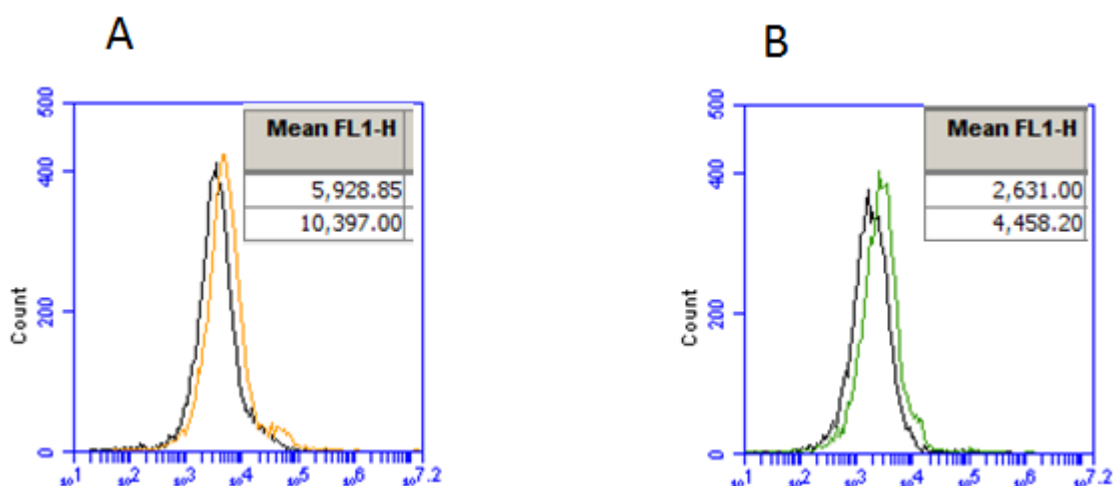


Figure 5.12 Flow cytometric analyses of intracellular ROS using DCF staining on SH SY5Y cells is shown with a treatment of A) 206.00 µg/ml of PEGylated gold nanoparticles (orange line); and B) 122.30 µg/ml of PEGylated gold-platinum nanoparticles (green line). The black line on both graphs indicates the control. The horizontal axis shows the fluorescence intensity. On the Mean FL1-H insets, the top values represent the control and the bottom values represent the treated fluorescence intensity of the SH SY5Y cells.

The flow cytometric analyses showed that intracellular ROS levels were higher PEGylated gold nanoparticles treated SH SY5Y cells with an average fluorescent intensity of 10,397.00 than in control cells with an average fluorescent intensity of 5,928.85 (Figure 5.12A). Treatment with PEGylated gold-platinum nanoparticles had similar effects, where intracellular ROS accumulation increased to an average fluorescent intensity of 4,458.20 from 2,631.00 of control (Figure 5.12B).

5.5 MITOCHONDRIAL MEMBRANE POTENTIAL

The mitochondrial function of the cells was evaluated through measurements of membrane potential, using the fluorescent dye, Rhodamine123 that is known to cross the mitochondrial membrane and accumulate in the mitochondrial matrix, only when the mitochondrial membrane potential (MMP) is preserved (Sakamuru *et al*, 2016). In

case of a loss of the MMP, the Rhodamine123 fluorescence intensity undergoes a significant reduction.

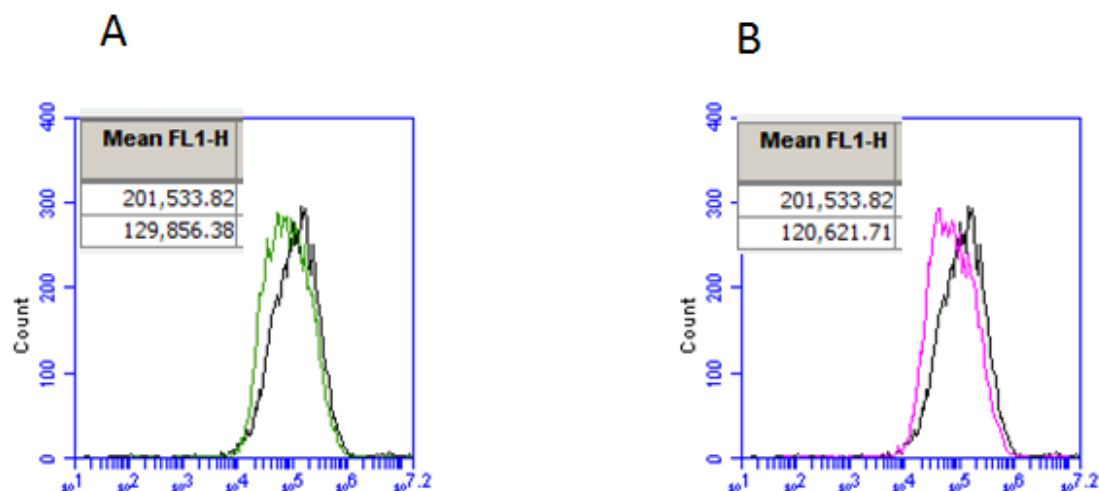


Figure 5.13 The mitochondrial membrane potential was quantitated by a flow cytometric analysis with rhodamine123. The U87 cells were treated with A) 116.70 $\mu\text{g/ml}$ of PEGylated gold nanoparticles (green line); and B) 103.60 $\mu\text{g/ml}$ of PEGylated gold-platinum nanoparticles (pink line). The black line on both graphs indicates the control. The horizontal axis shows the fluorescence intensity. On the Mean FL1-H insets, the top values represent the control and the bottom values represent the treated fluorescence intensity of the U87 cells.

As shown in Figure 5.13A, the mitochondrial incorporation of Rhodamine123 in U87 cells treated with 116.70 $\mu\text{g/ml}$ of PEGylated gold nanoparticles underwent a reduction compared to that measured on untreated cells (with a fluorescent intensity from 201,533.82 of the control to 129,856.32 of the treated). A similar trend was observed in Figure 5.13B where the U87 cells were treated with a concentration of 103.60 $\mu\text{g/ml}$ of PEGylated gold-platinum nanoparticles for 48 hours (with a fluorescent intensity from 201,533.82 of the control to 120,621.71 of the treated).

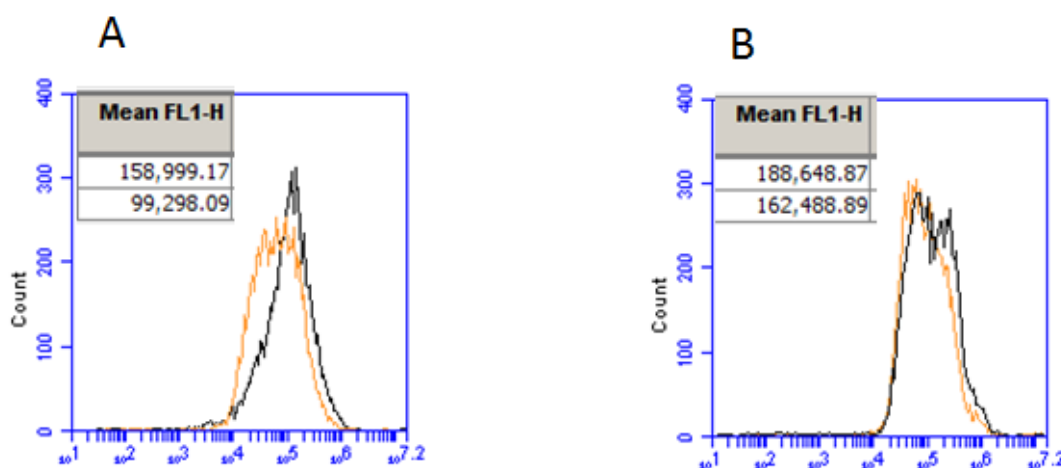


Figure 5.14 The mitochondrial membrane potential was quantitated by a flow cytometric analysis with rhodamine123. The SH SY5Y cells were treated with A) 206.00 µg/ml of PEGylated gold nanoparticles (orange line); and B) 122.30 µg/ml of PEGylated gold-platinum nanoparticles (green line). The black line on both graphs indicates the control. The horizontal axis shows the fluorescence intensity. On the Mean FL1-H insets, the top values represent the control and the bottom values represent the treated fluorescence intensity of the SH SY5Y cells.

As shown in Figure 5.14A, the membrane mitochondrial potential of SH SY5Y cells treated with 206.00 µg/ml of PEGylated gold nanoparticles underwent a reduction compared to that measured on control cells. The fluorescent intensity went from 188,648.87 of the control to 162,488.89 of the treated. A similar trend was observed (Figure 5.14B) when the U87 cells were treated with 122.30 µg/ml of PEGylated gold-platinum nanoparticles for 48 hours (with a fluorescent intensity from 201,533.82 of the control to 120,621.71 of the treated).

5.6 QUANTIFICATION OF THE CELLULAR UPTAKE

The cellular uptake of PEGylated gold and gold-platinum nanoparticles after 24 hours of incubation were quantified with ICP-MS. As shown by the EDS results, PEGylated gold nanoparticles are made up of metal gold elements, whereas PEGylated gold-platinum nanoparticles are made up of both gold and platinum elements. These elements were endocytosed by U87 and SH SY5Y cells and were quantified.

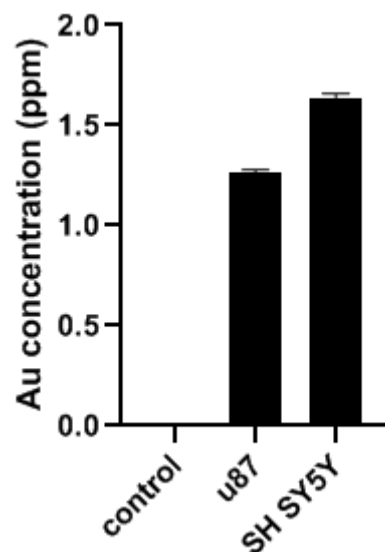


Figure 5.15 Cellular uptake of the IC₅₀ PEGylated gold nanoparticles concentration by U87 and SH SY5Y cells. The number of gold ions endocysed by the cells is quantified.

As shown by the EDS results in the chapter 4 (Figure 4.8), PEGylated gold nanoparticles are composed of metal gold elements. The U87 cells and SH SY5Y cells were treated with 125.5µg/ml and 319.3µg/ml of PEGylated gold nanoparticles, respectively. The ICP-MS ionized the PEGylated gold nanoparticles and quantified the gold ions inside the cells. Figure 5.15 shows a concentration of 1.35 ppm and 1.66 ppm of the gold ions was taken up by the cells, respectively.

Figure 5.16 shows the amounts of gold and platinum ions that were taken up by the U87 and SH SY5Y cells when they were incubated with 182.1µg/ml and 253.2µg/ml PEGylated gold-platinum nanoparticles, respectively, for 24 hours. PEGylated gold-platinum was ionized by the ICP-MS to form gold and platinum ions. These ions were quantified.

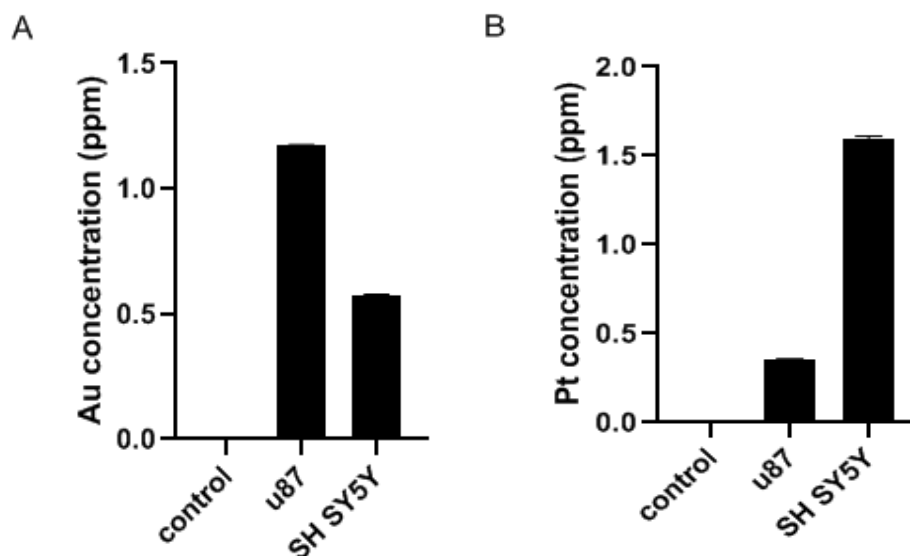


Figure 5.16 Cellular uptake of the IC₅₀ PEGylated gold-platinum nanoparticles concentration by U87 and SH SY5Y cells; A) the number of gold ions endocysed by the cells is quantified, (B) the number of platinum ions endocysed by the cells is quantified.

A concentration of 1.26 ppm (**Figure 5.16A**) of gold ions and 0.48 ppm (**Figure 5.16B**) of platinum ions was quantified inside the U87 cells. Also, it was shown that the intracellular gold and platinum ions concentration was 0.66 ppm (**Figure 5.16A**) and 1.63 ppm (**Figure 5.16B**) for SH SY5Y cells, respectively.

CHAPTER SIX

DISCUSSION

Homeostasis is the ability of biological systems to maintain a stable internal environment within narrow limits (Kotas and Medzhitov, 2015). The nervous system plays an important role in maintaining homeostasis by controlling and regulating other parts of the body (Butler, 2000). However, this important function can be compromised when the cells of the nervous system become cancerous. Two of the major cancers of the nervous system include glioblastoma multiforme (GBM) and neuroblastoma (NB). Current treatment for these cancers could involve a combination of surgery, radiotherapy and chemotherapy. These types of treatments have many limitations including specificity and selectivity to the target (Bianchi *et al.*, 2010).

The use of polyethylene glycol (PEG) is an innovative and reliable method in cancer treatment because of the ability of this compound to conjugate with proteins, enzymes, nanoparticles, liposomes and low molecular weight drugs. PEGylated metallic nanoparticles have been shown to have many advantages including: enhanced therapeutic efficacy, increased serum half-life, prolonged circulation time and protection from reticuloendothelial cells (Mishra *et al.*, 2016).

The purpose of this study was to synthesize and characterize functionalized metallic nanoparticles and evaluate their cytotoxic properties against nervous system cancer cell lines.

6.1 PHYSIOCHEMICAL PROPERTIES OF NANOPARTICLES

6.1.1 Synthesis of nanoparticles and Ultraviolet–visible spectroscopy

The nanoparticles were synthesized by using a chemical reduction method. In this method, a reducing agent donates electrons to metal ions. Metal ions accept these electrons, resulting in them to be reduced to zero valence metal atoms (nuclei). These nuclei cluster together and grow until a capping agent is introduced into the reaction, where it adsorbs into the surface of the nanoparticles in order to avoid overgrowing and aggregation on the nanoparticles (Phan and Nguyen, 2017). The chemical reduction of metal ions to metal nanoparticles is well reported in literature (Benaissi *et al.*, 2010; Abdulghani and Hussain, 2014).

6.1.1.1 Gold nanoparticles

The citrate-capped gold nanoparticles were synthesized using a modified chemical reduction method as previously described by Oliveira *et al.*, (2017). Sodium borohydride is a strong reducing agent that was used to reduce gold ions (Au^{3+}) to gold atoms (Au^0) and these atoms clustered until capped with citrate. Citrate-capped gold nanoparticles were thus formed and appeared as a red solution. Pluchery *et al.*, (2013) also reported on citrate-capped gold nanoparticles that were red in colour. This red colour is due to small gold nanoparticles reflecting red light, while absorbing blue light (Al-Qadi and Saadah, 2015). These citrate-capped gold nanoparticles were then functionalized with PEG using a modified method by Sosibo *et al.*, (2015). The thiols on the PEG interacted with the surface of the nanoparticles via covalent bonds.

The synthesis of these citrate-capped and PEGylated gold nanoparticles was confirmed with the UV-Vis spectra. An important characteristic of the UV-Vis spectra is the

surface plasmon resonance (SPR) which is caused by a collective oscillation of free electrons (conduction band electrons) on the surface of the nanoparticles, driven by the incident electric field (Huang and El-Sayed, 2010). This results in the absorption and scattering of incident light, which leads to an absorption band (also called SPR band) (Ahmad *et al.*, 2018). The position and width of this band is influenced by the size, shape and agglomeration state of the nanoparticles.

In this study, the synthesized citrate-capped and “PEGylated” gold nanoparticles showed well-defined, narrow absorption bands, with typical surface SPR peaks that are characteristic of gold nanoparticles, which are normally between 500-550 nm (Das and Dhar, 2014).

The citrate-capped gold nanoparticles had an absorption band at around 510 - 512 nm. For PEGylated gold nanoparticles, an absorption band was observed at around 518- 520 nm. This suggests that the PEGylated gold nanoparticles had a bigger particle size than citrate-capped gold nanoparticles (Shi *et al.*, 2012). Nanoparticles with increased size absorb red light at longer wavelengths and this way some blue light is reflected, hence the PEGylated gold nanoparticle solution appeared purplish in colour. This finding is similar to previous findings by Tejamaya *et al.*, (2012), whereby citrate-capped nanoparticles absorbed blue light (shorter wavelengths) and PEGylated nanoparticles absorbed red light (longer wavelengths).

Other important optical properties of gold nanoparticles that were characterized in this study include shape and size distribution. The width and symmetry of the SPR band can be applied to measure these optical properties. Gold nanoparticles with a single narrow and evenly distributed absorption band are said to be monodispersed and spherical, respectively (Kaur *et al.*, 2016). Abdelghany *et al.*, (2017) also reported that

symmetric and narrow absorption band indicate spherical nanoparticles with a narrow size distribution. Therefore, both the citrate-capped and PEGylated gold nanoparticles were spherical and monodispersed since their absorption bands were narrow and evenly symmetrical. Dzimitovics *et al.*, (2016) reported that nanoparticles with multiple peaks on the UV-Vis spectra have different shapes other than spherical. Gold nanoparticles with two peaks are rods and those with three peaks are triangles (Pourali *et al.*, 2017).

6.1.1.2 Gold-platinum nanoparticles

Citrate-capped gold-platinum bNPs were formed by chemically reducing Au³⁺ ions and Pt⁶⁺ ions into Au⁰ and Pt⁰ atoms in the presence of sodium borohydride. This was a modified method of Qu *et al.*, (2011). The size of gold-platinum nanoparticles were limited by the citrate capping. The citrate-capped gold-platinum nanoparticles appeared to be dark brown solution, even after they were PEGylated. This finding is similar to previous results by Chau *et al.*, (2017).

The strong SPR peak that was present in the gold nanoparticles disappeared in the gold-platinum nanoparticles such that, there was no visible peak in the visible region (400-800 nm). Chau *et al.*, (2017) also reported that there were no SPR peaks that were observed in their gold-platinum nanoparticles. The absence of an SPR peak in a UV-Vis spectrum is a common characteristic of platinum nanoparticles (Chopade *et al.*, 2015). Watanabe *et al.*, (2009) reported that there was no SPR peak in the UV-Vis spectra of platinum nanoparticles. However, Dobrucka *et al.*, (2019) and Palma *et al.*, (2016) reported on platinum nanoparticles with SPR peaks in the ultraviolet region (200 – 390 nm). Although, it was revealed that these platinum nanoparticles had agglomerated, hence there were SPR peaks.

It is possible that the platinum nanoparticles suppressed the surface plasma energy of gold nanoparticles in the present study. This happens when bNPs form a core/shell structure, where one metal (shell) covers the other metal (core). It is therefore possible that platinum was the shell that covered the gold (core). Jawad *et al.*, (2019) reported that gold had a preference to be in core due to greater reducing abilities of gold salt as compared to platinum salt. Previous studies by Tan *et al.*, (2017) showed similar findings. Okumu *et al.*, (2016) reported that the UV-Vis spectra of silver-platinum bNPs resembled that of platinum nanoparticles (where silver was the core and platinum the shell). Whereas, Dao *et al.*, (2013) showed that silver-platinum bNPs had a UV-Vis spectra resembled that of silver nanoparticles when platinum was at the core and silver at the shell.

6.1.2 High Resolution Transmission Electron Microscope (HRTEM)

The morphology and core sizes of the dried samples were studied using the High Resolution Transmission Electron Microscope (HRTEM). This microscope uses electron beams to produce images with high resolutions, since the wavelength of electrons is shorter (Kogure, 2013).

It was found that all the citrate-capped and PEGylated nanoparticles were monodispersed and had average core sizes of approximately 5 nm. HRTEM only analysed the core sizes of the nanoparticle without the organic citrate and PEG layers, hence the nanoparticle sizes were approximately the same. This is because the organic citrate and PEG layers had low electron density and were thus not sensitive to HRTEM (Manson *et al.*, 2011).

All the nanoparticles were mostly spherical in shape (which collaborated with the results obtained by the UV-Vis spectra) but the citrate-capped and PEGylated gold-

platinum nanoparticles formed chains. The spherical nanoparticles were connected to each other and formed branches. Platinum nanoparticles and platinum-bNPs have a tendency of having nanoparticles in close contact with each other forming nano-chains (Dao *et al.*, 2013). Chen *et al.*, (2015), Chau *et al.*, (2017) and Grasmik *et al.*, (2018) reported similar morphological findings.

The citrate-capped gold and gold-platinum nanoparticles appeared to have agglomerated. Citrate-capped nanoparticles tend to be stable under normal conditions. Iswarya *et al.*, (2017), Li *et al.*, (2018) and Contreras-Trigo *et al.*, (2018) have all synthesized spherical citrate-capped nanoparticles that did not aggregate. However, citrate-capped nanoparticles are fragile and tend to aggregate upon exposure to various stressors such as centrifugation (Alkiliary *et al.*, 2014). The cause of this agglomeration in this present study cannot be pin-pointed to a specific stressor. Although, the centrifugation process could have been the cause of this agglomeration because citrate molecules are weakly bound to the surface of nanoparticles and can be easily removed from the surface of nanoparticles (Chee and Lee, 2012). Tejamaya *et al.*, (2012) showed similar findings.

6.1.3 Energy-dispersive X-ray spectroscopy (EDS)

The compositional analysis of the nanoparticles was carried out by the Energy-dispersive X-ray spectroscopy (EDS). EDS is a technique that relies on the interaction between some source of X-ray radiation and sample (Neikov *et al.*, 2019).

The EDS spectra results of both the citrate-capped and PEGylated gold nanoparticles were quite similar. They indicated the presence of the metallic gold (Au) with a strong peak at 2.12 keV. There were also other weak metallic Au peaks that were observed. Ghann, *et al.*, (2011), Dzimitrowicz *et al.*, (2016) and Mioc *et al.*, (2018) have reported

similar patterns of metallic Au peaks, with the strongest peak at 2.12 keV. This suggests that gold nanoparticles were indeed synthesized and that gold nanoparticles in general have the same EDS spectra, despite their surface chemistry.

Citrate-capped and PEGylated gold-platinum nanoparticles showed multiple peaks of gold and platinum metals, with the highest at 2.12 keV. This confirmed the synthesis of gold-platinum nanoparticles. There were some peaks of Au and platinum (Pt) that were at the same energy levels, indicating that in bNPs, the metal distribution may have been constant at some points. Similar findings were reported by Jawad *et al.*, (2019) and Olajire *et al.*, (2017).

The electron beam that was used in these EDS measurements had a diameter that was larger than the diameter of the nanoparticles, hence elemental composition obtained also reflected the composition of both particle and its elemental surroundings. Citrate and PEG are organic compounds that are made up of carbon (C), hydrogen (H) and oxygen (O). The elemental O and C that were observed in the EDS spectra, suggesting that PEG and citrate molecules were present on the surface of the nanoparticles. The H is not present in the spectra because it has a low atomic number and it is difficult to detect low numbered elements (Kumar *et al.*, 2016). Similar findings were reported by Xu *et al.*, (2018).

The peak of other elements observed in the EDS results were impurities. The presence of nickel (Ni), C and copper (Cu) could have been due to the carbon coated copper grids and carbon coated nickel TEM grids (Shittu *et al.*, 2017). These TEM grids played a role in obtaining high electrical conductivity to prevent sample charging (Alvarez-Fraga *et al.*, 2019). The chloride (Cl) might have originated from Chloroplatinic acid (H₂PtCl₆) which was the precursor of gold-platinum nanoparticles.

6.1.4 Fourier-transform infrared spectroscopy (FTIR)

FTIR was carried out in order to understand the nature of the surface chemistry (potential functional groups that are on the surface) of the nanoparticles.

The citrate-capped gold and gold-platinum nanoparticles, have the citrate molecules on their surface. Citrate is a compound that is composed of three carboxylic acids. Carboxylic acids have absorption in the infrared region due the presence of carbonyl groups and hydroxyl groups (Ouellette *et al.*, 2015). A typical FTIR spectra of a citrate molecule has OH stretching, C=O stretching of COOH and asymmetric COO-stretching (Ou *et al.*, 2008). The citrate-capped gold and gold-platinum nanoparticles had symmetric stretching vibrations of carboxylate group COO⁻ at 1112 and 1167 cm⁻¹, respectively.

Furthermore, there were anti-symmetric stretching vibrations of COO⁻ at 1636 and 1625 cm⁻¹ for citrate-capped gold and gold-platinum, respectively. There was also a hydroxyl group OH infrared band at 3406 and 3466 cm⁻¹ for citrate-capped gold and citrate-capped gold-platinum, respectively. The exhibition of COO⁻ and OH groups generally indicate that the citrate ions have been linked to the surface of the nanoparticles as previously reported by Wulandari *et al.*, (2015). Park *et al.*, (2014) also reported similar findings, where the carbonyl and hydroxyl groups were observed.

FTIR was also assessed to confirm the covalent functionalization of PEG on the surface of the nanoparticles. PEG is a polyether that has a wide range of terminal functional groups (Pramanik *et al.*, 2015). In this study, it had an OH group. The FTIR absorption spectra analysis of PEGylated nanoparticles showed many characteristic peaks. PEGylated nanoparticles usually have peaks that are related to C–OH, C–H, C=O, and C–O bonds (Chen *et al.*, 2012; Alkilany *et al.*, 2015). The prominent peaks in this

current study had stretching vibrations at around 2866 and 1132 cm^{-1} which represent CH_2 of alkane and ether (C-O) stretching, respectively for PEGylated gold nanoparticles. Vibration characteristics at 1620 and 1073 cm^{-1} were observed for PEG gold-platinum nanoparticles, which represented C=O and C-O stretch. At 1399 cm^{-1} , a vibration was observed which represented a CH_2 scissoring. These results tend to suggest that the PEG chain was linked on the surface of the nanoparticles, as previously described in literature (Gajendiran *et al.*, 2014). Also, broad band in the 3300–3500 cm^{-1} region of the PEGylated nanoparticles was attributed to the OH group and suggested that this hydroxyl group played a role in linking the nanoparticles to the PEG chains. The OH band was broader in citrate-capped nanoparticles compared to PEGylated nanoparticles due to the overlapping of the OH band with the C-H band (Ouellette *et al.*, 2015). Khairuddin *et al.*, (2016) reported similar findings.

6.1.5 Dynamic Light Scattering (DLS)

Nanoparticles in suspension undergo Brownian motion. When a laser light is illuminated on these nanoparticles, they scatter the light and the intensity of this scattering light fluctuates. The analysis of this fluctuation yields the hydrodynamic size and size distribution of these nanoparticles (Bauer and Schnapp, 2007).

Hydrodynamic size refers to the overall size of the nanoparticles in a colloidal suspension (Lusvarghi *et al.*, 2018). That is, including the capping and stabilizing agent on the surface. The average hydrodynamic sizes were expected to be larger than the core sizes measured by TEM (Reznickova *et al.*, 2019). The hydrodynamic sizes of citrate-capped nanoparticles were measured to be around 8.5907 ± 0.36905 nm and 8.7045 ± 1.01798 nm for citrate-capped gold and citrate-capped gold-platinum nanoparticles, respectively. Thus, there was an increase compared to the sizes from

TEM. The hydrodynamic sizes of these nanoparticles also increased after they were PEGylated, with PEGylated gold nanoparticles at around 13.33 ± 0.91413 nm and PEGylated gold-platinum nanoparticles at 16.1833 ± 0.98656 nm. These results collaborated well with the FTIR and UV-Vis results, which suggest that PEGylation on the nanoparticles was successful. Previous studies by Manson *et al.*, (2011) and Tejamaya *et al.*, (2012) reported similar results.

The PDI was used to estimate the average dispersity (size distribution) of the nanoparticles in a solution (Masarudin *et al.*, 2015). When the PDI of nanoparticles is greater than 0.5, they are said to be polydispersed and when less than 0.7 (or closer to 0), then they are said to be monodispersed (Nobbmann and Morfesis, 2009). The average PDI of nanoparticles were measured to be around 0.2387 ± 0.5930 , 0.4173 ± 0.5930 , 0.2625 ± 0.1355 and 0.3985 ± 0.6024 for citrate-capped gold nanoparticles, citrate-capped gold-platinum, PEGylated gold nanoparticles and PEGylated gold-platinum nanoparticles, respectively. All of these values were less than 0.7, suggesting that the nanoparticles were monodispersed (Danaei *et al.*, 2018). These results were also well in agreement with previous studies (Arockiya *et al.*, 2014).

The stability of the nanoparticles in water dispersion was analysed by measuring the zeta potential. The zeta potential indicated the magnitude of the repulsive forces between the nanoparticles (Reznickova *et al.*, 2019). As mentioned before, the nanoparticles were capped with citrate in order to limit their size and prevent aggregation. The citrate ions on the surface of citrate-capped nanoparticles provided electrostatic forces that counteracted and exceeded the weak Van der Waals forces in between nanoparticles, preventing agglomeration. Citrate ions thus provided electrostatic stabilization of the nanoparticles (Pfeiffer *et al.*, 2014).

Nanoparticles with a zeta potential of less than -30 mV have excellent stability (Pate and Safier, 2016). The citrate-capped nanoparticles in this study had high zeta potential measurements of -26.27 ± 2.09 mV and -26.22 ± 2.57 mV for citrate-capped gold nanoparticles and citrate-capped gold-platinum, respectively. This suggests that these nanoparticles had moderate/ limited stability. Mahbubul *et al.*, (2009) reported that a zeta potential of less than -20 mV provided limited stability.

The highly negative zeta potential that were obtained in citrate-capped nanoparticles moved closer to zero after PEGylation. PEGylated gold and gold-platinum nanoparticles had a zeta potential of -10.97 ± 0.81 mV and -9.82 ± 1.89 mV, respectively. Nanoparticles with a zeta potential between -10 and +10 mV are considered approximately neutral (Clogston and Patri, 2011). The reason for this drop could be because PEG is a neutral polymer and has a tendency to absorb charged ions, thus the zeta potential moves closer to zero (Wang *et al.*, 2014). Cieslak *et al.*, (2017) and Charmi *et al.*, (2019) reported similar results, whereby PEGylated nanoparticles had a zeta potential that was closer to zero. However, PEG provides a steric stabilization, where its chains cover the surface of the nanoparticles (alternatively, covering the Van der Waals forces) and thus preventing agglomeration. These results are also well matched with the UV-Vis, FTIR and hydrodynamic size in that the PEGylation of the nanoparticles was successful. Previous studies by Nițică *et al.*, (2018) reported similar findings.

6.2 IN VITRO COLLOIDAL STABILITY

Nanoparticles were synthesized in order for potential *in vitro* applications in cancer treatment. The *in vitro* stability of the citrate-capped and PEGylated nanoparticles

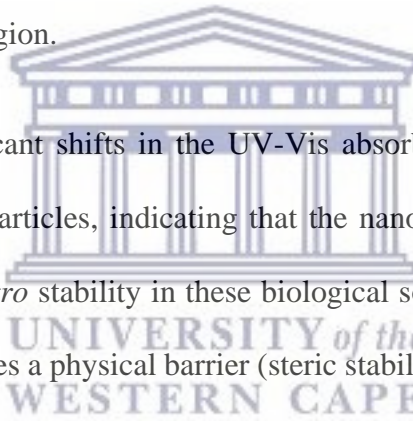
dispersed in water, DMEM medium, PBS and 0.5% BSA for up to 48 hours was assessed using UV-Vis absorption spectra.

Nanoparticles can be stable for long durations when dispersed in water compared to other fluids. The development of nanoparticle-based treatment is for ultimate use in biological systems and in most cases transmitted via the bloodstream and tissue fluids surrounding cells in the human body. These systems are known to have electrolytes, high ionic strength, salt, amino acids and bio-macromolecules (Kononenko *et al.*, 2017). These factors can influence the stability of nanoparticles (Freese *et al.*, 2012). It is therefore important to determine the *in vitro* stability of nanoparticle/drugs for any biological application.

Millipore water was used to disperse the nanoparticles during synthesis. Millipore water has very few charge-carrying ions that may interfere with the nanoparticles. All the results for the nanoparticles (both citrate-capped and PEGylated) were stable when they were dispersed in Millipore water.

Citrate-capped nanoparticles are stabilized by electrostatic forces. Electrostatic stabilization can be disrupted by high ionic strength, salt content and bio-macromolecules (Moore *et al.*, 2015). The ions on the surface of the nanoparticles can be desorbed or replaced by these factors, collapsing the electrostatic stabilization (Alkilany *et al.*, 2014). This results in aggregation of the nanoparticles, as a result of the weak Van der Waals forces are greater. Calderon-Jimenez *et al.*, (2017) reported that the high ionic strength in media resulted in aggregation of nanoparticles that were stabilized electrostatically. Park *et al.*, (2013) reported that citrate-capped nanoparticles agglomerated in the presence of PBS. Manson *et al.*, (2011) also showed that citrate-capped nanoparticles aggregated in the presence of PBS and BSA.

The citrate-capped gold nanoparticles were unstable in these biological solvents (DMEM medium, PBS and BSA), as their SPR band shifted to higher wavelengths. A shift in the wavelength of gold nanoparticles could suggest aggregation. There were small peaks for citrate-capped gold-platinum nanoparticles that were observed when they were dispersed in DMEM medium, suggesting that there was some sort of instability. However, the dispersity of citrate-capped gold-platinum on other biological solvents, there were no absorption bands that were observed. This does not necessarily mean that these nanoparticles were stable under these solvents. Agglomeration in platinum nanoparticles can cause an absorption band to be observed in the UV region of the UV-Vis spectrum. The UV-Vis spectra machine was not powerful enough to cover the whole UV region.



There were no significant shifts in the UV-Vis absorbance spectra observed of the PEGylated gold nanoparticles, indicating that the nanoparticles were intact and thus demonstrating an *in vitro* stability in these biological solvents. PEG is a polymer and unlike citrate, it provides a physical barrier (steric stability) that prevents nanoparticles from aggregating. It has the ability to provide colloidal stability and compatibility in biological media, salts and extreme pH (Guerrini *et al.*, 2018). Manson *et al.*, (2011) reported that PEGylated nanoparticles had stability in PBS and BSA. For the PEGylated gold-platinum nanoparticles, their UV-Vis spectra for the biological solvents did not show an SPR peak for up to 48 hours. This suggests that PEGylated nanoparticles were stable, due to the physical barrier on their surface.

6.3 CYTOTOXICITY AND QUANTIFICATION OF CELLULAR UPTAKE STUDIES

In this present study, it was observed that treatment of glioblastoma U87 and neuroblastoma SH SY5Y cell lines with citrate-capped and PEGylated nanoparticles

resulted in a dose-and time-dependent decrease in viability which were statistically significant when compared with the controls.

It has been reported that gold nanoparticles have very little toxicity to normal cells. Khan *et al.*, (2014) also reported on gold nanoparticles being non-toxic to cells. This non-toxicity, together with other properties (biocompatibility, inert nature and stability) makes gold nanoparticles perfect candidates for drug carriers in cancer treatment (Mioc *et al.*, 2018). However, there are various factors that may influence the cytotoxicity of gold nanoparticles on cancerous cells, such as the surface chemistry. The citrate ions on the surface of citrate-capped nanoparticles have been proposed to have cytotoxic effects. Surapaneni *et al.*, (2018) reported that citrate-capped gold nanoparticles induced cytotoxicity in triple negative breast cancer (TNBC) cells. Bastos *et al.*, 2017 showed that citrate-capped nanoparticles were cytotoxic to HepG2 cell lines, whereas Liu *et al.*, (2014) reported that citrate-capped gold nanoparticles were cytotoxic to A549 lung cancer cell lines.

The toxicity of PEGylated gold nanoparticles appears to be dependent on cell types. Toxicity against some cell lines has been established although in some cells this cytotoxicity was not significant (Zhang *et al.*, 2012). Seol *et al.*, (2013) reported that their synthesized PEGylated gold nanoparticles were non-toxic to EMT-6 cells whereas Tlotleng *et al.*, (2016) reported higher levels of cytotoxicity in the HepG2 cells than in HEK 293 cells. Bastos *et al.*, (2017) also showed that PEG had cytotoxic activity against HepG2 cells. PEG is also cytotoxic against HCC-1937 breast cancer cells (Massard *et al.*, 2018).

Another factor that might have had influenced the significant decrease in cell viability is the chemical composition of the gold-platinum nanoparticles. There are many

platinum-based products that are cytotoxic to cancerous cells, such as cisplatin, oxaliplatin and carboplatin (Chen *et al.*, 2013). Platinum nanoparticles have previously been shown to have significant cytotoxic effect on U87 cells (Kutwin *et al.*, 2017). The cytotoxic effects exerted by platinum nanoparticles on cancer cell lines but not normal cells were reported by Bendale *et al.*, (2017) whereas Mohammadi *et al.*, (2013) demonstrated a concentration-dependent toxicity of platinum nanoparticles against the HepG-2 and MCF-7 cells. No studies on neuroblastoma have been reported in literature. The findings on this study suggest that citrate-capped and PEGylated nanoparticles are cytotoxic to U87 and SH SY5Y cells. .

Since only the PEGylated nanoparticles showed stability under the biological solvents in addition to their other advantages such as increasing the circulation half-life of the nanoparticles in the human body, only their IC₅₀ values were determined. Also, PEGylated nanoparticles tend to be taken up more by cells compared to citrate-capped nanoparticles mainly because the latter are anionic. It is known that anionic nanoparticles/molecules tend to bind less efficiently to the negatively charged cell membranes, because they would repel each other (Xie *et al.*, 2017). Thus, PEGylated nanoparticles are neutral (as determined by the zeta potential) and tend to enter cells via the clathrin-mediated endocytosis (CME) pathway (Li *et al.*, 2014). Gold and platinum ions were satisfactorily quantified in the U87 and SH SY5Y cells using ICP-MS method, suggesting that PEGylated gold and gold-platinum nanoparticles were taken up by the cells after an incubation period of 24 hours.

The IC₅₀ values obtained were higher for SH SY5Y cells than the U87 cells, suggesting that these NPs are less sensitive to SH SY5Y cells than U87 cells hence, more nanoparticles may be required in order to elicit a 50% decrease in SH SY5Y cell

viability. This could probably account for why more of the PEGylated nanoparticles were taken up by the SH SY5Y cells (due to high concentration of treatment).

The IC₅₀ values obtained for 48 hours were then used for subsequent experiments, in order to understand the mode of action of the cytotoxicity of PEGylated nanoparticles against the above mentioned cell lines.

6.4 ASSESSMENT OF CYTO-MORPHOLOGICAL CHANGES

Following the cell viability studies, the morphology of the cells was investigated. The control SH SY5Y cells were pyramidal-shaped and no clusters were observed, characteristic of differentiated N-type neuroblastoma cells, known to be less aggressive than the undifferentiated cells (Jögi *et al.*, 2012).

On the other hand, SH SY5Y cells treated with PEGylated gold and gold-platinum nanoparticles appeared to be round-shaped and detached from the surface of the culture dish, consistent with shrinkage in the cytoplasm, which could have led to loss of cell-to-cell contact (Lee *et al.*, 2007). Previous studies by Waseem *et al.*, (2017) showed that treatment with oxaliplatin (a platinum agent) led to cell shrinkage, membrane bleb formation, aggregation, and detachment from the cell surface. Previous studies have also reported similar findings (Pallavicini *et al.*, 2015). Generally, neuroblastoma cell shrinkage has been linked to the programmed cell death process known as apoptosis (Bortner and Cidlowski, 2007).

U87 cells are poorly differentiated cells which are generally astrocyte-like in morphology, with longer protrusions, known to have an aggressive growth pattern, which possibly explains their unchanged morphology after treatment with PEGylated gold and gold-platinum NPs. There were however a few round cells and some cells

were floating. Kutwin *et al.*, (2017) and Li *et al.*, (2012) reported similar findings, where the morphology of U87 did not change significantly. No previous studies were found that reported on the effects of PEGylated NPs on the morphology of U87 cells. However, Hopkins *et al.*, (2018) reported that there was some change in morphology of treated D54MG human glioblastoma cells treated with chemically-functionalized single-walled carbon nanotubes, but such was not significant. It is also possible that the lack of morphological change in the U87 cells was due to the relatively low IC₅₀ values for these cells, implying a limited uptake of the treatment by the cells.

Taken together, these results tend to suggest that treatment with PEGylated gold and gold-platinum nanoparticles may have affected the growth and morphology of both U87 and SH SY5Y cells.

6.5 ASSESSMENT OF OXIDATIVE STRESS

ROS constitutes a pool of highly reactive oxidative species including superoxide anions, hydroxyl radicals, hydrogen peroxides, singlet oxygen, and alpha oxygen (Manke *et al.*, 2013). Elevated levels of intracellular ROS have been related to cytotoxicity (Aithal *et al.*, 2009) and a variety of metallic nanoparticles have been shown to dramatically increase ROS levels (Horie *et al.*, 2011; Thakor *et al.*, 2011; Martínez-Torres *et al.*, 2018).

In this study, oxidative stress was determined by the DCFH-DA assay which measures intracellular levels of ROS. The results obtained indicated an increase in ROS production after a 48 h treatment with the PEGylated gold and gold-platinum nanoparticles. Therefore, it is possible that the observed increase in ROS is one of the main mechanisms of cytotoxicity indicated by damage to intracellular structures. A study by Soenen *et al.*, (2014) showed that treatment of PC12 cells with PEGylated

gold nanoparticles resulted in increased ROS production while Farooq *et al.*, (2018) also showed that treatment of HeLa cells with PEGylated gold nanoparticles resulted in increased ROS production. Similar results were reported for HEK293 cells treated with platinum nanoparticles (Almeer *et al.*, 2018). All the results tend to show that PEGylated gold and gold-platinum NPs caused cytotoxicity by oxidative stress.

6.6 ASSESSMENT OF MITOCHONDRIAL MEMBRANE POTENTIAL (MMP)

High accumulation of ROS has been associated with mitochondrial dysfunction (Sakamuru *et al.*, 2016). Mitochondrial membrane potential ($\Delta\psi_m$) is a major determinant of the state of mitochondria and the cell as a whole (Li *et al.*, 2014). In this study, the mitochondrial membrane potential assay was used in conjunction with the intracellular ROS assay and the results obtained showed that there was a reduction in the mitochondrial membrane potential and an increase in ROS production (Zhao *et al.*, 2018). PEGylated nanoparticles have been reported to induce an increase in ROS production while decreasing the mitochondrial membrane potential (Kim *et al.*, 2017). Previous studies by Huang *et al.*, (2014) reported that PEGylated gold nanoparticles reduced the mitochondrial membrane potential in K562 cells. It can therefore be suggested that the high intracellular ROS was perhaps related to the destruction of the mitochondrial membrane potential (mitochondrial dysfunction) due to intracellular oxidative stress. Previous studies by Zhang *et al.*, (2015) and Wang *et al.*, (2018) have shown that when there was an increase in ROS, there was also a decrease in the mitochondrial membrane potential. It has been reported that intracellular ROS induces apoptosis by reducing the mitochondrial membrane potential. ROS affects the mitochondrial membrane, which down-regulates an anti-apoptotic gene B-cell

lymphoma 2 (BCI-2). This leads to the activation of caspase 3 (which results in apoptosis) (Yuan *et al.*, 2018).

6.7 CONCLUSION

In this study, metallic nanoparticles were chemically synthesized using sodium borohydride as a reducing agent and sodium citrate as a capping agent. These citrate-capped metallic nanoparticles were then functionalized with PEG.

Both these citrate-capped and PEGylated metallic nanoparticles were further characterized using various techniques, including the UV-Vis, HRTEM, EDS, FTIR and DLS to determine their physicochemical properties. The UV-Vis spectra confirmed the synthesis and functionalization of the citrate-capped and PEGylated gold and gold-platinum nanoparticles. The analysis of HRTEM images revealed that all the nanoparticles were spherical, well dispersed with an average core size of approximately 5nm. The EDS results confirmed the elemental compositions of gold and gold-platinum nanoparticles while the FTIR and DLS results confirmed that the nanoparticles were stable, citrate-capped and PEGylated.

In vitro studies showed that the PEGylated nanoparticles were stable in biological solvents. In this study, the PEGylated metallic nanoparticles were taken up by both the U87 and SH SY5Y cell lines and induced a potent decrease in cell viability. Thus, these PEGylated metallic nanoparticles were cytotoxic, possibly mediated by oxidative stress.

Further biological studies to explore the potential development of PEGylated gold and gold-platinum nanoparticles into anticancer drugs are recommended.

6.8 LIMITATIONS

This project experienced some time and budget constraints, necessitating an extension of study beyond the 12 months were initially available for the laboratory experiments, data management and analysis as well as for writing this mini-thesis. The procurement processes for major laboratory consumables took longer than expected while the booking of equipment for sample analysis also contributed to the delay at the different stages of experimentation.

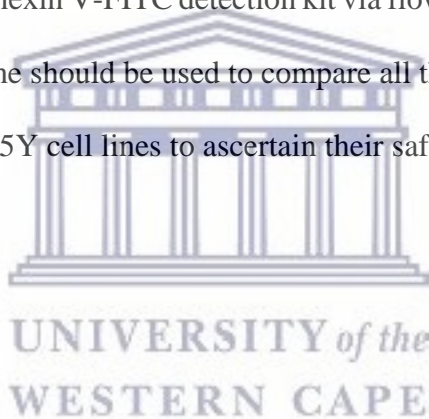
Also, only a few biological studies were found in literature that describe the effects of treatments with gold-platinum bimetallic NPs, hence there were very few reference sources with elaborate methodology for consultation. Thus, findings from this study were largely compared with the results of other bimetallic NPs.

6.9 FUTURE RECOMMENDATIONS

Future studies should focus on broadening the scope of this type of study to include more characterization methods and biological assays. A powerful UV-Vis spectrum that shows the whole UV-Vis region (200-800 nm) and beyond, could help in the observation of the SPR peak of the gold-platinum nanoparticles. Scanning Electron Microscopy (SEM) could be used to augment the TEM results and provide additional information on the morphology of the nanoparticles. Also XRD and SAED assessment could be useful in understanding the crystallinity of the nanoparticles. The nature of the gold-platinum nanoparticles (such as core-shell/ nanoalloy) can be determined by using the small-angle X-ray scattering (ASAXS).

Anti-cancer drugs are usually subjected to sterilization processes hence it would be proper to perform stability studies under an autoclave machine (with high temperatures and pressures) and possibly using the DLS (zeta potential) analysis.

This study investigated the short-term cytotoxic effects using the Cell Proliferation Reagent WST-1. Addition of the trypan blue exclusion assay and a clonogenic assay could help with validation of the cytotoxic potential of these nanoparticles for long-term periods. In addition, since platinum-based compounds have been reported to damage the DNA of cells, it would be suitable to use the comet assay or similar assays to analyze DNA content and damage while cell cycle arrest/apoptosis/necrosis could be evaluated using the Annexin V-FITC detection kit via flow cytometry. Finally, a normal (non-cancerous) cell line should be used to compare all the effects of the nanoparticles on the U87 and SH SY5Y cell lines to ascertain their safety as potential anticancer NP formulations.



REFERENCES

1. Abdelghany, A. M. et al. (2017) 'Effect of Gamma-irradiation on biosynthesized gold nanoparticles using *Chenopodium murale* leaf extract', *Journal of Saudi Chemical Society*. Elsevier, 21(5), pp. 528–537. doi: 10.1016/J.JSCS.2015.10.002.
2. Abdulghani, A. J. and Hussain, R. K. (no date) Synthesis of Gold Nanoparticles Via Chemical Reduction of Au (III) Ions by Isatin in Aqueous solutions: Ligand Concentrations and pH Effects, *Baghdad Science Journal*. Available at: <https://www.iasj.net/iasj?func=fulltext&aId=93354> (Accessed: 20 July 2019).
3. Ahmad, T. et al. (2018) 'Green synthesis of stabilized spherical shaped gold nanoparticles using novel aqueous *Elaeis guineensis* (oil palm) leaves extract', *Journal of Molecular Structure*. Elsevier, 1159, pp. 167–173. doi: 10.1016/J.MOLSTRUC.2017.11.095.
4. Ahmed, W., Jackson, M. J. and Ul Hassan, I. (2015) 'Nanotechnology to Nanomanufacturing', *Emerging Nanotechnologies for Manufacturing*. William Andrew Publishing, pp. 1–13. doi: 10.1016/B978-0-323-28990-0.00001-4.
5. Alkilany, A. M. et al. (2014) 'Colloidal Stability of Citrate and Mercaptoacetic Acid Capped Gold Nanoparticles upon Lyophilization: Effect of Capping Ligand Attachment and Type of Cryoprotectants', *Langmuir*. American Chemical Society, 30(46), pp. 13799–13808. doi: 10.1021/la504000v.
6. Alkilany, A. M., Bani Yaseen, A. I. and Kailani, M. H. (2015) 'Synthesis of Monodispersed Gold Nanoparticles with Exceptional Colloidal Stability with

- Grafted Polyethylene Glycol- g -polyvinyl Alcohol', *Journal of Nanomaterials*, 2015, pp. 1–9. doi: 10.1155/2015/712359.
7. Almeer, R. S. et al. (2018) 'Green Platinum Nanoparticles Interaction With HEK293 Cells: Cellular Toxicity, Apoptosis, and Genetic Damage.', *Dose-response : a publication of International Hormesis Society*. SAGE Publications, 16(4), p. 1559325818807382. doi: 10.1177/1559325818807382.
 8. Almenawer, S. A. et al. (2015) 'Biopsy versus partial versus gross total resection in older patients with high-grade glioma: a systematic review and meta-analysis', *Neuro-Oncology*. Oxford University Press, 17(6), pp. 868–881. doi: 10.1093/neuonc/nou349.
 9. Al-Qadi, K. and Saadah, B. (2015) 'Gold Nanoparticles: Size vs. Color'. Available at: <https://www.ideals.illinois.edu/handle/2142/75909> (Accessed: 20 July 2019).
 10. Alshatwi, A. A., Athinarayanan, J. and Vaiyapuri Subbarayan, P. (2015) 'Green synthesis of platinum nanoparticles that induce cell death and G2/M-phase cell cycle arrest in human cervical cancer cells', *Journal of Materials Science: Materials in Medicine*, 26(1), p. 7. doi: 10.1007/s10856-014-5330-1.
 11. Álvarez-Fraga, L. et al. (2019) 'Formation and stability of highly conductive semitransparent copper Meso-grids covered with graphene', *Applied Surface Science*. North-Holland, 493, pp. 32–40. doi: 10.1016/J.APSUSC.2019.06.219.
 12. Alvi, S. et al. (2017) 'Clinical manifestations of neuroblastoma with head and neck involvement in children', *International Journal of Pediatric*

- Otorhinolaryngology. Elsevier, 97, pp. 157–162. doi: 10.1016/J.IJPORL.2017.04.013.
13. An, K. and Somorjai, G. A. (2015) ‘Nanocatalysis I: Synthesis of Metal and Bimetallic Nanoparticles and Porous Oxides and Their Catalytic Reaction Studies’, *Catalysis Letters*. Springer US, 145(1), pp. 233–248. doi: 10.1007/s10562-014-1399-x.
14. Arockiya Aarthi Rajathi, F. et al. (2014) ‘Phytofabrication of gold nanoparticles assisted by leaves of Suaeda monoica and its free radical scavenging property’, *Journal of Photochemistry and Photobiology B: Biology*, 135, pp. 75–80. doi: 10.1016/j.jphotobiol.2014.03.016.
15. Baba, A. I. and Cătoi, C. (2007) ‘NERVOUS SYSTEM TUMORS’. The Publishing House of the Romanian Academy. Available at: <https://www.ncbi.nlm.nih.gov/books/NBK9547/> (Accessed: 21 April 2019).
16. Baker, M. J. et al. (2014) ‘Using Fourier transform IR spectroscopy to analyze biological materials.’, *Nature protocols*. NIH Public Access, 9(8), pp. 1771–91. doi: 10.1038/nprot.2014.110.
17. Bastos, V. et al. (2017) ‘Coating independent cytotoxicity of citrate- and PEG-coated silver nanoparticles on a human hepatoma cell line’, *Journal of Environmental Sciences*. Elsevier, 51, pp. 191–201. doi: 10.1016/J.JES.2016.05.028.
18. Bauer, M. M. T. and Schnapp, G. (2007) ‘Protein Production for Three-Dimensional Structural Analysis’, *Comprehensive Medicinal Chemistry II*. Elsevier, pp. 411–432. doi: 10.1016/B0-08-045044-X/00092-4.

19. Behzadi, S. et al. (2015) 'Determination of nanoparticles using UV-Vis spectra.', *Nanoscale*, 7(12), pp. 5134–9. doi: 10.1039/c4nr00580e.
20. Bell, N. et al. (2013) 'Store-operated Ca²⁺ entry in proliferating and retinoic acid-differentiated N- and S-type neuroblastoma cells', *Biochimica et Biophysica Acta (BBA) - Molecular Cell Research*. Elsevier, 1833(3), pp. 643–651. doi: 10.1016/J.BBAMCR.2012.11.025.
21. Benaissi, K. et al. (2010) 'Synthesis of platinum nanoparticles using cellulosic reducing agents', *Green Chem. The Royal Society of Chemistry*, 12(2), pp. 220–222. doi: 10.1039/B913218J.
22. Bendale, Y., Bendale, V. and Paul, S. (2017) 'Evaluation of cytotoxic activity of platinum nanoparticles against normal and cancer cells and its anticancer potential through induction of apoptosis', *Integrative Medicine Research*. Elsevier, 6(2), pp. 141–148. doi: 10.1016/J.IMR.2017.01.006.
23. Berthold, F. et al. (2017) 'Incidence, Survival, and Treatment of Localized and Metastatic Neuroblastoma in Germany 1979–2015', *Pediatric Drugs*. Springer, 19(6), pp. 577–593. doi: 10.1007/s40272-017-0251-3.
24. Beyer, K. (2012) Influence of Capping Agents on Silver Nanoparticle (Ag-NP) Toxicity to Nitrifying Bacteria. Available at: https://wri.csusb.edu/documents/KelseyBeyer_FinalReport_12March2013.pdf (Accessed: 18 June 2019).
25. Bhattacharjee, S. (2016) 'DLS and zeta potential – What they are and what they are not?', *Journal of Controlled Release*, 235, pp. 337–351. doi: 10.1016/j.jconrel.2016.06.017.

26. Bianchi, S., Bigazzi, R. and Campese, V. M. (2010) 'Intensive Versus Conventional Therapy to Slow the Progression of Idiopathic Glomerular Diseases', *American Journal of Kidney Diseases*. W.B. Saunders, 55(4), pp. 671–681. doi: 10.1053/J.AJKD.2009.11.006.
27. Bortner, C. D. and Cidlowski, J. A. (2007) 'Cell shrinkage and monovalent cation fluxes: role in apoptosis.', *Archives of biochemistry and biophysics*. NIH Public Access, 462(2), pp. 176–88. doi: 10.1016/j.abb.2007.01.020.
28. Brinsko, S. P. et al. (2011) 'Examination of the Stallion for Breeding Soundness', *Manual of Equine Reproduction*. Mosby, pp. 176–206. doi: 10.1016/B978-0-323-06482-8.00022-3.
29. Brisse, H. J. et al. (2011) 'Guidelines for Imaging and Staging of Neuroblastic Tumors: Consensus Report from the International Neuroblastoma Risk Group Project', *Radiology*. Radiological Society of North America, Inc., 261(1), pp. 243–257. doi: 10.1148/radiol.11101352.
30. Bunker, A. (2012) 'Poly(Ethylene Glycol) in Drug Delivery, Why Does it Work, and Can We do Better? All Atom Molecular Dynamics Simulation Provides Some Answers', *Physics Procedia*. Elsevier, 34, pp. 24–33. doi: 10.1016/J.PHPRO.2012.05.004.
31. Bustos, A. R. M., Encinar, J. R. and Sanz-Medel, A. (2013) 'Mass spectrometry for the characterisation of nanoparticles', *Analytical and Bioanalytical Chemistry*, 405(17), pp. 5637–5643. doi: 10.1007/s00216-013-7014-y.
32. Butler, A. B. (2000) 'Nervous System', *The Laboratory Fish*. Academic Press, pp. 331–355. doi: 10.1016/B978-012529650-2/50026-3.

33. Butler, A. B. (2000) 'Nervous System', *The Laboratory Fish*. Academic Press, pp. 331–355. doi: 10.1016/B978-012529650-2/50026-3.
34. Butt, A. and Verkhatsky, A. (2018) 'Neuroglia: Realising their true potential', *Brain and Neuroscience Advances*. SAGE Publications Sage UK: London, England, 2, p. 239821281881749. doi: 10.1177/2398212818817495.
35. Calderón-Jiménez, B. et al. (2017) 'Silver Nanoparticles: Technological Advances, Societal Impacts, and Metrological Challenges', *Frontiers in Chemistry*. Frontiers, 5, p. 6. doi: 10.3389/fchem.2017.00006.
36. Chandra, S. and Kumar, A. (2012) 'Modulation of synthetic parameters of cobalt nanoparticles: TEM, EDS, spectral and thermal studies', *Spectrochimica Acta Part A: Molecular and Biomolecular Spectroscopy*. Elsevier, 98, pp. 23–26. doi: 10.1016/J.SAA.2012.07.065.
37. Charmi, J. et al. (2019) 'Polyethylene glycol (PEG) decorated graphene oxide nanosheets for controlled release curcumin delivery', *Heliyon*. Elsevier, 5(4), p. e01466. doi: 10.1016/J.HELIYON.2019.E01466.
38. Chau, J. L. H., Chen, C.-Y. and Yang, C.-C. (2017) 'Facile synthesis of bimetallic nanoparticles by femtosecond laser irradiation method', *Arabian Journal of Chemistry*. Elsevier, 10, pp. S1395–S1401. doi: 10.1016/J.ARABJC.2013.04.014.
39. Chee, S.-S. and Lee, J.-H. (2012) 'Synthesis of tin nanoparticles through modified polyol process and effects of centrifuging and drying on nanoparticles', *Transactions of Nonferrous Metals Society of China*. Elsevier, 22, pp. s707–s711. doi: 10.1016/S1003-6326(12)61791-9.

40. Chen, D.-J. et al. (2015) 'One-pot wet-chemical co-reduction synthesis of bimetallic gold–platinum nanochains supported on reduced graphene oxide with enhanced electrocatalytic activity', *Journal of Power Sources*. Elsevier, 287, pp. 363–369. doi: 10.1016/J.JPOWSOUR.2015.04.080.
41. Chen, T. et al. (2012) 'PEG-nanolized ultrasmall selenium nanoparticles overcome drug resistance in hepatocellular carcinoma HepG2 cells through induction of mitochondria dysfunction', *International Journal of Nanomedicine*, p. 3939. doi: 10.2147/IJN.S30940.
42. Chen, X. et al. (2013) 'Platinum-based agents for individualized cancer treatment.', *Current molecular medicine*, 13(10), pp. 1603–12. Available at: <http://www.ncbi.nlm.nih.gov/pubmed/24206132> (Accessed: 19 July 2019).
43. Chopade, B. et al. (2015) 'Novel platinum–palladium bimetallic nanoparticles synthesized by *Dioscorea bulbifera*: anticancer and antioxidant activities', *International Journal of Nanomedicine*. Dove Press, 10(1), p. 7477. doi: 10.2147/IJN.S91579.
44. Chowdhury, S. et al. (2016) 'Process Optimization of Silver Nanoparticle Synthesis Using Response Surface Methodology', *Procedia Engineering*. Elsevier, 148, pp. 992–999. doi: 10.1016/J.PROENG.2016.06.552.
45. Cieślak, A. et al. (2017) 'Stealth nanocarriers based sterosomes using PEG post-insertion process', *European Journal of Pharmaceutics and Biopharmaceutics*. Elsevier, 115, pp. 31–38. doi: 10.1016/J.EJPB.2017.02.008.

46. Clogston, J. D. and Patri, A. K. (2011) 'Zeta Potential Measurement', in *Methods in molecular biology* (Clifton, N.J.), pp. 63–70. doi: 10.1007/978-1-60327-198-1_6.
47. Colon, N. C. and Chung, D. H. (2011) 'Neuroblastoma.', *Advances in pediatrics*. NIH Public Access, 58(1), pp. 297–311. doi: 10.1016/j.yapd.2011.03.011.
48. Contreras-Trigo, B. et al. (2018) 'Slight pH Fluctuations in the Gold Nanoparticle Synthesis Process Influence the Performance of the Citrate Reduction Method', *Sensors*, 18(7), p. 2246. doi: 10.3390/s18072246.
49. Cooper, G. M. (2000) 'The Development and Causes of Cancer'. Sinauer Associates. Available at: <https://www.ncbi.nlm.nih.gov/books/NBK9963/> (Accessed: 15 February 2019).
50. Cox, J. D. et al. (2010) 'Chapter 1 – Physical and Biologic Basis of Radiation Therapy', in *Radiation Oncology. Content Repository Only!*, pp. 3–49. Available at: <https://www.sciencedirect.com/science/article/pii/B9780323049719000019> (Accessed: 9 July 2019).
51. Dahman, Y. and Dahman, Y. (2017) 'Nanoparticles', *Nanotechnology and Functional Materials for Engineers*. Elsevier, pp. 93–119. doi: 10.1016/B978-0-323-51256-5.00005-8.
52. Danaei, M. et al. (2018) 'Impact of Particle Size and Polydispersity Index on the Clinical Applications of Lipidic Nanocarrier Systems', *Pharmaceutics*, 10(2), p. 57. doi: 10.3390/pharmaceutics10020057.

53. Dao, A. T. N. et al. (2013) 'Enhanced electronic properties of Pt@Ag heterostructured nanoparticles.', *Sensors* (Basel, Switzerland). Multidisciplinary Digital Publishing Institute (MDPI), 13(6), pp. 7813–26. doi: 10.3390/s130607813.
54. Das, S. and Dhar, B. B. (2014) 'Green synthesis of noble metal nanoparticles using cysteine-modified silk fibroin: catalysis and antibacterial activity', *RSC Adv. The Royal Society of Chemistry*, 4(86), pp. 46285–46292. doi: 10.1039/C4RA06179A.
55. Dasari, S. and Tchounwou, P. B. (2014) 'Cisplatin in cancer therapy: molecular mechanisms of action.', *European journal of pharmacology*. NIH Public Access, 740, pp. 364–78. doi: 10.1016/j.ejphar.2014.07.025.
56. Davis, M. E. (2016) 'Glioblastoma: Overview of Disease and Treatment.', *Clinical journal of oncology nursing*. NIH Public Access, 20(5 Suppl), pp. S2–8. doi: 10.1188/16.CJON.S1.2-8.
57. Diallo, A. et al. (2015) 'Green synthesis of Co₃O₄ nanoparticles via *Aspalathus linearis*: Physical properties', *Green Chemistry Letters and Reviews*. Taylor & Francis, 8(3–4), pp. 30–36. doi: 10.1080/17518253.2015.1082646.
58. Dobrucka, R. (2019) 'Biofabrication of platinum nanoparticles using *Fumariae herba* extract and their catalytic properties', *Saudi Journal of Biological Sciences*. Elsevier, 26(1), pp. 31–37. doi: 10.1016/J.SJBS.2016.11.012.
59. Dowling, A. P. (2004) 'Development of nanotechnologies', *Materials Today*. Elsevier, 7(12), pp. 30–35. doi: 10.1016/S1369-7021(04)00628-5.

60. Dubois, L. G. et al. (2014) 'Gliomas and the vascular fragility of the blood brain barrier', *Frontiers in Cellular Neuroscience*. *Frontiers*, 8, p. 418. doi: 10.3389/fncel.2014.00418.
61. Dumba, M., Jawad, N. and McHugh, K. (2014) 'Neuroblastoma and nephroblastoma: an overview and comparison', *Cancer Imaging*. *BioMed Central*, 14(Suppl 1), p. O15. doi: 10.1186/1470-7330-14-S1-O15.
62. Dykman, L. A. and Khlebtsov, N. G. (2011) 'Gold nanoparticles in biology and medicine: recent advances and prospects.', *Acta naturae*. National Research University Higher School of Economics, 3(2), pp. 34–55. Available at: <http://www.ncbi.nlm.nih.gov/pubmed/22649683> (Accessed: 21 April 2019).
63. Dzimitrowicz, A. et al. (2016) 'Preparation and characterization of gold nanoparticles prepared with aqueous extracts of Lamiaceae plants and the effect of follow-up treatment with atmospheric pressure glow microdischarge', *Arabian Journal of Chemistry*. Elsevier. doi: 10.1016/J.ARABJC.2016.04.004.
64. Elhissi, A. (2013) 'Introduction to Nanotechnology', *Nanobiomaterials in Clinical Dentistry*. William Andrew Publishing, pp. 3–16. doi: 10.1016/B978-1-4557-3127-5.00001-5.
65. Farooq, M. U. et al. (2018) 'Gold Nanoparticles-enabled Efficient Dual Delivery of Anticancer Therapeutics to HeLa Cells.', *Scientific reports*. Nature Publishing Group, 8(1), p. 2907. doi: 10.1038/s41598-018-21331-y.
66. Fichtner, M. (2009) 'Nanoscale Materials For Hydrogen and Energy Storage', *Frontiers of Nanoscience*. Elsevier, 1, pp. 270–297. doi: 10.1016/B978-0-08-044965-4.50009-2.

67. Foss, C. A. and Rahman, A. (2016) 'Optical Properties of Nanoparticle Pair Structures', Reference Module in Materials Science and Materials Engineering. Elsevier. doi: 10.1016/B978-0-12-803581-8.02410-3.
68. Freese, C. et al. (2012) 'Uptake and cytotoxicity of citrate-coated gold nanospheres: Comparative studies on human endothelial and epithelial cells', Particle and Fibre Toxicology. BioMed Central, 9(1), p. 23. doi: 10.1186/1743-8977-9-23.
69. Gajendiran, M. et al. (2014) 'Gold nanoparticle conjugated PLGA-PEG-SA-PEG-PLGA multiblock copolymer nanoparticles: synthesis, characterization, in vivo release of rifampicin', J. Mater. Chem. B. The Royal Society of Chemistry, 2(4), pp. 418-427. doi: 10.1039/C3TB21113D.
70. Ganesh Kumar, C. et al. (2016) 'Synthesis, characterization, and applications of nanobiomaterials for antimicrobial therapy', Nanobiomaterials in Antimicrobial Therapy. William Andrew Publishing, pp. 103-152. doi: 10.1016/B978-0-323-42864-4.00004-X.
71. Genzen, J. R. et al. (2009) 'Ependymal cells along the lateral ventricle express functional P2X(7) receptors.', Purinergic signalling. Springer, 5(3), pp. 299-307. doi: 10.1007/s11302-009-9143-5.
72. Ghann, W. E. et al. (2011) 'Synthesis and biological studies of highly concentrated lisinopril-capped gold nanoparticles for CT tracking of angiotensin converting enzyme (ACE)', in Cullum, B. M. and McLamore, E. S. (eds). International Society for Optics and Photonics, p. 80250H. doi: 10.1117/12.885526.

73. Gladson, C. L., Prayson, R. A. and Liu, W. M. (2010) 'The Pathobiology of Glioma Tumors', *Annual Review of Pathology: Mechanisms of Disease*, 5(1), pp. 33–50. doi: 10.1146/annurev-pathol-121808-102109.
74. Goodarzi, S. et al. (2017) 'Fullerene: biomedical engineers get to revisit an old friend', *Materials Today*. Elsevier, 20(8), pp. 460–480. doi: 10.1016/J.MATTOD.2017.03.017.
75. Grasmik, V. et al. (2018) 'Synthesis and biological characterization of alloyed silver–platinum nanoparticles: from compact core–shell nanoparticles to hollow nanoalloys', *RSC Advances*. The Royal Society of Chemistry, 8(67), pp. 38582–38590. doi: 10.1039/C8RA06461J.
76. Gritsch, L., Meng, D. and Boccaccini, A. R. (2017) 'Nanostructured biocomposites for tissue engineering scaffolds', *Biomedical Composites*. Woodhead Publishing, pp. 501–542. doi: 10.1016/B978-0-08-100752-5.00021-4.
77. Guerrini, L., Alvarez-Puebla, R. and Pazos-Perez, N. (2018) 'Surface Modifications of Nanoparticles for Stability in Biological Fluids', *Materials*, 11(7), p. 1154. doi: 10.3390/ma11071154.
78. Guo, J. et al. (2017) 'Gold nanoparticles enlighten the future of cancer theranostics.', *International journal of nanomedicine*. Dove Press, 12, pp. 6131–6152. doi: 10.2147/IJN.S140772.
79. Hackley, V. A. and Clogston, J. D. (2011) 'Measuring the Hydrodynamic Size of Nanoparticles in Aqueous Media Using Batch-Mode Dynamic Light

- Scattering’, in *Methods in molecular biology* (Clifton, N.J.), pp. 35–52. doi: 10.1007/978-1-60327-198-1_4.
80. Hanif, F. et al. (2017) ‘Glioblastoma Multiforme: A Review of its Epidemiology and Pathogenesis through Clinical Presentation and Treatment’, *Asian Pacific journal of cancer prevention : APJCP*. Shahid Beheshti University of Medical Sciences, 18(1), pp. 3–9. doi: 10.22034/APJCP.2017.18.1.3.
81. Heinz, H. et al. (2017) ‘Nanoparticle decoration with surfactants: Molecular interactions, assembly, and applications’, *Surface Science Reports*. North-Holland, 72(1), pp. 1–58. doi: 10.1016/J.SURFREP.2017.02.001.
82. Hopkins, S. et al. (2018) ‘Effects of Chemically-Functionalized Single-Walled Carbon Nanotubes on the Morphology and Vitality of D54MG Human Glioblastoma Cells’, *Neuroglia*, 1(2), pp. 327–338. doi: 10.3390/neuroglia1020022.
83. Horie, M. et al. (2011) ‘Evaluation of cellular influences of platinum nanoparticles by stable medium dispersion’, *Metallomics*, 3(11), p. 1244. doi: 10.1039/c1mt00060h.
84. Housman, G. et al. (2014) ‘Drug resistance in cancer: an overview.’, *Cancers*. Multidisciplinary Digital Publishing Institute (MDPI), 6(3), pp. 1769–92. doi: 10.3390/cancers6031769.
85. Huang, P.-S. and Gao, T. (2018) ‘Current development of 1D and 2D metallic nanomaterials for the application of transparent conductors in solar cells: Fabrication and modeling’, *Nano-Structures & Nano-Objects*. Elsevier, 15, pp. 119–139. doi: 10.1016/J.NANOSO.2017.09.001.

86. Huang, X. and El-Sayed, M. A. (2010) 'Gold nanoparticles: Optical properties and implementations in cancer diagnosis and photothermal therapy', *Journal of Advanced Research*. Elsevier, 1(1), pp. 13–28. doi: 10.1016/J.JARE.2010.02.002.
87. Huang, Y.-C. et al. (2014) 'Pegylated gold nanoparticles induce apoptosis in human chronic myeloid leukemia cells.', *BioMed research international*. Hindawi Limited, 2014, p. 182353. doi: 10.1155/2014/182353.
88. Hulla, J., Sahu, S. and Hayes, A. (2015) 'Nanotechnology', *Human & Experimental Toxicology*. SAGE Publications Sage UK: London, England, 34(12), pp. 1318–1321. doi: 10.1177/0960327115603588.
89. Ishola, T. A. and Chung, D. H. (2007) 'Neuroblastoma', *Surgical Oncology*. Elsevier, 16(3), pp. 149–156. doi: 10.1016/J.SURONC.2007.09.005.
90. Ismail, E. H. et al. (2018) 'Successful Green Synthesis of Gold Nanoparticles using a *Corchorus olitorius* Extract and Their Antiproliferative Effect in Cancer Cells.', *International journal of molecular sciences*. Multidisciplinary Digital Publishing Institute (MDPI), 19(9). doi: 10.3390/ijms19092612.
91. Iswarya, V. et al. (2017) 'Modulatory effects of Zn²⁺ ions on the toxicity of citrate- and PVP-capped gold nanoparticles towards freshwater algae, *Scenedesmus obliquus*', *Environmental Science and Pollution Research*, 24(4), pp. 3790–3801. doi: 10.1007/s11356-016-8131-x.
92. Jawad, M. et al. (2019) 'Plasmonic effects and size relation of gold-platinum alloy nanoparticles', *Advances in Nano Research*. Techno-Press, 7(3), p. 167. doi: 10.12989/ANR.2019.7.3.167.

93. Jensen, W. B. and Culp, B. (2003) 'The KLM-Shell Labels Question Why do the labels for the electron orbits in the Bohr model begin with the letter K?', *Chemical Education Today* 996 *Journal of Chemical Education* •, 80(8). doi: 10.1021/ed080p996.
94. Jögi, A. et al. (2012) 'Cancer cell differentiation heterogeneity and aggressive behavior in solid tumors.', *Upsala journal of medical sciences*. Taylor & Francis, 117(2), pp. 217–24. doi: 10.3109/03009734.2012.659294.
95. Johnston, M. V., Wang, S. and Reinard, M. S. (2006) 'Nanoparticle Mass Spectrometry: Pushing the Limit of Single Particle Analysis', *Applied Spectroscopy*, 60(10), p. 264A–272A. doi: 10.1366/000370206778664671.
96. Kaszuba, M. et al. (2010) 'High-concentration zeta potential measurements using light-scattering techniques.', *Philosophical transactions. Series A, Mathematical, physical, and engineering sciences*. The Royal Society, 368(1927), pp. 4439–51. doi: 10.1098/rsta.2010.0175.
97. Katifelis, H. et al. (2018) 'Ag/Au bimetallic nanoparticles induce apoptosis in human cancer cell lines via P53 , CASPASE-3 and BAX/BCL-2 pathways', *Artificial Cells, Nanomedicine, and Biotechnology*, 46(sup3), pp. S389–S398. doi: 10.1080/21691401.2018.1495645.
98. Kaur, P., Thakur, R. and Chaudhury, A. (2016) 'Biogenesis of copper nanoparticles using peel extract of Punica granatum and their antimicrobial activity against opportunistic pathogens', *Green Chemistry Letters and Reviews*, 9(1), pp. 33–38. doi: 10.1080/17518253.2016.1141238.

99. Kembhavi, S. A. et al. (2015) 'Imaging in neuroblastoma: An update.', *The Indian journal of radiology & imaging*. Wolters Kluwer -- Medknow Publications, 25(2), pp. 129–36. doi: 10.4103/0971-3026.155844.
100. Khairuddin et al. (2016) 'FTIR studies on the effect of concentration of polyethylene glycol on polymerization of Shellac', *Journal of Physics: Conference Series*. IOP Publishing, 776(1), p. 012053. doi: 10.1088/1742-6596/776/1/012053.
101. Khan, A. K. et al. (2014) 'Gold Nanoparticles: Synthesis and Applications in Drug Delivery', *Tropical Journal of Pharmaceutical Research*, 13(7), pp. 1169–1177. doi: 10.4314/tjpr.v13i7.23.
102. Khan, W. S. (2013) 'Nanotechnology Emerging Trends, Markets, and Concerns', *Nanotechnology Safety*. Elsevier, pp. 1–16. doi: 10.1016/B978-0-444-59438-9.00001-1.
103. Kim, S.-W. et al. (2017) 'PEGylated anticancer-carbon nanotubes complex targeting mitochondria of lung cancer cells', *Nanotechnology*, 28(46), p. 465102. doi: 10.1088/1361-6528/aa8c31.
104. Kiran Aithal, B. et al. (2009) 'Juglone, a naphthoquinone from walnut, exerts cytotoxic and genotoxic effects against cultured melanoma tumor cells', *Cell Biology International*, 33(10), pp. 1039–1049. doi: 10.1016/j.cellbi.2009.06.018.
105. Kogure, T. (2013) 'Electron Microscopy', *Developments in Clay Science*. Elsevier, 5, pp. 275–317. doi: 10.1016/B978-0-08-098259-5.00011-1.

106. Kononenko, V. et al. (2017) 'Phototoxicity of Mesoporous TiO₂ + Gd Microbeads With Theranostic Potential', *Advances in Biomembranes and Lipid Self-Assembly*. Academic Press, 26, pp. 153–171. doi: 10.1016/BS.ABL.2017.06.002.
107. Konwar Boruah, S. et al. (2012) 'Green Synthesis Of Gold Nanoparticles Using Camellia Sinensis And Kinetics Of The Reaction', *Advanced Materials Letters*, 3(6), pp. 481–486. doi: 10.5185/amlett.2012.icnano.103.
108. Kotas, M. E. and Medzhitov, R. (2015) 'Homeostasis, Inflammation, and Disease Susceptibility', *Cell*. Cell Press, 160(5), pp. 816–827. doi: 10.1016/J.CELL.2015.02.010.
109. Kovalevich, J. and Langford, D. (2013) 'Considerations for the Use of SH-SY5Y Neuroblastoma Cells in Neurobiology', in *Methods in molecular biology* (Clifton, N.J.), pp. 9–21. doi: 10.1007/978-1-62703-640-5_2.
110. Kriel, J. et al. (2018) 'Coordinated autophagy modulation overcomes glioblastoma chemoresistance through disruption of mitochondrial bioenergetics', *Scientific Reports*. Nature Publishing Group, 8(1), p. 10348. doi: 10.1038/s41598-018-28590-9.
111. Kristan, W. B. (2016) 'Early evolution of neurons', *Current Biology*. Cell Press, 26(20), pp. R949–R954. doi: 10.1016/J.CUB.2016.05.030.
112. Kutwin, M. et al. (2017) 'Investigation of platinum nanoparticle properties against U87 glioblastoma multiforme', *Archives of Medical Science*, 6(6), pp. 1322–1334. doi: 10.5114/aoms.2016.58925.

113. Kwist, K., Bridges, W. C. and Burg, K. J. L. (2016) ‘The effect of cell passage number on osteogenic and adipogenic characteristics of D1 cells.’, *Cytotechnology*. Springer, 68(4), pp. 1661–7. doi: 10.1007/s10616-015-9883-8.
114. Laudon, M. et al. (2011) Nanotech Conference & Expo 2011 : technical proceedings of the 2011 NSTI Nanotechnology Conference and Expo : June 13-16, 2011, Boston, Massachusetts, U.S.A., TechConnect Briefs. Nano Science and Technology Institute. Available at: <https://briefs.techconnect.org/papers/cytotoxic-studies-of-peg-functionalized-zno-nanoparticles-on-mcf-7-cancer-cells/> (Accessed: 15 February 2019).
115. Ledur, P F et al. (2017) ‘Culture conditions defining glioblastoma cells behavior: what is the impact for novel discoveries?’ *Oncotarget* vol. 8,40 69185-69197. 11 Aug. 2017, doi:10.18632/oncotarget.20193
116. Lee, J., Park, S. H. and Kim, Y. Z. (2018) ‘Prognostic Evaluation of Neurological Assessment of the Neuro-Oncology Scale in Glioblastoma Patients.’, *Brain tumor research and treatment*. Korean Brain Tumor Society, 6(1), pp. 22–30. doi: 10.14791/btrt.2018.6.e1.
117. Lee, M. K. et al. (2007) ‘Resveratrol protects SH-SY5Y neuroblastoma cells from apoptosis induced by dopamine’, *Experimental & Molecular Medicine*, 39(3), pp. 376–384. doi: 10.1038/emm.2007.42.
118. Li, C.-C. et al. (2013) ‘Effects of capping agents on the dispersion of silver nanoparticles’, *Colloids and Surfaces A: Physicochemical and Engineering Aspects*. Elsevier, 419, pp. 209–215. doi: 10.1016/J.COLSURFA.2012.11.077.

119. Li, H. S. et al. (2012) 'PDCD5 promotes cisplatin-induced apoptosis of glioma cells via activating mitochondrial apoptotic pathway', *Cancer Biology & Therapy*, 13(9), pp. 822–830. doi: 10.4161/cbt.20565.
120. Li, H.-J. et al. (2018) 'Gold Nanoparticles Grafted with PLL-b-PNIPAM: Interplay on Thermal/pH Dual-Response and Optical Properties', *Molecules*, 23(4), p. 921. doi: 10.3390/molecules23040921.
121. Li, N. et al. (2014) 'A Systematic Assessment of Mitochondrial Function Identified Novel Signatures for Drug-Induced Mitochondrial Disruption in Cells', *Toxicological Sciences*. Narnia, 142(1), pp. 261–273. doi: 10.1093/toxsci/kfu176.
122. Li, Y., Kröger, M. and Liu, W. K. (2014) 'Endocytosis of PEGylated nanoparticles accompanied by structural and free energy changes of the grafted polyethylene glycol', *Biomaterials*. Elsevier, 35(30), pp. 8467–8478. doi: 10.1016/J.BIOMATERIALS.2014.06.032.
123. Liu, Q. et al. (2012) 'Preparation of Cu nanoparticles with NaBH₄ by aqueous reduction method', *Transactions of Nonferrous Metals Society of China*. Elsevier, 22(1), pp. 117–123. doi: 10.1016/S1003-6326(11)61149-7.
124. Liu, Z. et al. (2014) 'Effects of Internalized Gold Nanoparticles with Respect to Cytotoxicity and Invasion Activity in Lung Cancer Cells', *PLoS ONE*. Edited by H. G. Munshi. Public Library of Science, 9(6), p. e99175. doi: 10.1371/journal.pone.0099175.

125. Lodish, H. et al. (2000) 'Overview of Neuron Structure and Function'. W. H. Freeman. Available at: <https://www.ncbi.nlm.nih.gov/books/NBK21535/> (Accessed: 21 April 2019).
126. Lovinger, D. M. (2008) 'Communication networks in the brain: neurons, receptors, neurotransmitters, and alcohol.', *Alcohol research & health: the journal of the National Institute on Alcohol Abuse and Alcoholism*. National Institute on Alcohol Abuse and Alcoholism, 31(3), pp. 196–214. Available at: <http://www.ncbi.nlm.nih.gov/pubmed/23584863> (Accessed: 19 June 2019).
127. Lue, J.-T. (2001) 'A review of characterization and physical property studies of metallic nanoparticles', *Journal of Physics and Chemistry of Solids*. Pergamon, 62(9–10), pp. 1599–1612. doi: 10.1016/S0022-3697(01)00099-3.
128. Lusvarghi, S. et al. (2018) 'Chemical and Biophysical Approaches for Complete Characterization of Lectin–Carbohydrate Interactions', *Methods in Enzymology*. Academic Press, 598, pp. 3–35. doi: 10.1016/BS.MIE.2017.06.010.
129. Mahbulul, I. M. and Mahbulul, I. M. (2019) 'Stability and Dispersion Characterization of Nanofluid', *Preparation, Characterization, Properties and Application of Nanofluid*. William Andrew Publishing, pp. 47–112. doi: 10.1016/B978-0-12-813245-6.00003-4.
130. Maney, V. and Singh, M. (2017) 'An in vitro assessment of novel chitosan/bimetallic PtAu nanocomposites as delivery vehicles for doxorubicin', *Nanomedicine*. Future Medicine Ltd London, UK, 12(21), pp. 2625–2640. doi: 10.2217/nmm-2017-0228.

131. Manke, A., Wang, L. and Rojanasakul, Y. (2013) 'Mechanisms of nanoparticle-induced oxidative stress and toxicity.', *BioMed research international*. Hindawi, 2013, p. 942916. doi: 10.1155/2013/942916.
132. Manson, J. et al. (2011) 'Polyethylene glycol functionalized gold nanoparticles: the influence of capping density on stability in various media', *Gold Bulletin*. Springer-Verlag, 44(2), pp. 99–105. doi: 10.1007/s13404-011-0015-8.
133. Măntele, W. and Deniz, E. (2017) 'UV–VIS absorption spectroscopy: Lambert-Beer reloaded', *Spectrochimica Acta Part A: Molecular and Biomolecular Spectroscopy*, 173, pp. 965–968. doi: 10.1016/j.saa.2016.09.037.
134. Maple, B. R. et al. (2005) 'Characterization of displaced bipolar cells in the tiger salamander retina', *Vision Research*. Pergamon, 45(6), pp. 697–705. doi: 10.1016/J.VISRES.2004.09.038.
135. Martínez-Torres, A. C. et al. (2018) 'Chitosan gold nanoparticles induce cell death in HeLa and MCF-7 cells through reactive oxygen species production.', *International journal of nanomedicine*. Dove Press, 13, pp. 3235–3250. doi: 10.2147/IJN.S165289.
136. Masarudin, M. J. et al. (2015) 'Factors determining the stability, size distribution, and cellular accumulation of small, monodisperse chitosan nanoparticles as candidate vectors for anticancer drug delivery: application to the passive encapsulation of [(14)C]-doxorubicin.', *Nanotechnology, science and applications*. Dove Press, 8, pp. 67–80. doi: 10.2147/NSA.S91785.
137. Massard, C. et al. (2018) 'Cytotoxicity Study of Gold Nanoparticles on the Basal-Like Triple-Negative HCC-1937 Breast Cancer Cell Line', *Journal of*

- Biomaterials and Nanobiotechnology. Scientific Research Publishing, 09(01), pp. 13–25. doi: 10.4236/jbnb.2018.91002.
138. McEwen, B. S. (2016) ‘Central Role of the Brain in Stress and Adaptation: Allostasis, Biological Embedding, and Cumulative Change’, *Stress: Concepts, Cognition, Emotion, and Behavior*. Academic Press, pp. 39–55. doi: 10.1016/B978-0-12-800951-2.00005-4.
139. Mendivil Palma, M. I. et al. (2016) ‘Synthesis and Properties of Platinum Nanoparticles by Pulsed Laser Ablation in Liquid’, *Journal of Nanomaterials*. Hindawi, 2016, pp. 1–11. doi: 10.1155/2016/9651637.
140. Menéndez-Manjón, A. and Barcikowski, S. (2011) ‘Hydrodynamic size distribution of gold nanoparticles controlled by repetition rate during pulsed laser ablation in water’, *Applied Surface Science*. North-Holland, 257(9), pp. 4285–4290. doi: 10.1016/J.APSUSC.2010.12.037.
141. Mioc, M. et al. (2018) ‘The Cytotoxic Effects of Betulin-Conjugated Gold Nanoparticles as Stable Formulations in Normal and Melanoma Cells.’, *Frontiers in pharmacology*. Frontiers Media SA, 9, p. 429. doi: 10.3389/fphar.2018.00429.
142. Mishra, P., Nayak, B. and Dey, R. K. (2016) ‘PEGylation in anti-cancer therapy: An overview’, *Asian Journal of Pharmaceutical Sciences*. Elsevier, 11(3), pp. 337–348. doi: 10.1016/J.AJPS.2015.08.011.
143. Mody, V. V et al. (2010) ‘Introduction to metallic nanoparticles.’, *Journal of pharmacy & bioallied sciences*. Wolters Kluwer -- Medknow Publications, 2(4), pp. 282–9. doi: 10.4103/0975-7406.72127.

144. Mohamed, M. A. et al. (2017) 'Fourier Transform Infrared (FTIR) Spectroscopy', Membrane Characterization. Elsevier, pp. 3–29. doi: 10.1016/B978-0-444-63776-5.00001-2.
145. Mohammadi, H. et al. (2013) 'Evaluation of synthesized platinum nanoparticles on the MCF-7 and HepG-2 cancer cell lines', International Nano Letters. Springer Berlin Heidelberg, 3(1), p. 28. doi: 10.1186/2228-5326-3-28.
146. Moore, T. L. et al. (2015) 'Nanoparticle colloidal stability in cell culture media and impact on cellular interactions', Chemical Society Reviews. Royal Society of Chemistry, 44(17), pp. 6287–6305. doi: 10.1039/C4CS00487F.
147. Mughal, A. A. et al. (2018) 'Patterns of Invasive Growth in Malignant Gliomas—The Hippocampus Emerges as an Invasion-Spared Brain Region', Neoplasia. Elsevier, 20(7), pp. 643–656. doi: 10.1016/J.NEO.2018.04.001.
148. Mullassery, D. and Losty, P. D. (2016) 'Neuroblastoma', Paediatrics and Child Health. Churchill Livingstone, 26(2), pp. 68–72. doi: 10.1016/J.PAED.2015.11.005.
149. Nadagouda, M. N. and Varma, R. S. (2008) 'Green synthesis of silver and palladium nanoparticles at room temperature using coffee and tea extract', Green Chemistry. The Royal Society of Chemistry, 10(8), p. 859. doi: 10.1039/b804703k.
150. Neikov, O. D. et al. (2019) 'Powder Characterization and Testing', Handbook of Non-Ferrous Metal Powders. Elsevier, pp. 3–62. doi: 10.1016/B978-0-08-100543-9.00001-4.

151. Neikov, O. D. et al. (2019) 'Powder Characterization and Testing', Handbook of Non-Ferrous Metal Powders. Elsevier, pp. 3–62. doi: 10.1016/B978-0-08-100543-9.00001-4.
152. Nilapwar, S. M. et al. (2011) 'Absorption Spectroscopy', in Methods in enzymology, pp. 59–75. doi: 10.1016/B978-0-12-385118-5.00004-9.
153. Nițică, Ștefan et al. (2018) 'PEGylated Gold Nanoparticles with Interesting Plasmonic Properties Synthesized Using an Original, Rapid, and Easy-to-Implement Procedure', Journal of Nanomaterials. Hindawi, 2018, pp. 1–7. doi: 10.1155/2018/5954028.
154. Nobbmann, U. and Morfesis, A. (2009) 'Light scattering and nanoparticles', Materials Today. Elsevier, 12(5), pp. 52–54. doi: 10.1016/S1369-7021(09)70164-6.
155. Okumu, F. and Matoetoe, M. (2016) 'Kinetics and Morphological Analysis of Silver Platinum Bimetallic Nanoparticles', Acta Metallurgica Sinica (English Letters), 29(4), pp. 320–325. doi: 10.1007/s40195-016-0395-0.
156. Olajire, A. A. and Adesina, O. O. (2017) 'Green Approach to Synthesis of Pt and Bimetallic Au@Pt Nanoparticles Using Carica Papaya Leaf Extract and Their Characterization', Journal of Nanostructures. University of Kashan, 7(4), pp. 338–344. doi: 10.22052/JNS.2017.54219.
157. Oliveira, J. P. et al. (2017) 'A helpful method for controlled synthesis of monodisperse gold nanoparticles through response surface modeling', Arabian Journal of Chemistry. Elsevier. doi: 10.1016/J.ARABJC.2017.04.003.

158. Ornes, S. (2016) 'Core Concept: Quantum dots.', Proceedings of the National Academy of Sciences of the United States of America. National Academy of Sciences, 113(11), pp. 2796–7. doi: 10.1073/pnas.1601852113.
159. Ou, X. et al. (2008) 'Photocatalytic reaction by Fe(III)–citrate complex and its effect on the photodegradation of atrazine in aqueous solution', Journal of Photochemistry and Photobiology A: Chemistry. Elsevier, 197(2–3), pp. 382–388. doi: 10.1016/J.JPHOTOCHEM.2008.02.001.
160. Ouellette, R. J. et al. (2015) 'Carboxylic Acids', Organic Chemistry Study Guide. Elsevier, pp. 361–384. doi: 10.1016/B978-0-12-801889-7.00020-0.
161. Pal, S. K. and Hurria, A. (2012) 'Chemotherapy', Management of Cancer in the Older Patient. W.B. Saunders, pp. 89–94. doi: 10.1016/B978-1-4377-1398-5.10009-8.
162. Pallavicini, P. et al. (2015) 'Gold nanostars coated with neutral and charged polyethylene glycols: A comparative study of in-vitro biocompatibility and of their interaction with SH-SY5Y neuroblastoma cells', Journal of Inorganic Biochemistry, 151, pp. 123–131. doi: 10.1016/j.jinorgbio.2015.05.002.
163. Park, J. R. and Bagatell, R. (2016) 'Neuroblastoma', Lanzkowsky's Manual of Pediatric Hematology and Oncology. Academic Press, pp. 473–490. doi: 10.1016/B978-0-12-801368-7.00024-7.
164. Park, J. and Shumaker-Parry, J. S. (2014) 'Structural Study of Citrate Layers on Gold Nanoparticles: Role of Intermolecular Interactions in Stabilizing Nanoparticles', Journal of the American Chemical Society, 136(5), pp. 1907–1921. doi: 10.1021/ja4097384.

165. Park, K. and Lee, Y. (2013) 'The Stability of Citrate-Capped Silver Nanoparticles in Isotonic Glucose Solution for Intravenous Injection', *Journal of Toxicology and Environmental Health, Part A*. Taylor & Francis, 76(22), pp. 1236–1245. doi: 10.1080/15287394.2013.849215.
166. Paszkiewicz, M. et al. (2016) 'Synthesis and Characterization of Monometallic (Ag, Cu) and Bimetallic Ag-Cu Particles for Antibacterial and Antifungal Applications', *Journal of Nanomaterials*. Hindawi, 2016, pp. 1–11. doi: 10.1155/2016/2187940.
167. Pate, K. and Safier, P. (2016) 'Chemical metrology methods for CMP quality', *Advances in Chemical Mechanical Planarization (CMP)*. Woodhead Publishing, pp. 299–325. doi: 10.1016/B978-0-08-100165-3.00012-7.
168. Pawar, R. S., Upadhaya, P. G. and Patravale, V. B. (2018) 'Quantum Dots: Novel Realm in Biomedical and Pharmaceutical Industry', *Handbook of Nanomaterials for Industrial Applications*. Elsevier, pp. 621–637. doi: 10.1016/B978-0-12-813351-4.00035-3.
169. Perera, J., Weerasekera, M. and Kottegoda, N. (2015) 'Slow release anti-fungal skin formulations based on citric acid intercalated layered double hydroxides nanohybrids', *Chemistry Central Journal*, 9(1), p. 27. doi: 10.1186/s13065-015-0106-3.
170. Pfeiffer, C. et al. (2014) 'Interaction of colloidal nanoparticles with their local environment: the (ionic) nanoenvironment around nanoparticles is different from bulk and determines the physico-chemical properties of the nanoparticles',

- Journal of the Royal Society Interface. The Royal Society, 11(96), p. 20130931.
doi: 10.1098/RSIF.2013.0931.
171. Phan, C. M. and Nguyen, H. M. (2017) 'Role of Capping Agent in Wet Synthesis of Nanoparticles', *The Journal of Physical Chemistry A*. American Chemical Society, 121(17), pp. 3213–3219. doi: 10.1021/acs.jpca.7b02186.
172. Philips, A. et al. (2018) 'Brain Tumours: Rise in Glioblastoma Multiforme Incidence in England 1995–2015 Suggests an Adverse Environmental or Lifestyle Factor', *Journal of Environmental and Public Health*. Hindawi, 2018, pp. 1–10. doi: 10.1155/2018/7910754.
173. Pinzaru, I. et al. (2018) 'Stable PEG-coated silver nanoparticles – A comprehensive toxicological profile', *Food and Chemical Toxicology*. Pergamon, 111, pp. 546–556. doi: 10.1016/J.FCT.2017.11.051.
174. Pitkethly, M. (2008) 'Nanotechnology: past, present, and future', *Nano Today*. Elsevier, 3(3–4), p. 6. doi: 10.1016/S1748-0132(08)70029-X.
175. Pluchery, O., Remita, H. and Schaming, D. (2013) 'Demonstrative experiments about gold nanoparticles and nanofilms: an introduction to nanoscience', *Gold Bulletin*. Springer Berlin Heidelberg, 46(4), pp. 319–327. doi: 10.1007/s13404-013-0122-9.
176. Pourali, P. et al. (2017) 'Biosynthesis of gold nanoparticles by two bacterial and fungal strains, *Bacillus cereus* and *Fusarium oxysporum*, and assessment and comparison of their nanotoxicity in vitro by direct and indirect assays', *Electronic Journal of Biotechnology*. Elsevier, 29, pp. 86–93. doi: 10.1016/J.EJBT.2017.07.005.

177. Qu, J. et al. (2011) 'Coalescence of Ag₂S and Au nanocrystals at room temperature', *Journal of Materials Chemistry*. The Royal Society of Chemistry, 21(32), p. 11750. doi: 10.1039/c1jm12358k.
178. Rawat, R. S. (2015) 'Dense Plasma Focus - From Alternative Fusion Source to Versatile High Energy Density Plasma Source for Plasma Nanotechnology', *Journal of Physics: Conference Series*, 591, p. 012021. doi: 10.1088/1742-6596/591/1/012021.
179. Rezaei, M., Tabaian, S. H. and Haghshenas, D. F. (2012) 'Nucleation and growth of Pd nanoparticles during electrocrystallization on pencil graphite', *Electrochimica Acta*. Pergamon, 59, pp. 360–366. doi: 10.1016/J.ELECTACTA.2011.10.081.
180. Reznickova, A. et al. (2019) 'PEGylated gold nanoparticles: Stability, cytotoxicity and antibacterial activity', *Colloids and Surfaces A: Physicochemical and Engineering Aspects*. Elsevier, 560, pp. 26–34. doi: 10.1016/J.COLSURFA.2018.09.083.
181. Rich, B. S. and La Quaglia, M. P. (2012) 'Neuroblastoma', *Pediatric Surgery*. Mosby, pp. 441–458. doi: 10.1016/B978-0-323-07255-7.00031-3.
182. Rick, J., Tsai, M.-C. and Hwang, B. J. (2015) 'Biosensors Incorporating Bimetallic Nanoparticles.', *Nanomaterials* (Basel, Switzerland). Multidisciplinary Digital Publishing Institute (MDPI), 6(1). doi: 10.3390/nano6010005.
183. Riss, T. L. et al. (2004) *Cell Viability Assays, Assay Guidance Manual*. Eli Lilly & Company and the National Center for Advancing Translational

- Sciences. Available at: <http://www.ncbi.nlm.nih.gov/pubmed/23805433> (Accessed: 14 July 2019).
184. Rockwood, A. L., Kushnir, M. M. and Clarke, N. J. (2018) 'Mass Spectrometry', Principles and Applications of Clinical Mass Spectrometry. Elsevier, pp. 33–65. doi: 10.1016/B978-0-12-816063-3.00002-5.
185. Roco, M. C. (2011) 'The long view of nanotechnology development: the National Nanotechnology Initiative at 10 years', Journal of Nanoparticle Research. Springer Netherlands, 13(2), pp. 427–445. doi: 10.1007/s11051-010-0192-z.
186. Roopan, S. M. and Elango, G. (2016) 'Self-assembly of transition metal nanoparticles using marine sources', Fabrication and Self-Assembly of Nanobiomaterials. William Andrew Publishing, pp. 459–483. doi: 10.1016/B978-0-323-41533-0.00015-5.
187. Saidi, T. and Douglas, T. S. (2017) 'Nanotechnology in South Africa – Challenges in evaluating the impact on development', South African Journal of Science. Academy of Science of South Africa, 113(7/8), pp. 1–2. doi: 10.17159/sajs.2017/a0217.
188. Sakamuru, S., Attene-Ramos, M. S. and Xia, M. (2016) 'Mitochondrial Membrane Potential Assay.', Methods in molecular biology (Clifton, N.J.). NIH Public Access, 1473, pp. 17–22. doi: 10.1007/978-1-4939-6346-1_2.
189. Schnorr, J. M. and Swager, T. M. (2011) 'Emerging Applications of Carbon Nanotubes †', Chemistry of Materials. American Chemical Society, 23(3), pp. 646–657. doi: 10.1021/cm102406h.

190. Scimeca, M. et al. (2018) 'Energy Dispersive X-ray (EDX) microanalysis: A powerful tool in biomedical research and diagnosis.', *European journal of histochemistry : EJH*. PAGEPress, 62(1), p. 2841. doi: 10.4081/ejh.2018.2841.
191. Seol, S. K. et al. (2013) 'One-Step Synthesis of PEG-Coated Gold Nanoparticles by Rapid Microwave Heating', *Journal of Nanomaterials*. Hindawi, 2013, pp. 1–6. doi: 10.1155/2013/531760.
192. Sharma, A., Goyal, A. K. and Rath, G. (2018) 'Recent advances in metal nanoparticles in cancer therapy', *Journal of Drug Targeting*, 26(8), pp. 617–632. doi: 10.1080/1061186X.2017.1400553.
193. Sharma, G. et al. (2019) 'Novel development of nanoparticles to bimetallic nanoparticles and their composites: A review', *Journal of King Saud University - Science*. Elsevier, 31(2), pp. 257–269. doi: 10.1016/J.JKSUS.2017.06.012.
194. Shi, W. et al. (2012) 'Synthesis and Characterization of Gold Nanoparticles with Plasmon Absorbance Wavelength-Tunable from Visible to Near Infrared Region', *ISRN Nanomaterials*. Hindawi, 2012, pp. 1–9. doi: 10.5402/2012/659043.
195. Shittu, K. O. et al. (2017) 'Application of gold nanoparticles for improved drug efficiency', *Advances in Natural Sciences: Nanoscience and Nanotechnology*. IOP Publishing, 8(3), p. 035014. doi: 10.1088/2043-6254/aa7716.
196. Shukla, G. et al. (2017) 'Advanced magnetic resonance imaging in glioblastoma: a review', *Chinese Clinical Oncology*, 6(4). doi: 10.21037/ccov0i0.15820.

197. Sizoo, E. M. et al. (2010) 'Symptoms and problems in the end-of-life phase of high-grade glioma patients', *Neuro-Oncology*. Oxford University Press, 12(11), pp. 1162–1166. doi: 10.1093/neuonc/nop045.
198. Smith, C. and Ironside, J. W. (2007) 'Diagnosis and pathogenesis of gliomas', *Current Diagnostic Pathology*. Churchill Livingstone, 13(3), pp. 180–192. doi: 10.1016/J.CDIP.2007.04.002.
199. Smith, S. J. et al. (2010) 'Urine catecholamine levels as diagnostic markers for neuroblastoma in a defined population: implications for ophthalmic practice.', *Eye (London, England)*. NIH Public Access, 24(12), pp. 1792–6. doi: 10.1038/eye.2010.125.
200. Soenen, S. J. et al. (2014) 'The Cellular Interactions of PEGylated Gold Nanoparticles: Effect of PEGylation on Cellular Uptake and Cytotoxicity', *Particle & Particle Systems Characterization*. John Wiley & Sons, Ltd, 31(7), pp. 794–800. doi: 10.1002/ppsc.201300357.
201. Sosibo, N. M. et al. (2015) 'Facile Attachment of TAT Peptide on Gold Monolayer Protected Clusters: Synthesis and Characterization.', *Nanomaterials (Basel, Switzerland)*. Multidisciplinary Digital Publishing Institute (MDPI), 5(3), pp. 1211–1222. doi: 10.3390/nano5031211.
202. Spear, J. C., Ewers, B. W. and Batteas, J. D. (2015) '2D-nanomaterials for controlling friction and wear at interfaces', *Nano Today*. Elsevier, 10(3), pp. 301–314. doi: 10.1016/J.NANTOD.2015.04.003.

203. Srinoi, P. et al. (2018) 'Bimetallic Nanoparticles: Enhanced Magnetic and Optical Properties for Emerging Biological Applications'. Preprints. doi: 10.20944/PREPRINTS201804.0104.V1.
204. Stauffer, E., Dolan, J. A. and Newman, R. (2008) 'Gas Chromatography and Gas Chromatography—Mass Spectrometry', in *Fire Debris Analysis*. Elsevier, pp. 235–293. doi: 10.1016/B978-012663971-1.50012-9.
205. Suk, J. S. et al. (2016) 'PEGylation as a strategy for improving nanoparticle-based drug and gene delivery.', *Advanced drug delivery reviews*. NIH Public Access, 99(Pt A), pp. 28–51. doi: 10.1016/j.addr.2015.09.012.
206. Surapaneni, S. K., Bashir, S. and Tikoo, K. (2018) 'Gold nanoparticles-induced cytotoxicity in triple negative breast cancer involves different epigenetic alterations depending upon the surface charge', *Scientific Reports*. Nature Publishing Group, 8(1), p. 12295. doi: 10.1038/s41598-018-30541-3.
207. Tai, L. (2012) 'Cell Biology of the Nervous System', *Basic Neurochemistry*. Academic Press, pp. 3–25. doi: 10.1016/B978-0-12-374947-5.00001-8.
208. Tan, C. et al. (2017) 'A self-supporting bimetallic Au@Pt core-shell nanoparticle electrocatalyst for the synergistic enhancement of methanol oxidation', *Scientific Reports*. Nature Publishing Group, 7(1), p. 6347. doi: 10.1038/s41598-017-06639-5.
209. Tejamaya, M. et al. (2012) 'Stability of Citrate, PVP, and PEG Coated Silver Nanoparticles in Ecotoxicology Media', *Environmental Science & Technology*. American Chemical Society, 46(13), pp. 7011–7017. doi: 10.1021/es2038596.

210. Thakor, A. S. et al. (2011) 'Oxidative stress mediates the effects of Raman-active gold nanoparticles in human cells.', *Small* (Weinheim an der Bergstrasse, Germany). NIH Public Access, 7(1), pp. 126–36. doi: 10.1002/sml.201001466.
211. Tlotleng, N. et al. (2016) 'Cytotoxicity, intracellular localization and exocytosis of citrate capped and PEG functionalized gold nanoparticles in human hepatocyte and kidney cells', *Cell Biology and Toxicology*, 32(4), pp. 305–321. doi: 10.1007/s10565-016-9336-y.
212. Tosun, M. et al. (2017) 'Anatomic Origin and Molecular Genetics in Neuroblastoma', in *Neuroblastoma - Current State and Recent Updates*. InTech. doi: 10.5772/intechopen.69568.
213. Vasile, F., Dossi, E. and Rouach, N. (2017) 'Human astrocytes: structure and functions in the healthy brain.', *Brain structure & function*. Springer, 222(5), pp. 2017–2029. doi: 10.1007/s00429-017-1383-5.
214. Verly, I. R. N. et al. (2017) 'Catecholamines profiles at diagnosis: Increased diagnostic sensitivity and correlation with biological and clinical features in neuroblastoma patients', *European Journal of Cancer*. Pergamon, 72, pp. 235–243. doi: 10.1016/J.EJCA.2016.12.002.
215. Walton, J. D. et al. (2004) 'Characteristics of stem cells from human neuroblastoma cell lines and in tumors.', *Neoplasia* (New York, N.Y.). Neoplasia Press, 6(6), pp. 838–45. doi: 10.1593/neo.04310.
216. Wang, A. et al. (2014) 'Gold Nanoparticles: Synthesis, Stability Test, and Application for the Rice Growth', *Journal of Nanomaterials*. Hindawi, 2014, pp. 1–6. doi: 10.1155/2014/451232.

217. Wang, E. C. and Wang, A. Z. (2014) 'Nanoparticles and their applications in cell and molecular biology.', *Integrative biology: quantitative biosciences from nano to macro*. NIH Public Access, 6(1), pp. 9–26. doi: 10.1039/c3ib40165k.
218. Wang, S. et al. (2018) 'Sotetsuflavone inhibits proliferation and induces apoptosis of A549 cells through ROS-mediated mitochondrial-dependent pathway', *BMC Complementary and Alternative Medicine*. BioMed Central, 18(1), p. 235. doi: 10.1186/s12906-018-2300-z.
219. Waseem, M. et al. (2017) 'Melatonin pre-treatment mitigates SHSY-5Y cells against oxaliplatin induced mitochondrial stress and apoptotic cell death.', *PLoS one*. Public Library of Science, 12(7), p. e0180953. doi: 10.1371/journal.pone.0180953.
220. Watanabe, A. et al. (2009) 'In vitro free radical scavenging activity of platinum nanoparticles', *Nanotechnology*, 20(45), p. 455105. doi: 10.1088/0957-4484/20/45/455105.
221. Whatmore, R. W. (2006) 'Nanotechnology—what is it? Should we be worried?', *Occupational Medicine*. Narnia, 56(5), pp. 295–299. doi: 10.1093/occmed/kql050.
222. Wittekind, C. and Neid, M. (2005) 'Cancer Invasion and Metastasis', *Oncology*, 69(1), pp. 14–16. doi: 10.1159/000086626.
223. Wu, D. and Yotnda, P. (2011) 'Production and detection of reactive oxygen species (ROS) in cancers.', *Journal of visualized experiments: JoVE*. MyJoVE Corporation, (57). doi: 10.3791/3357.

224. Wulandari, P. et al. (2015) 'Characterization of citrates on gold and silver nanoparticles', *Journal of Colloid and Interface Science*. Academic Press, 438, pp. 244–248. doi: 10.1016/J.JCIS.2014.09.078.
225. Xie, X. et al. (2017) 'The Effect of shape on Cellular Uptake of Gold Nanoparticles in the forms of Stars, Rods, and Triangles', *Scientific Reports*. Nature Publishing Group, 7(1), p. 3827. doi: 10.1038/s41598-017-04229-z.
226. Xu, H. et al. (2017) 'Geographic Variations in the Incidence of Glioblastoma and Prognostic Factors Predictive of Overall Survival in US Adults from 2004–2013', *Frontiers in Aging Neuroscience*. Frontiers Media SA, 9. doi: 10.3389/FNAGI.2017.00352.
227. Xu, M. et al. (2018) 'Synthesis and Comparative Biological Properties of Ag-PEG Nanoparticles with Tunable Morphologies from Janus to Multi-Core Shell Structure.', *Materials* (Basel, Switzerland): Multidisciplinary Digital Publishing Institute (MDPI), 11(10). doi: 10.3390/ma11101787.
228. Yamada, M., Foote, M. and Prow, T. W. (2015) 'Therapeutic gold, silver, and platinum nanoparticles', *Wiley Interdisciplinary Reviews: Nanomedicine and Nanobiotechnology*, 7(3), pp. 428–445. doi: 10.1002/wnan.1322.
229. Yuan, Y.-G. et al. (2018) 'Silver Nanoparticles Potentiates Cytotoxicity and Apoptotic Potential of Camptothecin in Human Cervical Cancer Cells', *Oxidative Medicine and Cellular Longevity*. Hindawi, 2018, pp. 1–21. doi: 10.1155/2018/6121328.
230. Zabłocka, A. et al. (2015) 'Neurotrophic Activity of Cultured Cell Line U87 is Up-Regulated by Proline-Rich Polypeptide Complex and Its Constituent

- Nonapeptide.’, *Cellular and molecular neurobiology*. Springer, 35(7), pp. 977–86. doi: 10.1007/s10571-015-0192-8.
231. Zaleska-Medynska, A. et al. (2016) ‘Noble metal-based bimetallic nanoparticles: the effect of the structure on the optical, catalytic and photocatalytic properties’, *Advances in Colloid and Interface Science*. Elsevier, 229, pp. 80–107. doi: 10.1016/J.CIS.2015.12.008.
232. Zhang, M., Shi, J. and Jiang, L. (2015) ‘Modulation of mitochondrial membrane integrity and ROS formation by high temperature in *Saccharomyces cerevisiae*’, *Electronic Journal of Biotechnology*. Pontificia Universidad Católica de Valparaíso, 18(3), pp. 202–209. doi: 10.1016/j.ejbt.2015.03.008.
233. Zhang, Y. et al. (2012) ‘Effect of Size, Shape, and Surface Modification on Cytotoxicity of Gold Nanoparticles to Human HEP-2 and Canine MDCK Cells’, *Journal of Nanomaterials*. Hindawi, 2012, pp. 1–7. doi: 10.1155/2012/375496.
234. Zhao, M.-X. et al. (2018) ‘The Apoptosis Effect on Liver Cancer Cells of Gold Nanoparticles Modified with Lithocholic Acid.’, *Nanoscale research letters*. Springer, 13(1), p. 304. doi: 10.1186/s11671-018-2653-8.
235. Zimmermann, S., Dziadziuszko, R. and Peters, S. (2014) ‘Indications and limitations of chemotherapy and targeted agents in non-small cell lung cancer brain metastases’, *Cancer Treatment Reviews*. W.B. Saunders, 40(6), pp. 716–722. doi: 10.1016/J.CTRV.2014.03.005.

236. Zuber, A. et al. (2016) 'Detection of gold nanoparticles with different sizes using absorption and fluorescence based method', *Sensors and Actuators B: Chemical*. Elsevier, 227, pp. 117–127. doi: 10.1016/J.SNB.2015.12

